Collision of a dipolar vortex with a semi-infinite wall

Berkvens, P.P.J.

Award date:
2004

TU/e technische universiteit eindhoven
Eindhoven University of Technology

Department of Applied Physics
Fluid Dynamics Laboratory
Building: Cascade
P.O. Box 513
5600 MB Eindhoven

Title: **Collision of a dipolar vortex with a semi-infinite wall**

Author: P.P.J. Berkvens

Report number: R-1645-A

Date: July 2004

Group : Vortex Dynamics, Department of Applied Physics, Eindhoven University of Technology, The Netherlands

Advisor : prof. dr. ir. G.J.F. van Heijst (TU/e)

Abstract

In this study the evolution of a dipolar vortex colliding with a no-slip wall with a sharp edge was investigated. In absence of any obstructions the dipolar vortex moves in a straight path. The wall has been placed at different distances relative to the straight path of the undisturbed dipole. The behaviour of the vortex is strongly influenced by the offset-value. If the offset is large enough the vortex will not be influenced at all. If the offset becomes smaller, however, a patch of secondary vorticity is generated at the sharp edge and at the side of the wall. This patch removes some of the vorticity of one of the poles of the dipolar vortex. The dipole then becomes asymmetrical and starts to move in a curved path. If the offset becomes even smaller, or negative, the dipolar vortex will split and the two poles merge with the secondary vorticity from the wall and form two new dipolar vortices which move away from the wall in a curved path. This behaviour was investigated using both numerical simulations and laboratory experiments. The experiments were performed in a rotating tank as well as in a stratified fluid.

Contents

Chapter 1

Introduction

The large-scale geophysical flow of air and water in the atmosphere and oceans, respectively, can be considered to be two-dimensional. This is caused by three phenomena. Rotation of the earth causes the flow to behave quasi-two-dimensionally due to the implications of the Taylor-Proudman theorem (explained in section 2.1). Density stratification of the fluid causes fluid particles to remain in a thin layer having the same density as the fluid particles themselves. Therefore the flow in these layers can be considered to be two-dimensional. Finally the flow is restricted by the dimensions of the domain, the horizontal scales ($\geq$ 1000 km) being much larger than the vertical scales (1 - 10 km). These large-scale flows are often very stable and can exist for a long time and have a strong influence on the weather and climate on earth.

Important features of large-scale two-dimensional flows in the atmosphere are vortices. High and low pressure areas are examples of such vortical structures. They can have a diameter of $O(10^3)$ km while the vertical dimensions are limited by the thickness of the atmosphere being $O(10^0)$ km. A high pressure area is, on the northern hemisphere, a vortex rotating in anticyclonic direction while a low pressure area corresponds with a vortex with cyclonic rotation. These vortices interact with each other. A vortex at a certain distance from another vortex will induce a velocity at the position of the other vortex and vice versa. This causes both vortices to move. Of course this principle is not limited to two vortices. Two vortices of oppositely signed strength can form a pair, called a dipolar vortex. This structure will translate through the fluid. If the two vortices are of equal, but opposite, strength the dipolar vortex will move in a straight path. An interesting problem is to see how such a dipolar vortex behaves near a solid boundary. This kind of interaction can take place between, for example, large-scale atmospheric vortices and mountain ridges. Earlier research on this subject has been performed by, for example, Barker and Crow [1] who describe experiments in which a dipolar vortex collides with a solid wall. A numerical study was performed by Orlandi [2]. In both studies an infinitely long wall was used and the collision was symmetrical.

In this study the emphasis is on a dipolar vortex colliding with a wall of *finite* length.

The offset, which is the distance between the undisturbed path of the dipolar vortex and the top of the wall, was varied. In the numerical simulations, as described in chapter 5, the offset was varied over a broad range. At large offsets the dipolar vortex is not influenced by the presence of the wall while at the other extreme (a large negative offset) the collision was symmetrical and the wall could be considered infinitely long. The latter is the same situation as studied by Orlandi. Experiments were also performed in both a rotating fluid, see chapter 6, and in a stratified fluid (described in chapter 7). In both types of experiments problems creating the dipolar vortex were encountered. Therefore only a few experiments were successful and could be compared to the results form the numerical simulations.

Chapter 2

Theory

2.1 Equations of motion

An incompressible flow can be described with two equations, the law of conservation of mass and the law of conservation of momentum. These are also known as the continuity equation and the Navier-Stokes equation, respectively, formulated as:

$$\nabla \cdot \mathbf{v} = \mathbf{0}, \tag{2.1}$$

$$\frac{D\mathbf{v}}{Dt} = -\frac{1}{\rho}\nabla p + \nu\nabla^2\mathbf{v} + \mathbf{g}. \tag{2.2}$$

In these equations is $\mathbf{v}$ the velocity, ρ the density of the fluid, p the local pressure, ν the kinematic viscosity and $\mathbf{g}$ is the gravitational acceleration. In equation (2.2) only the gravitational force is taken into account, but other external forces may be added.

The presence of background rotation changes the flow behaviour dramatically. The rotation induces an apparent force, the so-called Coriolis force $\mathbf{F_{cor}}$:

$$\mathbf{F}_{cor} = -2\rho\boldsymbol{\Omega} \times \mathbf{v}. \tag{2.3}$$

In this equation $\mathbf{v}$ is the velocity of the flow relative to the rotating frame and $\boldsymbol{\Omega}$ is the angular velocity of the entire system. On the northern hemisphere this force deflects a moving particle to the right while on the southern hemisphere the particle is deflected to the left. Since the Coriolis force is directed perpendicular to the velocity it does no work. Relative to a co-rotating frame, the flow is then governed by (see e.g. [3]):

$$\frac{D\mathbf{v}}{Dt} = -2\boldsymbol{\Omega} \times \mathbf{v} - \frac{1}{\rho}\nabla P + \nu\nabla^2\mathbf{v}. \tag{2.4}$$

In this equation P is the reduced pressure, defined as

$$P = p - p_{stat} \tag{2.5}$$

with p the pressure and p_{stat} the static pressure; the latter defined as the pressure when $\mathbf{v} = 0$, which can be written as

$$p_{stat} = -\rho\Phi_{gr} + \frac{1}{2}\rho\Omega^2 r^2. \tag{2.6}$$

Here Φ_{gr} is the gravitational potential and r is the distance to the axis of rotation. Equation (2.4) can be non-dimensionalized using these non-dimensional variables:

$$\tilde{\mathbf{v}} = \frac{\mathbf{v}}{U}, \quad \tilde{P} = \frac{P}{\rho\Omega UL}, \quad \tilde{t} = t\Omega, \quad \tilde{r} = \frac{r}{L}, \tag{2.7}$$

with U a characteristic velocity and L a characteristic length-scale. Using these the Navier-Stokes equation (2.4) can be written as

$$\frac{\partial\tilde{\mathbf{v}}}{\partial\tilde{t}} + Ro(\tilde{\mathbf{v}}\cdot\tilde{\nabla})\tilde{\mathbf{v}} + 2\mathbf{k}\times\tilde{\mathbf{v}} = -\tilde{\nabla}\tilde{P} + E\tilde{\nabla}^2\tilde{\mathbf{v}}. \tag{2.8}$$

Here $\mathbf{k}$ is the unit vector pointing in the same direction as the axis of rotation. The two dimensionless numbers Ro and E are the Rossby and Ekman number, respectively, defined as:

$$Ro = \frac{U}{\Omega L}, \quad E = \frac{\nu}{\Omega L^2}. \tag{2.9}$$

The Rossby number is the ratio of inertial forces and the Coriolis force while the Ekman number is the ratio of the viscous forces and the Coriolis force. Equation (2.8) can be simplified significantly using the following assumptions: the flow is quasi-stationary and both $Ro \ll 1$ and $E \ll 1$. If these assumptions are applied equation (2.8) reduces to the geostrophic balance,

$$2\mathbf{k}\times\tilde{\mathbf{v}} = -\tilde{\nabla}\tilde{P}. \tag{2.10}$$

This equation describes a balance between the Coriolis force and the pressure force. By taking the curl of equation (2.10) and using the continuity equation (2.1) it can be derived that the velocity of the flow is independent of the z-coordinate:

$$\frac{\partial\mathbf{v}}{\partial z} = 0. \tag{2.11}$$

This is the Taylor-Proudman-theorem, which expresses that the velocity in a flow satisfying the assumptions made for the geostrophic balance is two-dimensional i.e. the velocity is independent of the z-coordinate. One implication of this theorem is that the vorticity

$$\omega = \nabla\times\mathbf{v} \tag{2.12}$$

is directed perpendicular to the plane of the flow.

2.2 The Lamb dipolar vortex

Since the flow is assumed to be two-dimensional in the x, y-plane, the vorticity vector $\boldsymbol{\omega}$ is directed in the z-direction and can be written as $\boldsymbol{\omega} = (0, 0, \omega_z)$. If the fluid is also assumed to be incompressible the two-dimensional continuity equation (2.1) becomes

$$\frac{\partial u}{\partial x} + \frac{\partial v}{\partial y} = 0. \tag{2.13}$$

This equation indicates that the flow can be described by a scalar function, the so-called stream function ψ, which is defined by:

$$\begin{aligned} u &\equiv \frac{\partial \psi}{\partial y}, \\ v &\equiv -\frac{\partial \psi}{\partial x}. \end{aligned} \tag{2.14}$$

In two-dimensional flows the relation between the vorticity

$$\omega_z = \frac{\partial v}{\partial x} - \frac{\partial u}{\partial y} \tag{2.15}$$

and the stream function ψ is then given by the Poisson equation:

$$\omega_z = -\nabla^2 \psi. \tag{2.16}$$

To solve this equation Lamb assumed a linear ω_z,ψ relationship (Lamb, 1932 [4]) within a circle of radius a while the vorticity in the exterior, $r > a$, is zero:

$$\omega_z = \begin{cases} -k^2\psi & r < a, \\ 0, & r > a \end{cases} \tag{2.17}$$

in which k is a constant. For this vorticity distribution the following solution can be found:

$$\psi(r,\theta) = \begin{cases} -\frac{2U_0}{kJ_0(ak)} J_1(kr)\sin\theta & r \leq a, \\ -U_0(r - \frac{a^2}{r})\sin\theta & r > a. \end{cases} \tag{2.18}$$

Here r is the distance to the centre of the circle and U_0 is the uniform velocity of the exterior flow at infinity. This velocity can also be regarded as the velocity of the dipolar vortex in a stationary fluid. J_0 and J_1 are the zeroth and first order Bessel function, respectively. The angle θ is the angle with the uniform flow at infinity U_0. Since the stream function must be continuous at $r = a$ it is necessary that $J_1(ka) = 0$, therefore $k = 3.832/a$. The streamline pattern of a Lamb dipole is shown in figure 2.1.

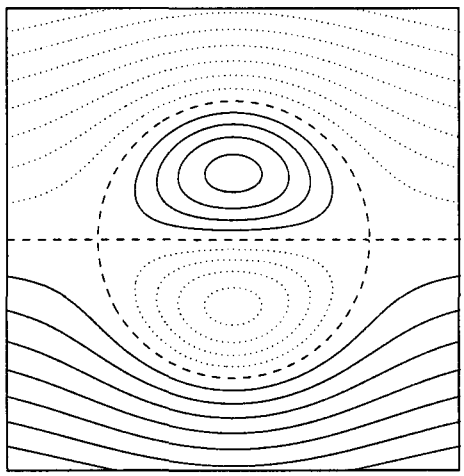

Figure 2.1: *Contours of the stream function of a Lamb dipolar vortex. Positive streamlines are solid, negative dotted and the dashed line indicates the line where the stream function is equal to zero in the frame moving with the dipole. This is the separatrix and it has radius* a.

2.3 Potential flow and conformal mapping

A two-dimensional flow can be described by so-called potential theory when the fluid is irrotational. Assuming that this is the case, i.e.

$$\frac{\partial v}{\partial x} - \frac{\partial u}{\partial y} = 0, \tag{2.19}$$

a scalar function ϕ, the velocity potential, can be defined as

$$\begin{aligned} u &\equiv \frac{\partial \phi}{\partial x}, \\ v &\equiv \frac{\partial \phi}{\partial y}. \end{aligned} \tag{2.20}$$

It is useful to introduce the complex potential w which is a function of the complex coordinate z, $w{=}w(z)$, with $z = x + iy$. The complex potential can be written as a function of both ϕ and ψ:

$$w(z) \equiv \phi(x, y) + i\psi(x, y), \tag{2.21}$$

while the derivative is related to the velocity components u and v via

$$\frac{dw}{dz} = u - iv. \tag{2.22}$$

The flow due to a potential or point vortex of strength Γ, which is located at z_0, can be described with the complex potential

$$w(z) = -\frac{i\Gamma}{2\pi}\ln(z - z_0). \tag{2.23}$$

The stream function ψ, which is the imaginary part of (2.23), is equal to

$$\psi = -\frac{\Gamma}{2\pi}\ln(r) \tag{2.24}$$

with r the distance to the vortex centre. The velocity generated by such a vortex is purely azimuthal and is given by

$$\begin{aligned} v_r &\equiv 0, \\ v_\theta &\equiv \frac{\Gamma}{2\pi r}. \end{aligned} \tag{2.25}$$

If more than one potential vortex is present the complex potentials of all vortices can be added to calculate the complex potential of the entire system of point vortices.

Since the subject of this investigation is the influence of a wall on a dipolar vortex the wall has to be taken into account as well. The influence of an infinitely long wall on the flow due to a point vortex can be investigated by introducing a so-called mirror vortex. This is a vortex of opposite strength that is placed at the mirror position of original vortex. The wall can then be ignored because the velocity at the position of the wall is purely tangential and no streamlines cross the wall. Since the fluid is inviscid the no-slip condition at the wall does not need to be satisfied. In figure 2.2 the principle of the mirror image is shown.

If the wall is not infinitely long the mirror technique cannot be used directly. It is necessary to first use a technique called 'conformal mapping'; this method is explained in more detail by for example Paterson (1983) [5]. To calculate the flow around a semi-infinite wall the following mapping will convert the flow in the entire z-space to the upper half plane of the ζ-space, see e.g. Spiegel [6]:

$$\zeta = z^{1/2}. \tag{2.26}$$

For the case of a *dipole* consisting of one pole of strength $-\Gamma$ located at $z_- = r_- e^{\,i\theta_-}$ and a pole of strength $+\Gamma$ at $z_+ = r_+ e^{\,i\theta_+}$ the transformation to the ζ-space maps the poles to

$$\begin{aligned} \zeta_- &\equiv r_-^{1/2} e^{\,i\theta_-/2}, \\ \zeta_+ &\equiv r_+^{1/2} e^{\,i\theta_+/2}. \end{aligned} \tag{2.27}$$

To represent the infinite wall two mirror vortices must be introduced, as shown in figure 2.3. Using equation (2.23) it is possible to calculate the potential velocity due to the dipolar vortex. The positions of the four poles are (a,b) and $(c,-d)$ for the two positive poles, one

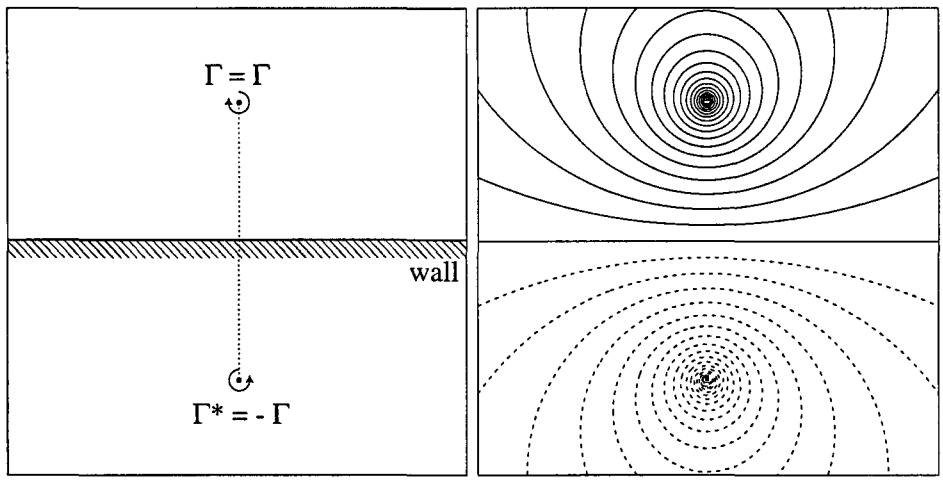

Figure 2.2: *Graph showing the principle of mirroring a vortex in the wall (left figure). The original vortex has strength* Γ *while the image vortex* Γ^* *has strength* $-\Gamma$*. The right figure shows the streamline pattern of this configuration. Solid lines indicate real streamlines while the dashed streamlines are in the wall and therefore not real. The straight streamline is at the position of the wall, no streamlines cross the wall.*

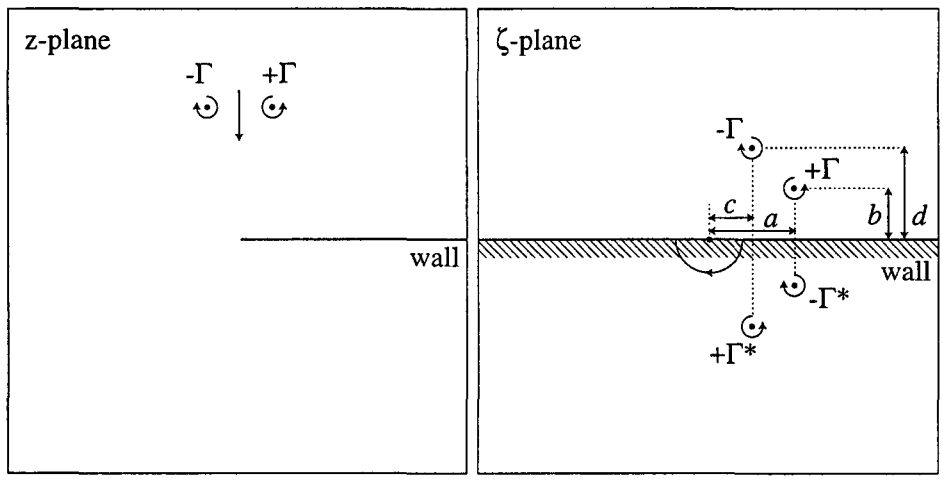

Figure 2.3: *The conformal mapping of the entire domain around the semi-infinite wall to the upper half plane of the* ζ*-space. This was done according to the mapping described in equation (2.26). The two image poles are indicated by an asterisk (*).*

real and one image vortex, and $(a,\text{-}b)$ and (c,d) for the negative poles. These positions can be calculated using equation (2.27). Then the potential velocity can be described with

$$w_\zeta(\zeta) = -\frac{i\Gamma}{2\pi} \cdot \Big\{ \ln[\zeta - (a+ib)] - \ln[\zeta - (c+id)] \\ - \ln[\zeta - (a-ib)] + \ln[\zeta - (c-id)] \Big\}. \tag{2.28}$$

This is still in the non-physical ζ-plane. To return to the real z-plane every ζ in equation (2.28) is replaced by $z^{1/2}$. The potential velocity in the z-plane, w_z, is

$$w_z(z) = -\frac{i\Gamma}{2\pi} \cdot \Big\{ \ln[z^{1/2} - (a+ib)] - \ln[z^{1/2} - (c+id)] \\ - \ln[z^{1/2} - (a-ib)] + \ln[z^{1/2} - (c-id)] \Big\}. \tag{2.29}$$

The stream function ψ is the imaginary part of the calculated complex potential, therefore only the real parts of the logarithmic functions need to be considered. The real part of $\ln(z)$ is equal to the logarithmic of the absolute value of z, $\ln(|x+iy|)$. The stream function ψ is equal to

$$\psi(z) = \frac{\Gamma}{2\pi} \cdot \Big\{ \ln[|z^{1/2} - (a+ib)|] - \ln[|z^{1/2} - (c+id)|] \\ - \ln[|z^{1/2} - (a-ib)|] + \ln[|z^{1/2} - (c-id)|] \Big\}. \tag{2.30}$$

The square root of a complex number $z = x + iy$ is defined as:

$$(x+iy)^{1/2} = \pm\frac{1}{2^{1/2}} \cdot \Big\{ [(x^2+y^2)^{1/2} + x]^{1/2} + \\ i \cdot \mathrm{sgn}(y) \cdot [(x^2+y^2)^{1/2} - x]^{1/2} \Big\}, \tag{2.31}$$

in which the plus sign is used for the upper half plane ($y > 0$) and the minus sign for the lower half plane ($y < 0$). It is now possible to calculate the irrotational flow in the vicinity of a semi-infinite wall due to a dipolar vortex. The streamline pattern and a vector diagram of this flow are shown in figure 2.4.

2.4 Boundary layers

In section 2.3 the influence of viscosity was neglected to approximate the flow around the wall due to a dipolar vortex. In reality, however, the no-slip condition requires that the normal and the tangential components of the fluid velocity at the wall are zero. Since the velocity away from the wall is non-zero a (viscous) adjustment has to be present: the boundary layer. The fluid can be divided in two domains, the boundary layer around a solid wall and a potential flow further away from the wall.

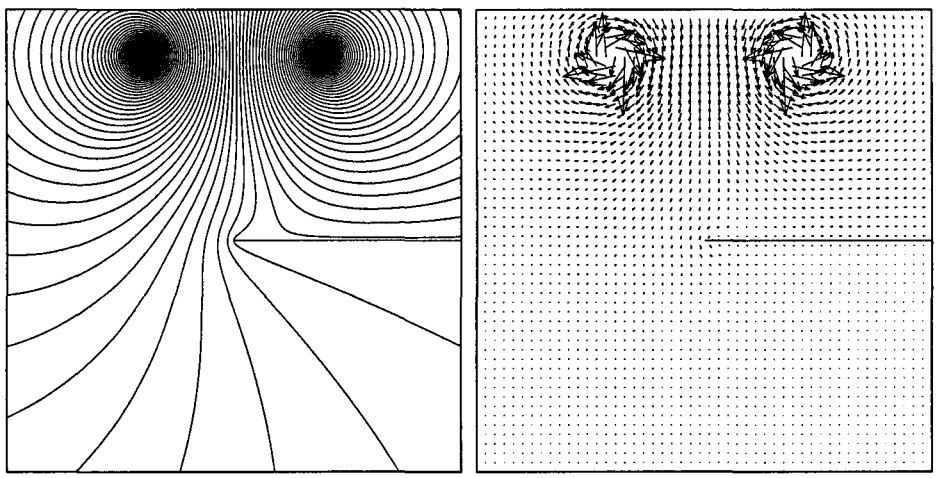

Figure 2.4: *Streamline and velocity field of a dipolar vortex in the vicinity of a semi-infinite wall. No streamlines cross the wall.*

An important dimensionless number in the theory of boundary layers is the Reynolds number, *Re*. This number gives the ratio of inertial and friction forces and is defined as

$$Re \equiv \frac{Ud}{\nu}. \tag{2.32}$$

Here U is a typical velocity in the flow and d a characteristic length. The thickness δ of the laminar boundary layer developing along a semi-infinite flat plate can be estimated at

$$\delta \sim x \cdot Re_x^{-1/2} \tag{2.33}$$

with x the horizontal distance to the edge of the plate as shown in figure 2.5 and Re_x the Reynolds number defined as

$$Re_x = \frac{Ux}{\nu}. \tag{2.34}$$

The higher the Reynolds number the thinner the boundary layer. Since usually $Re \gg 1$ the scaled boundary layer thickness is $\delta/x \ll 1$. Equation (2.33) only gives a rough approximation of the thickness of the boundary layer. The Blasius solution gives a quasi-exact representation of δ, see e.g. Kundu, 1990 [3]. It describes the velocity distribution in the boundary layer as a function of the similarity variable η which is defined as

$$\eta = y\sqrt{\frac{U}{\nu x}}. \tag{2.35}$$

This solution is shown graphically in figure 2.6. The thickness δ_{99} is defined as the distance from the wall to the point where $u = 0.99U$. Since this is at $\eta = 4.9$ the boundary-layer thickness δ_{99} is described by

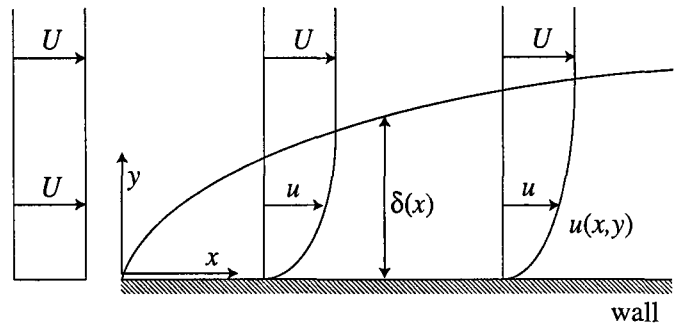

Figure 2.5: *A schematic overview of a boundary layer. The boundary layer is formed at a semi-infinite plate placed in the flow. The thickness of the layer is $\delta(x)$ and U is the velocity of the main flow.*

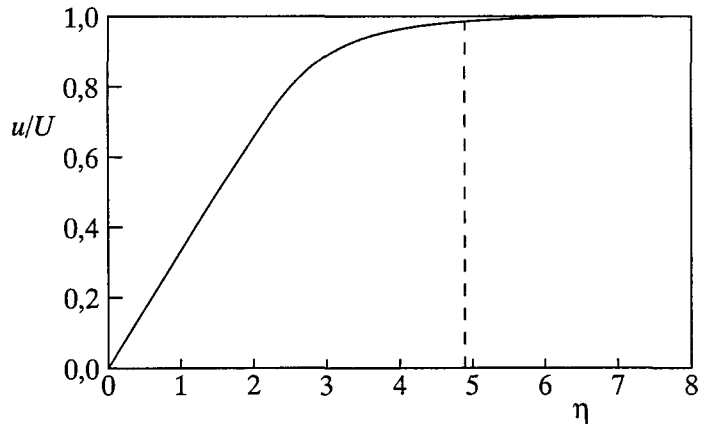

Figure 2.6: *The velocity distribution in the boundary layer according to the Blasius solution; the dashed line intersects the graph at $u/U = 0.99$.*

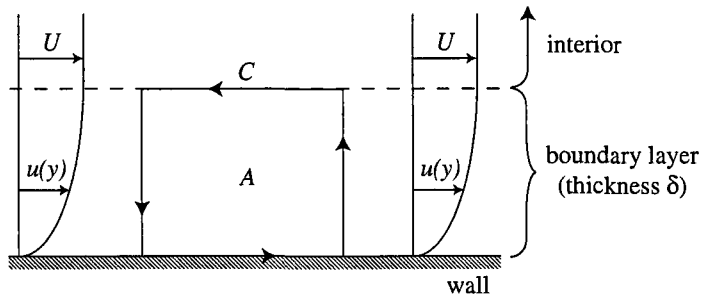

Figure 2.7: *Schematic overview of the contour C and surface A used in equation (2.37).*

$$\frac{\delta_{99}}{x} = \frac{4.9}{\sqrt{Re_x}} \tag{2.36}$$

In the boundary layer vorticity is generated: this is the so-called secondary vorticity. For example consider a wall and a main flow U parallel to it in positive x-direction (see figure 2.7). Since $\frac{\partial u}{\partial y} \neq 0$ the vorticity ω_z is, according to equation (2.15), also non-zero. The amount of vorticity generated in the boundary layer can be described using the circulation Γ defined as

$$\Gamma = \oint_C \mathbf{v} \cdot d\mathbf{r} = \iint_A \omega_z dA \tag{2.37}$$

with A the area enclosed by the closed contour C. To calculate the vorticity present in the boundary layer the contour C is chosen as indicated in figure 2.7. Since the velocity at and perpendicular to the wall are both equal to zero the amount of circulation Γ present in a part of the boundary layer of length l, $A = \delta l$, can be calculated:

$$\Gamma = -Ul. \tag{2.38}$$

The total circulation in the boundary layer depends only on the velocity of the main flow (U).

2.5 Boundary-layer separation

Sofar the main flow along the wall was assumed to be uniform. If the velocity of the fluid near the wall is not uniform, however, the boundary layer may separate. It will then roll up into a new vortex which will influence the path of the main dipole. The separation process is explained in this section.

In the inviscid external flow the pressure p can be calculated using the Bernoulli equation:

$$p + \frac{1}{2}\rho U^2 = \textit{constant along a streamline} \tag{2.39}$$

which, after taking the derivative to x, becomes:

$$\frac{\partial p}{\partial x} = -\rho U \frac{\partial U}{\partial x}. \tag{2.40}$$

Using the Bernoulli equation and the conservation laws (2.1) and (2.2), and assuming that $Re \gg 1$ the Prandtl boundary-layer equations can be derived, see for example Schlichting and Gersten 2000 [7]:

$$\frac{\partial u}{\partial x} + \frac{\partial v}{\partial y} = 0, \tag{2.41}$$

$$u\frac{\partial u}{\partial x} + v\frac{\partial u}{\partial y} = U\frac{\partial U}{\partial x} + \nu\frac{\partial^2 u}{\partial y^2}, \tag{2.42}$$

$$\frac{\partial p}{\partial y} = 0. \tag{2.43}$$

Using equation (2.40) the pressure gradient can be calculated outside the boundary layer. Since the pressure is constant in the y-direction, as shown in equation (2.43), the pressure inside the boundary layer is the same as that in main flow directly above the boundary layer. While $\frac{\partial U}{\partial x} > 0$ the pressure gradient, $\frac{\partial p}{\partial x} < 0$, supports the main flow. If the velocity of the main flow decreases, $\frac{\partial U}{\partial x} < 0$, the pressure gradient changes sign as well and will have an adverse effect on the velocity in the positive x-direction. It can cause the fluid in the boundary layer close to the wall to move in backward direction as shown in figure 2.8. This can be explained using equations (2.40) and (2.42) and the no-slip condition at the wall ($\mathbf{v} = \mathbf{0}$). From these equations it follows that

$$\nu\rho\frac{\partial^2 u}{\partial y^2}|_{y=0} = \frac{\partial p}{\partial x}. \tag{2.44}$$

Since the velocity in the boundary layer must adapt gradually to the main flow the second derivative of the velocity, $\frac{\partial^2 u}{\partial y^2}$, in the boundary layer near the main flow must be negative. If the gradient of the pressure is negative the sign of $\frac{\partial^2 u}{\partial y^2}$ is, according to equation (2.44), negative at the wall. The curvature of the velocity profile has the same sign all through the boundary layer, as shown in figure 2.8 *A*. If the pressure gradient is positive, however, the second derivative of the velocity at the wall is also positive. Since it is still negative near the main flow there must be a point of inflection in the velocity profile. It depends on the strength of the pressure gradient if the the boundary layer really separates. Figure 2.8 *B* already has a point of inflection in the velocity profile but the boundary layer has not yet separated because the pressure gradient is unable to overcome the viscous forces. In figure 2.8 *C* the shear at the wall is equal to zero, $\frac{\partial u}{\partial y} = 0$. This is called the separation point since if the pressure gradient increases even further the fluid near the wall will be flowing in backward direction. This is shown in figure 2.8 *D*.

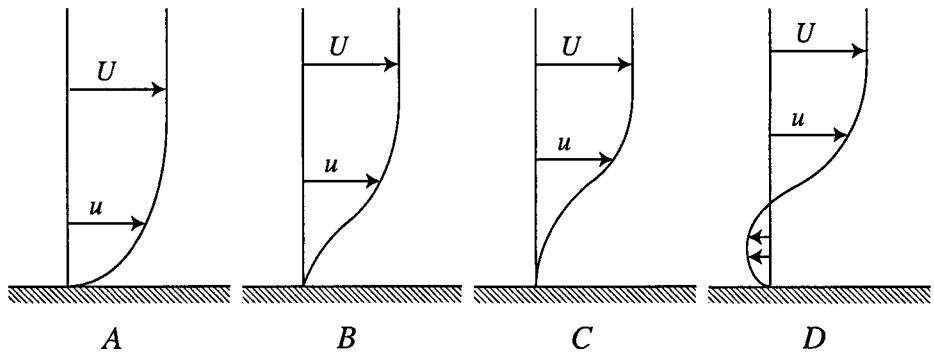

Figure 2.8: *A schematic overview of the separation proces at the wall. In figure A the velocity gradient is positive and the pressure gradient is therefore negative, no separation will take place. Figure B has a negative velocity gradient and thus a positive pressure gradient but still no separation has occurred. Next, in figure C, the pressure gradient is still positive and separation has begun although there is no flow in negative x-direction yet. Finally, in figure D, the fluid flows in opposite direction relative to the main flow.*

Chapter 3

Experimental set-up

Experiments were carried out in both a stratified fluid and in a rotating fluid. The stratified fluid has a vertical gradation in the density and therefore different fluid layers in which the motion is quasi-two-dimensional, while in the rotating tank the fluid behaves quasi-two-dimensional due to the Taylor-Proudman effect.

3.1 Stratification

The experiments in the stratified fluid were performed in a 1 m $\times$ 1 m perspex tank with a depth of 0.3 m. The tank is first filled with about 7 cm of fresh water, after that salt water with a density of 13.4% brix was added at the bottom of the tank, this layer is also 7 cm deep. Since the salt water was added slowly the two layers do not mix. A sharp interface between fresh and salt water is the result. In time the sharp interface will become a more gradual transition due to mass diffusion. The thickness of the layer in which experiments were performed was 0.5 cm.

In order to generate a dipolar vortex fluid is injected through a nozzle with an inner diameter of 2 mm (see e.g. van Heijst & Flór 1989 [8]). This is done using syringes that

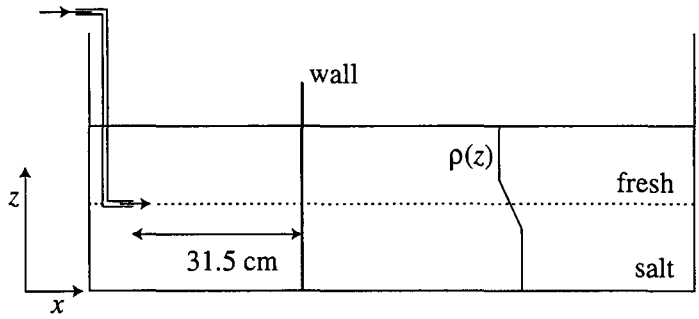

Figure 3.1: *Set-up for the experiments in the stratified fluid.*

are emptied via an automated mechanism so that the flow rate and injected volume are constant in the different experiments. In all experiments 3.3 ml of fluid was injected in 0.6 s. The distance from the tip of the nozzle to the plate is 31.5 cm. The injected fluid has the same density as the fluid at the level of the nozzle. Immediately after injection the flow forms a three-dimensional turbulent motion that moves away from the nozzle in a conical shape. This shape grows in both horizontal and vertical direction until the cone collapses into a flat layer due to gravity. This is described in more detail by Flór and van Heijst (1994) [9]. After this collapse the turbulent motion organizes into a dipolar vortex due to the inverse energy cascade which is characteristic for two-dimensional flows.
The flow in the water was visualized using either dye in the injected fluid or particles at the interface between fresh and salt water. These particles can be tracked as explained in section 3.3 to give a qualitative flow measurement. In the dye experiments dye was also put at the wall to visualise the secondary vorticity. In both cases the tank was illuminated by fluorescent tubes.

3.2 Background rotation

The tank in which the experiments are performed is 150 cm $\times$ 100 cm in size and is filled with 20 cm of tap water. The tank is placed on a table that rotates at a constant angular velocity $\Omega = 0.70$ rad s^{-1}. Experiments are not started for at least 45 minutes after setting the tank in motion. During this time the fluid can adjust to the rotating tank and get in solid body rotation. Since the water surface will adopt a parabolic form due to centrifugal forces the bottom has a specially designed parabolic shape to ensure a uniform water depth. This is necessary to avoid curved paths of a dipole due to the β-plane effect as described by Velasco Fuentes and van Heijst, 1994 [10].

As explained in section 2.1 the flow in a rotating fluid is quasi-two-dimensional due to the Taylor-Proudman theorem. In the derivation of this theorem the viscosity was neglected, i.e. $E \ll 1$. In reality this assumption is only valid in the so-called interior of the flow, which is the entire fluid volume except for the boundary layers at the bottom and sidewalls of the tank. There the velocity of the flow must adapt gradually to the no-slip condition at the bottom. The boundary layer at the bottom is a so-called Ekman boundary layer and is very thin compared to the water depth, its thickness δ_E being equal to

$$\delta_E = (\frac{\nu}{\Omega})^{1/2}, \tag{3.1}$$

see Pedlosky [11]. Since the tank used for the experiments rotates at 0.70 rad s^{-1} and the kinematic viscosity ν of the water is equal to 10^{-6} m^2 s^{-1} for fresh water of 20 ^{o}C the Ekman layer is 1.2 mm thick. Since this layer is very thin the entire flow can be considered quasi-two-dimensional.

The dipolar vortex is created by dragging an open cylinder with a diameter of 70 mm through the fluid while lifting it at the same time. To assure that the cylinder is moved

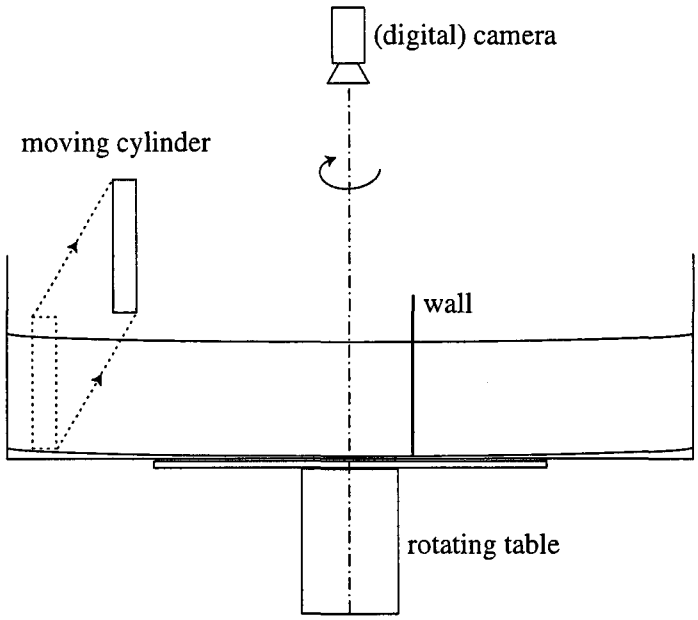

Figure 3.2: *Set-up for the experiments in the rotating tank. The camera is mounted in a co-rotating frame. The fluid is illuminated from the sides using 4 slide projectors (not shown).*

in a straight line a guiding rail was attached to the side of the tank. The cylinder was initially standing on the bottom of the tank, after which it was lifted out of the water. While being lifted the cylinder moved 9 cm in horizontal direction. The distance from the starting position of the cylinder to the wall is 49 cm. The relative flow is recorded by a camera mounted in the co-rotating frame. In figure 3.2 an overview of the set-up is given. Fluorescent tubes were used for the dye experiments, while slide projectors were used for the particles experiments.

3.3 Particle tracking

Dye can be used to visualize the flow. If, however, more qualitative information is required particle experiments have to be performed. In this section the process of particle tracking is explained as used for the particle experiments in both the rotating tank and the stratified fluid.

To do particle tracking in the rotating tank small tracer particles with a diameter of 250 μm are spread in the fluid, most of them float on the surface. These particles are illuminated using 4 slide projectors of 250 W each. A co-rotating digital camera was used to capture frames of the flow and tracer particles. In the stratified fluid the tracer particles

must have a density that is equal to the density level at which experiments are performed. Therefore small polystyrene spheres were used with a diameter varying between 1 and 2 mm which have a density corresponding to a 7.5 % brix solution. In both cases the camera used is a SMD 1M15 digital camera which captures images of 1024 $\times$ 1024 pixels in 12 bit greyscale at 7.5 frames per second.

The technique used for particle tracking is called High-resolution Particle Velocimetry (HPV). This is a combination of both PIV, Particle Image Velocimetry, and PTV, Particle Tracking Velocimetry.
PIV is a technique that uses two frames which it divides in small square areas of which the particle patterns are analyzed. These areas have fixed positions and sizes that are the same in all frames. The displacement of the particle pattern between the two frames is calculated for each area. Since the time interval between the two frames is known the velocity in each square can be determined. To get proper results there should be at least 4 to 8 particles in each area, the actual minimum depends on for instance the velocity. This process is explained in figure 3.3. It is performed on each area so the number of areas in which the total frame is divided is also the number of velocity vectors that is obtained using the PIV technique.
PTV is another method that can be used to calculate a velocity field from successive images. This technique is not as computer time efficient as PIV but it is capable of calculating the velocity of a single tracer particle. For good results the particle displacement between successive frames must be smaller than the distance between the particles. Then each particle in the first frame, i, should be matched to a particle in the next frame, $i+1$. An algorithm is used that searches for the particle in frame $i+1$ that is closest to the position of the particle in frame i. If the closest particle is not optimal when considering all other particles it may be matched to a particle further away. Then the particles in frame $i+1$ are matched to the particles in frame $i+2$. This is done for a sequence of frames resulting in a particle path. From this path the velocity of the particle is determined. The disadvantage of this technique is that at higher particle densities or velocities the matching is often incorrect since the closest particle in the next frame is not necessarily the same particle. To solve this problem it is possible to use results obtained using the PIV technique as a prediction for the position of the particle in the next frame. Then the closest particle to that predicted position is probably the correct one. This is called the HPV technique. It can calculate the velocity of each tracer particle at higher densities or velocities than PTV. A more precise description of PIV, PTV and HPV is given by Bastiaans *et al.* 2002 [12]. In all particle experiments the HPV technique was used.

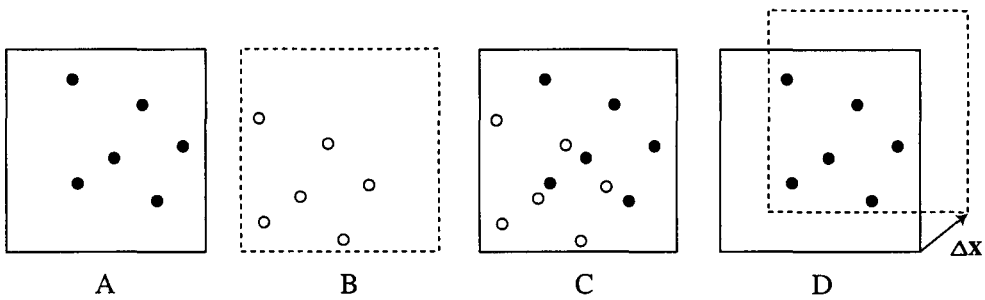

Figure 3.3: *Figure A and B show one of the small areas of the entire captured image, figure A belonging to frame i while B refers to frame* $i + 1$. *This is the same area, only a little later, with the particles now in different positions. This is visible in figure C in which the two frames are overlayed. The last figure displays the maximum correlation between the particle patterns and gives the displacement* $\Delta \boldsymbol{x}$.

Chapter 4

Potential Model

4.1 Analytical-numerical model

In this section a model for the paths of the two poles of the dipolar vortex is derived. The model is based on potential flow theory, in which the dipole is described by two point vortices. The path is approximated by calculating the velocity of the pole analytically and then multiplying the velocity with a short time interval Δt. This gives a small displacement from which the new position of the pole is calculated. This process is repeated a number of times and results in a path. Therefore this approach is called the analytical-numerical model.

In section 2.3 a description of the potential velocity due to a potential dipolar vortex was derived. The result was given in equation (2.29) and shown in figure 2.4. Apart from the stream function the velocity can also be calculated from the velocity potential using equation (2.22). The velocity at a position (x,y) in the z-plane due to a pole of strength Γ located at (a,b) in the ζ-plane is determined by

$$u = -\frac{\Gamma}{4\pi}\frac{F_2}{F_1^2 + F_2^2}, \tag{4.1}$$

$$v = \frac{\Gamma}{4\pi}\frac{F_1}{F_1^2 + F_2^2}, \tag{4.2}$$

with F_1 and F_2 two functions defined as

$$F_1 = x \pm 2^{-1/2}\{a \cdot [(x^2+y^2)^{1/2} + x]^{1/2} - b \cdot \mathrm{sgn}(y)[(x^2+y^2)^{1/2} - x]^{1/2}\}, \tag{4.3}$$

and

$$F_2 = y \pm 2^{-1/2}\{b \cdot [(x^2+y^2)^{1/2} + x]^{1/2} + a \cdot \mathrm{sgn}(y)[(x^2+y^2)^{1/2} - x]^{1/2}\} \tag{4.4}$$

where the plus signs are used if $y < 0$ and the minus signs if $y > 0$.

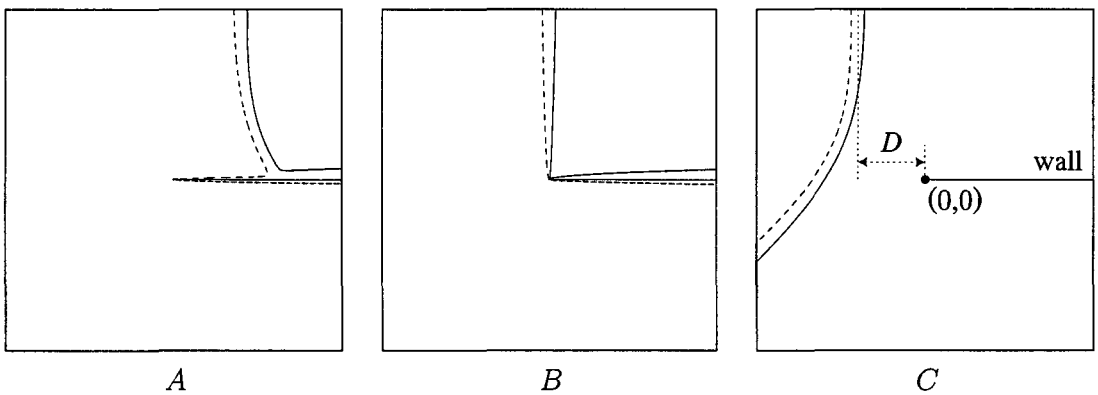

Figure 4.1: *Paths of a potential dipolar vortex starting at different positions. The origin of the plane is at the edge of the wall as indicated in figure C, there also the offset D is shown. The offsets δ in figures A, B and C are -5, 0 and 5, respectively. The strength of the two poles are $\Gamma_+ = -\Gamma_- = 1$. The dashed line indicates the path of the negative pole and the solid line represents the positive pole.*

To determine the velocity components u and v of a pole the velocity at the position of the pole must be calculated while ignoring the contribution of the pole itself. For example, the velocity of the positive pole is calculated using only the negative pole and the two image vortices. The contributions of all three poles can be added.

In figure 4.1 three examples are shown of the paths of the two poles of a dipolar vortex starting at different offsets. The dimensionless offset δ is defined as

$$\delta = \frac{D}{d} \tag{4.5}$$

where D is the distance between the straight path and the edge of the wall (as indicated in figure 4.1 C and d is the distance between the two poles. Figure 4.1 A shows that the dipole moves in a curved path towards the wall. Then the two poles separate and start moving along the wall. The negative pole moves closer to the wall than the positive one. Also the paths are not parallel to the wall. These effects are caused by the presence of the edge. With an infinitely long wall the approach would have been symmetrical. The difference between these two situations is shown in figure 4.2. Figure 4.2 A shows the dipole far from the edge; this situation is comparable with an infinitely long wall. Figure 4.1 B shows the paths of the two poles if the starting position is straight above the edge of the wall. While approaching the wall the two poles move closer together. At the wall the negative pole moves around the edge while the positive pole stays above the wall. Both then move to the right. The last figure (C) shows the curved path of the two poles, this is again caused by the presence of the wall, without it the dipolar vortex would move in a straight line.

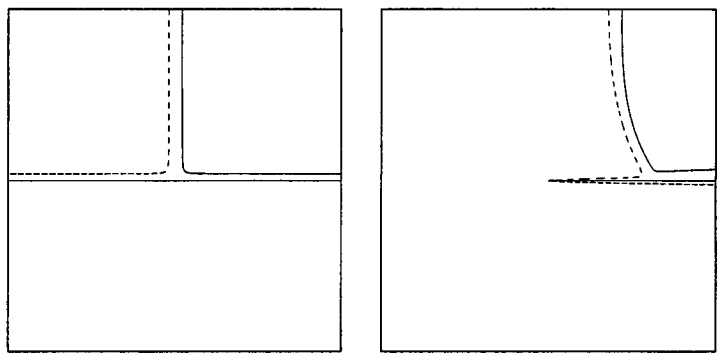

Figure 4.2: *Paths of two potential dipolar vortices. Figure A shows the path if the dipolar vortex is far from the edge, $\delta = -5000$. In figure B the offset is much smaller, $\delta = -5$. The strength of the vortices is the same as in figure 4.1. The dashed line indicates the path of the negative pole and the solid line represents the positive pole.*

4.2 Analytical models

In the previous section the path of the two poles was calculated. While the velocity was calculated analytically the path could not be determined analytically, a combination of both analytical and numerical calculations was needed. It is possible to calculate the paths of the two vortices analytically if the dipole moves towards an infinitely long wall. Also it is possible to derive an analytical expression for the path of a single pole around the edge of a semi-infinite wall. Finally the paths of two vortices of unequal strength are determined while ignoring the influence of the wall.

4.2.1 Paths of a dipole moving towards an infinitely long wall

If a dipolar vortex moves towards an infinite wall the paths can be calculated using the mirror principle. Two new poles are placed in the lower half plane as shown in figure 4.3. The positions of the poles are (x_1,y_1) and $(-x_1,y_1)$ for the real vortices and $(x_1,-y_1)$ and $(-x_1,-y_1)$ for the image vortices. Since the paths are symmetric in both x and y-axis only the path of the vortex in the first quadrant is calculated. The governing equation for this system of n point vortices is (see Newton 2001, [13]):

$$\frac{\partial x_j}{\partial t} = -\sum_{i=1,\, i\neq j}^{n} \frac{\Gamma_i(y_j - y_i)}{2\pi r_{ij}^2}, \tag{4.6}$$

$$\frac{\partial y_j}{\partial t} = \sum_{i=1,\, i\neq j}^{n} \frac{\Gamma_i(x_j - x_i)}{2\pi r_{ij}^2} \tag{4.7}$$

where r_{ij} is the distance between the vortices i and j. This is a system of Hamiltonian form:

$$\Gamma_j \frac{\partial x_j}{\partial t} = \frac{\partial H}{\partial y_j}, \quad \Gamma_j \frac{\partial y_j}{\partial t} = -\frac{\partial H}{\partial x_j} \tag{4.8}$$

with the Hamiltonian H

$$H \equiv -\frac{1}{4\pi} \sum_{i=1,\, i\neq j}^{n} \Gamma_i \Gamma_j \ln(r_{ij}) \tag{4.9}$$

a conserved quantity. For the system considered here the Hamiltonian is equal to:

$$H = -\frac{\Gamma^2}{4\pi} \ln\left(\frac{\sqrt{x_1^2 + y_1^2}}{2x_1 y_1}\right). \tag{4.10}$$

Since this is a conserved quantity the paths of the poles are described with

$$\frac{\sqrt{x_1^2 + y_1^2}}{2x_1 y_1} = c' \quad \text{or} \quad y_1^2 = \frac{x_1^2}{c x_1^2 - 1}. \tag{4.11}$$

where c and c' are (different) constants. The pole in the first quadrant moves initially (far from the wall) at $x_1 = c^{-1/2}$ and then deflects to the right, therefore x_1 is always larger than $c^{-1/2}$. The paths for different constants c are plotted in figure 4.3. The path that is calculated using this technique resembles the path calculated with the analytical-numerical combination far from the edge as shown in figure 4.2.

4.2.2 Path of a single vortex near the edge

If a single point vortex is placed near the edge of a semi-infinite wall it will start to move. Here an expression for the path is derived. In figure 4.4 the starting situation is shown, both in the real z-space in the ζ-space. The starting position of the vortex is (r_0, θ_0) in the z-plane. The transformation $\zeta = z^{1/2}$ maps the starting position to $(r_0' = r_0^{1/2},\ \theta_0' = \theta_0/2)$ where the prime indicates coordinates in the ζ-plane.

The equation of motion in the ζ-plane for a vortex of strength Γ located at $\zeta_v = \xi_v + i\eta_v$ is

$$\frac{d\zeta_v}{dt} = \frac{i\Gamma}{2\pi(\zeta_v - \overline{\zeta_v})} \tag{4.12}$$

where the subscript v indicates the position of the vortex. This equation implies that there is a Hamiltonian structure:

$$\Gamma \frac{d\zeta_v}{dt} = \frac{\partial H_\zeta}{\partial \eta_v} + i\frac{\partial H_\zeta}{\partial \xi_v} \tag{4.13}$$

with

$$H_\zeta(\zeta_v) = \frac{\Gamma^2}{4\pi} \ln(2\eta_v) \tag{4.14}$$

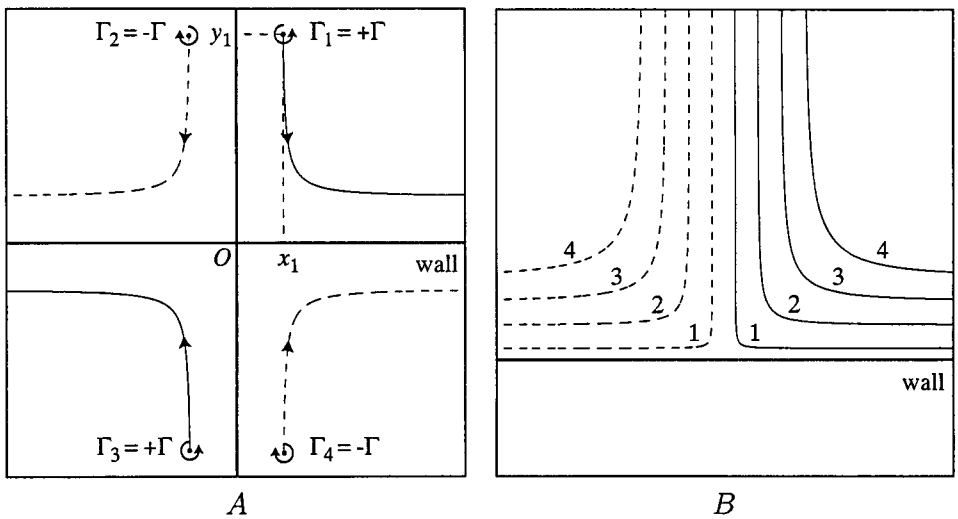

Figure 4.3: *Dipole approaching an infinite wall. Figure A shows the starting position of the two poles (Γ_1 and Γ_2 are located at (x_1,y_1) and $(-x_1,y_1)$ respectively) and their mirror images (Γ_4 and Γ_3 at positions $(x_1,-y_1)$, and $(-x_1,-y_1)$ respectively). Also the paths they describe are plotted. Figure B shows the paths of the real vortices for different starting positions. Solid lines represent the path of a positive pole, dashed lines the path of a negative pole.*

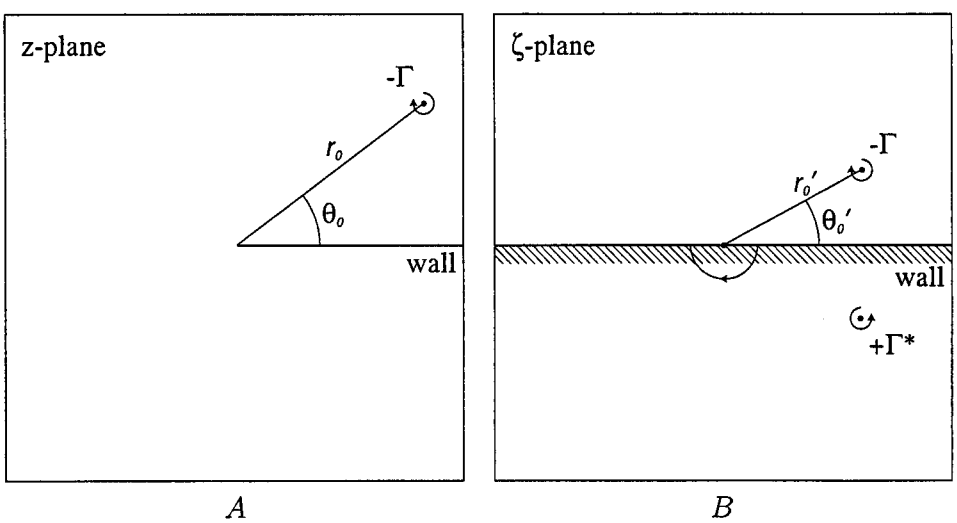

Figure 4.4: *Monopole near a semi-infinite wall, in the z-plane (figure A) and in ζ-plane (figure B), $r_0' = r_0^{1/2}$ and $\theta_0' = \theta_0/2$*

the Hamiltonian in the ζ-plane. The Hamiltonian H_z in the z-plane can now be calculated using (see Saffman [14], 1992)

$$H_z(\zeta_v) = H_\zeta(\zeta_v) + \frac{\Gamma^2}{4\pi} \ln |\frac{\partial z}{\partial \zeta}|_{(\zeta=\zeta_v)}. \tag{4.15}$$

Since $\eta_v = r' \sin(\theta'_v)$ and $|\partial z/\partial \zeta| = 2r'$ equation (4.15) can be written as

$$H_z(\zeta_v) = \frac{\Gamma^2}{4\pi} \ln(4{r'_v}^2 \sin(\theta')). \tag{4.16}$$

The pole will start to move in the z-plane following isolines of the Hamiltonian H_z which are described with

$$r_v \cdot \sin(\theta_v/2) = \text{const} \tag{4.17}$$

these paths are shown in figure 4.5 A. Transformed back to the ζ-space the paths are described by

$${r'_v}^2 \cdot \sin(\theta'_v) = \text{const}, \tag{4.18}$$

as is shown in figure 4.5 B. It is clear that the vortex in the ζ-plane does not move in a straight line. This is surprising since two poles of equal but opposite strength (the real and the image vortex) move in a straight line parallel to the wall. This strange behaviour was described first by Routh in 1881. He noted that singularities in a flow can be mapped conformally but only at a fixed instant. If at the position of the singularities a velocity is induced, for example by a mirror vortex, the singularity will describe a trajectory which can not be transformed the way constant potential lines are, Karweit, 1975 [15]. Therefore the path of a singularity may not be mapped conformally.

4.2.3 Two poles of unequal strength in absence of a wall

In the case when the dipole approaches a *no-slip* wall secondary vorticity will be generated at the wall while the two poles move away from each other (see section 4.2.1). Part of the secondary vorticity will form a vortex and merge with the original pole to form a new dipolar structure. The secondary vorticity vortex is less intense and the two vortices will not move in a straight line. In this section the paths of the two poles are calculated while ignoring the influence of the wall.

Again the vortices are considered to be point vortices. In figure 4.6 the situation is shown, two vortices of strength Γ_a and Γ_b at a distance d apart. Both poles induce a velocity at the position of the other pole. This velocity is perpendicular to the line connecting the poles, therefore the distance d between the poles remains constant. The two poles will move in circular paths with radii r_a and r_b around a point O. The induced velocities are:

$$v_a = \frac{\Gamma_b}{2\pi(-d)}, \quad v_b = \frac{\Gamma_a}{2\pi d}. \tag{4.19}$$

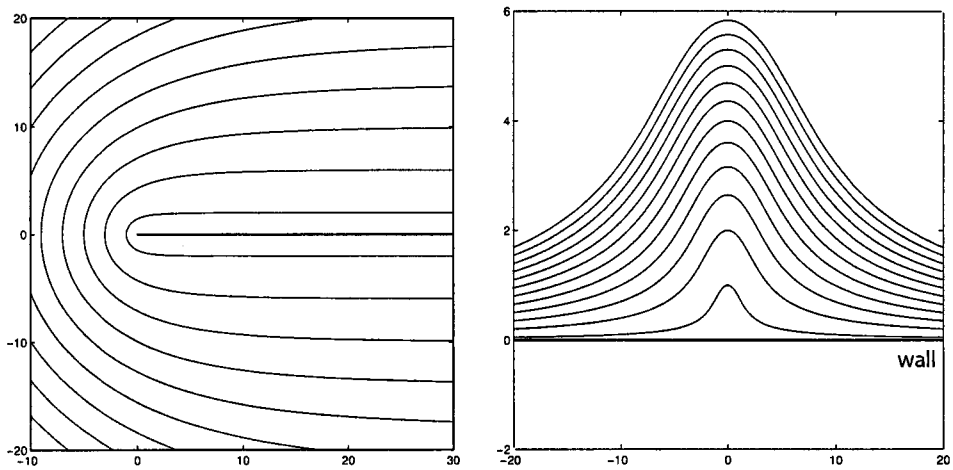

Figure 4.5: *Paths of a monopole near a semi-infinite wall, both in the z-plane (figure A) and in the ζ-plane (figure B).*

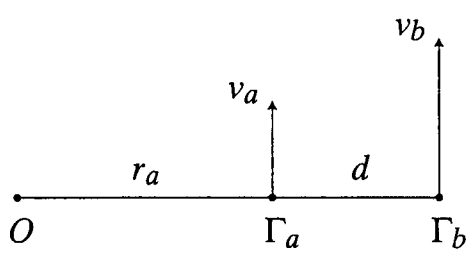

Figure 4.6: *Two opposite signed point vortices a distance d apart rotating around a common centre O.*

Since the angular velocity Ω around point O of the two poles is the same

$$\Omega = \frac{v_a}{r_a} = \frac{v_b}{r_b} \tag{4.20}$$

an equation for the radii of the paths of the poles can be derived:

$$r_b = \frac{d\,\Gamma_a}{\Gamma_a + \Gamma_b} \quad \text{and} \quad r_a = r_b - d. \tag{4.21}$$

The potential models derived in the previous section will be used in chapters 5, 6 and 7 to explain the paths of the poles as observed in numerical simulations and experiments.

Chapter 5

Numerical simulations

5.1 General descriptions

5.1.1 Starting conditions

The numerical code used to perform simulations solves the time dependent incompressible Navier-Stokes equation. The numerical code is based on the code as described in Verzicco *et al.* [16]. The Calculations were performed on a square domain in which a wall and a Lamb dipolar vortex are positioned. The length of the domain is 20 times the radius of the Lamb dipolar vortex (a from equation (2.17)), a is also the length scale used to make all other distances dimensionless. A schematic overview of the numerical domain, defined as $\{0 \leq x \leq 20,\ 0 \leq y \leq 20\}$, is shown in figure 5.1. The centre of the dipolar vortex at $t = 0$ is at (10,10). The wall is at $x = 6$ while the length of the wall is varied. The offset D is the distance from the straight path of the dipole to the top of the wall. This distance is non-dimensionalized by scaling it with the radius a of the dipole:

$$\delta \equiv \frac{D}{a} \tag{5.1}$$

with δ the dimensionless offset.

The resolution used for the numerical simulations is 401 $\times$ 401 grid points. The grid is not equidistant but is denser near the wall. To make sure that this resolution is high enough to get good results some simulations were repeated at a 301 $\times$ 301 grid. The results were essentially the same. Still the higher resolution was chosen as a good compromise between resolution for analysis and machine time.
All simulations were performed at Reynolds number Re = 1000. Some simulations were repeated at different Reynolds numbers (between Re = 100 and Re = 4000) but the evolution of the vortex remained the same. The dimensionless offset δ was varied between 3.0 and -4.0 in steps of 1.0, also simulations were performed at $\delta = 0.5$ and $\delta = -0.5$.

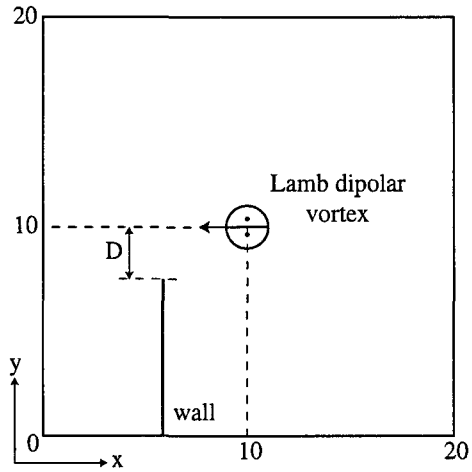

Figure 5.1: *Schematic overview of the starting conditions of the numerical simulations. The distance* D *was varied.*

5.1.2 Generation of secondary vorticity

As the dipolar vortex approaches the wall it induces a flow near the wall, which results in a boundary layer due to the no-slip condition. In this boundary layer secondary vorticity is generated as explained in section 2.4. In general there are four different possibilities, depending on the flow near the wall: these are shown in figure 5.2. The vorticity can be positive or negative, depending on the direction of the main flow. The sign of the vorticity follows directly from equation (2.15). In case of a main flow in x-direction at the top of the wall there are two possibilities; if the flow is in negative x-direction ($U < 0$)

$$\frac{\partial u}{\partial y} < 0 \tag{5.2}$$

and positive secondary vorticity is generated (figure 5.2 A). On the other hand, if $U > 0$,

$$\frac{\partial u}{\partial y} > 0 \tag{5.3}$$

the secondary vorticity is negative (figure 5.2 B). In this way also the sign of the secondary vorticity at the wall due to a flow with velocity v in y-direction can be explained, here for the right side of the wall. If the velocity of the main flow $V > 0$ the secondary vorticity is also positive since

$$\frac{\partial v}{\partial x} > 0, \tag{5.4}$$

as is shown in the upper part of figure 5.2 C. If the velocity is in opposite direction ($V < 0$) the sign of the gradient also changes sign, i.e.:

$$\frac{\partial v}{\partial x} < 0 \tag{5.5}$$

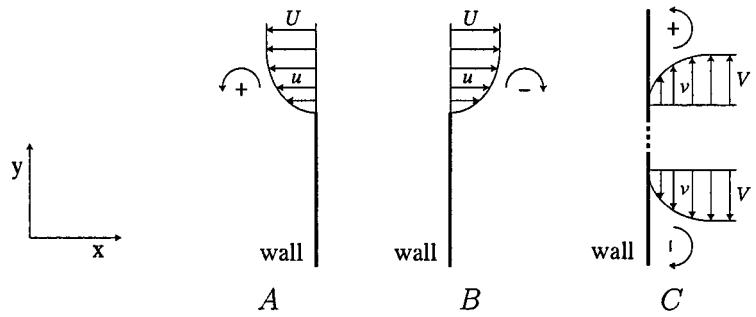

Figure 5.2: *Schematic overview of the secondary vorticity produced at the wall due to the no slip condition. Figures A and B show the secondary vorticity generation at the top of the wall due to a flow U in the x-direction. The last figure (C) gives the vorticity generation due to a flow V in y-direction. In both cases the generated vorticity can be either positive or negative depending on the direction of the flow.*

and thus negative secondary vorticity is generated (see figure 5.2 *C*, lower velocity profile). At the left side of the wall the generated secondary vorticity has the opposite sign for a main flow in the same direction. The vorticity at the top of the wall can be advected by the main flow. Also the vorticity sheet at the wall may detach according to the process described in paragraph 2.5.

5.1.3 Influence of the offset on the evolution of the dipolar vortex

The trajectories of the two poles of the dipolar vortex depend strongly on the offset; generally there are four different possibilities. The wall can be far away from the dipole, the offset is large, and therefore it has no influence on the path of the dipolar vortex. It will move in a straight line, an example is described in subsection 5.2.1.
If the path of the dipole is closer to the wall its path will be influenced. Secondary vorticity is generated at the top of the wall and this will interact with the pole closest to the wall. The latter will lose some vorticity to the secondary vorticity patch. This results in a deflection of the path of the dipole away from the wall. This is described in more detail in subsection 5.2.2.
It is also possible that the two poles of the dipolar vortex are split in two separate monopolar vortices. The secondary vorticity that is generated at the wall merges with the two now separated poles and two new dipoles are formed as set out in subsection 5.2.3. Since the original poles are much stronger than the newly formed poles the dipoles describe a curved path.
If the wall is completely blocking the path of the dipole, corresponding to a large negative offset, the two newly formed dipoles will be symmetrical. This was described by Orlandi in 1990 [2] and shown here in subsection 5.2.4.

5.2 Detailed description for four different offsets

5.2.1 Offset $\delta = 3.0$

As described above the path of the vortex is not influenced by the wall in this case. In figure 5.3 the time evolution of the vorticity distribution of a Lamb dipolar vortex is shown. Figure 5.4 shows the velocity close to the wall. At $t = 1$ the dipolar vortex approaches the wall and at the top of the wall negative vorticity is produced due to a flow in positive x-direction. This is the same situation as shown in figure 5.2 B. As the dipole moves closer to the wall ($t = 3$) more negative vorticity is generated. This patch of negative vorticity is advected to the right and induces a velocity in positive y-direction at the right side of the wall. This flow also generates positive secondary vorticity, which is advected to the top of the wall where it separates and moves with the flow to the right. The dipole is now ($t = 4$) above the wall and more vorticity is generated which gathers in an irregular patch of both positive and negative vorticity. At $t = 5$ the dipolar vortex has moved past the wall. The irregular patch evolves into more organised patches of positive and negative vorticity due to the inverse energy cascade typical for two-dimensional flows. This becomes more clear at $t = 7$ where a dipolar structure has formed with a single negative vortex and two patches of positive vorticity. This structure still induces a flow next to the wall in positive y-direction and positive vorticity continues to be generated. Finally at $t = 9$ a clear dipolar vortex has emerged from the chaotic patch of vorticity. It moves in a curved path back to the wall because the negative pole is more intense than the positive. The original dipolar vortex has continued to move in a straight line.

5.2.2 Offset $\delta = 1.0$

The path of the dipole is now closer to the wall and the trajectory is no longer a straight line. The vorticity plots of the dipolar vortex at different moments are shown in figure 5.5, while the velocity close to the wall is shown in figure 5.6. At $t = 1$ the dipole has moved from the starting position towards the wall. The main flow above the wall is in negative x-direction, this in contrast to the flow in positive x-direction at an offset of 3 (described in subsection 5.2.1). A patch of positive vorticity is generated at the top due to this flow. At $t = 3$ the dipolar vortex has moved closer to the wall. The flow above the wall is still in negative x-direction and the strength of the secondary vorticity patch increases. Also the main flow advects the vorticity patch to the left. At the right side of the wall the flow is in downward direction and negative secondary vorticity is generated. The next frame is at $t = 4$, when the original dipolar vortex is right above the wall. The positive secondary-vorticity patch merges with the original positive-vorticity pole. The negative secondary vorticity has moved to the top of the wall due to the mirror principle explained in section 2.3, and the velocity above the wall is now in positive x-direction. Therefore negative vorticity is generated. This vorticity patch strips off some of the vorticity of the positive pole of the original vortex as is clear at $t = 5$. Since the negative pole of the dipole is not influenced it is now stronger than the positive pole. The dipole will move

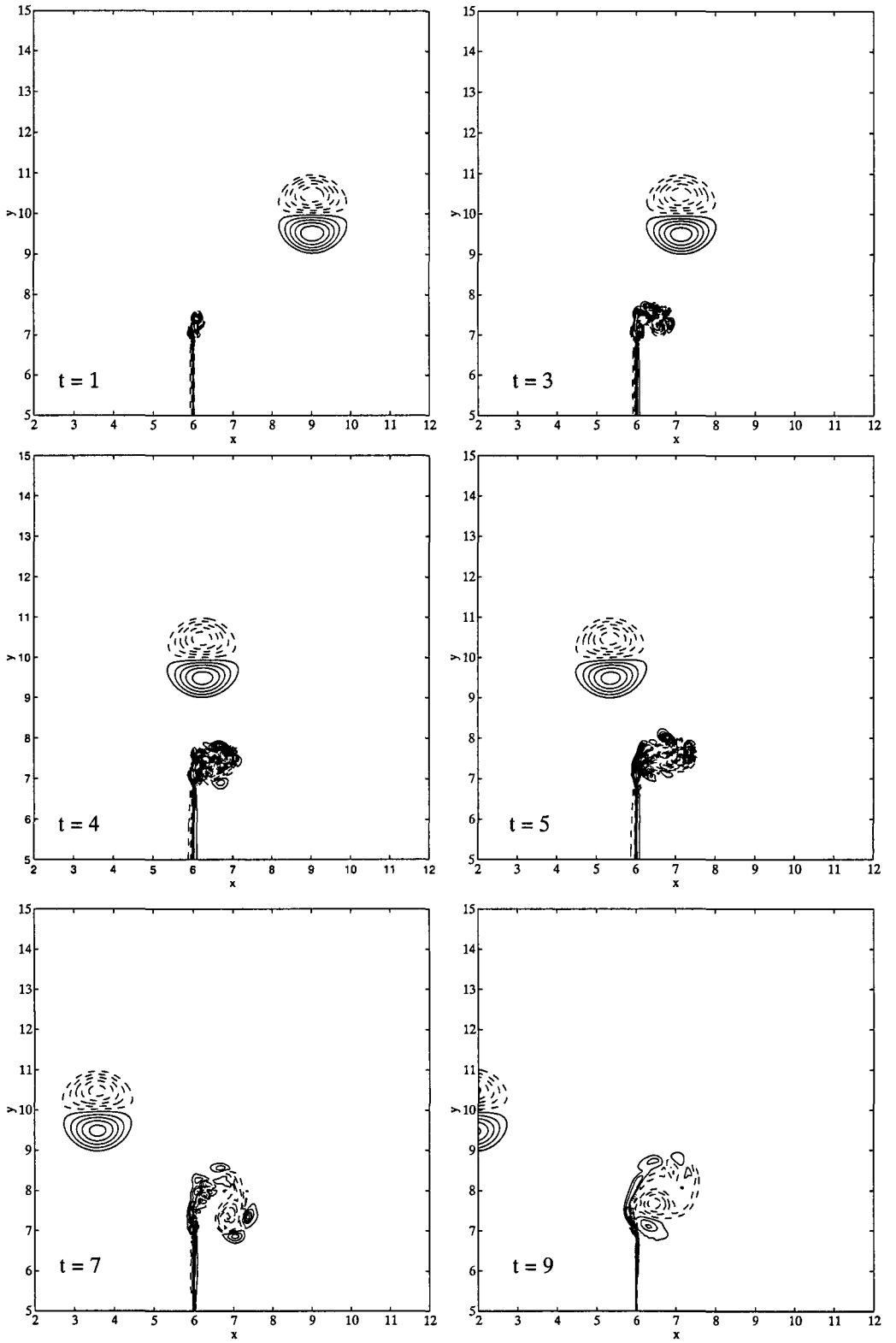

Figure 5.3: *Vorticity contour plots of a dipolar vortex approaching the wall. At* $t = 0$ *the offset is* $\delta = 3.0$. *Dashed lines indicate negative vorticity while solid lines represent positive vorticity.*

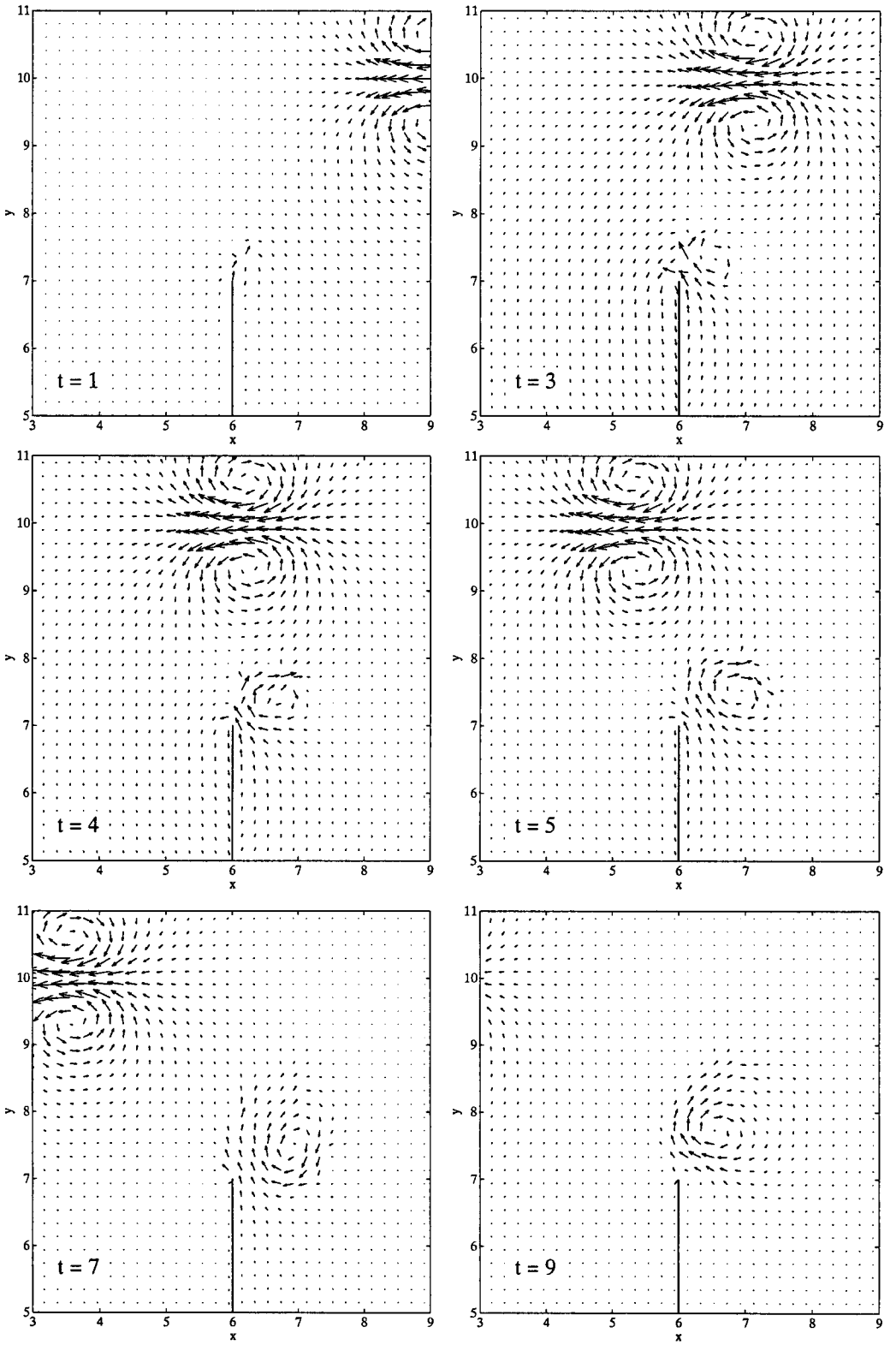

Figure 5.4: *Velocity plots of the same numerical simulation as used in figure 5.3. Only the area around the wall is shown.*

in a curved path as is visible at $t = 7$ and $t = 9$. The disorganised patch of secondary vorticity and original positive vorticity at the right of the wall organises into a dipolar vortex which moves towards the wall because the negative pole is more intense. There the dipolar vortex splits: the negative pole moves up while the positive patch moves down. Again due to these vortices secondary vorticity is generated and new dipolar structures are formed.

5.2.3 Offset $\delta = 0.0$

Here the wall is right in front of the lower, positive, pole of the dipolar vortex. The first two frames from figures 5.7 and 5.8, $t = 1$ and $t = 3$, are comparable to the first frames of the situation described in subsection 5.2.2. Here too positive vorticity is generated at the top of the wall while negative vorticity is generated at the right hand side of the wall. However, at $t = 4$ the situations are no longer comparable. Now the original positive pole collides with the wall while the negative pole remains above the wall. Still, due to the flow around the wall secondary vorticity is generated, both positive (at the top) and negative (at the right side). In the next frame, $t = 5$, the dipole really splits up, the negative pole moves in upward direction while the positive pole moves in downward direction. The negative pole forms a new dipolar structure with the positive secondary vorticity and the positive pole with the negative secondary vorticity. In both cases the original pole is more intense than the newly formed poles. This becomes more distinct at $t = 7$ and $t = 9$ where the curved path of the two new dipoles becomes apparent. Production of vorticity at the top and side of the wall continues.

5.2.4 Offset $\delta = -4.0$

With this offset the wall blocks the the path of the dipole completely, neither pole of the dipolar vortex will move past the wall. Also since the top of the wall is far from the dipole (at a distance $4a$) it does not have any influence on the collision behaviour. As will become clear, the collision is symmetrical in the line $y = 10$. Figures 5.9 and 5.10 are used to explain evolution of the collision. At $t = 1$ the dipolar vortex has moved towards the wall and induces a velocity at the right-hand side. Since the dipole is not too close to the wall, at a distance of about $3a$, times the radius of the dipole, the influence of the top is still noticeable. Figure 5.10 shows that the absolute velocity at the wall is smaller for $y > 10$ than it is for $y < 10$. However, the velocity is small in both cases and not much secondary vorticity is generated. The next frame, $t = 3$, already shows a more symmetrical velocity distribution at the wall. The secondary vorticity at the wall is positive for $y > 10$ and negative for $y < 10$, as explained in figure 5.2. At $t = 4$ the dipole collides with the wall and the velocity profile at the wall is completely symmetrical. Since the velocities at the wall in the previous, asymmetrical, frames are much smaller than the velocity at $t = 4$ the influence of the asymmetry on the amount of generated secondary vorticity is negligible. Now two patches of vorticity are visible at the wall near the vortex. In the next frame, $t = 5$, the two original poles merge with the secondary vorticity patches and start

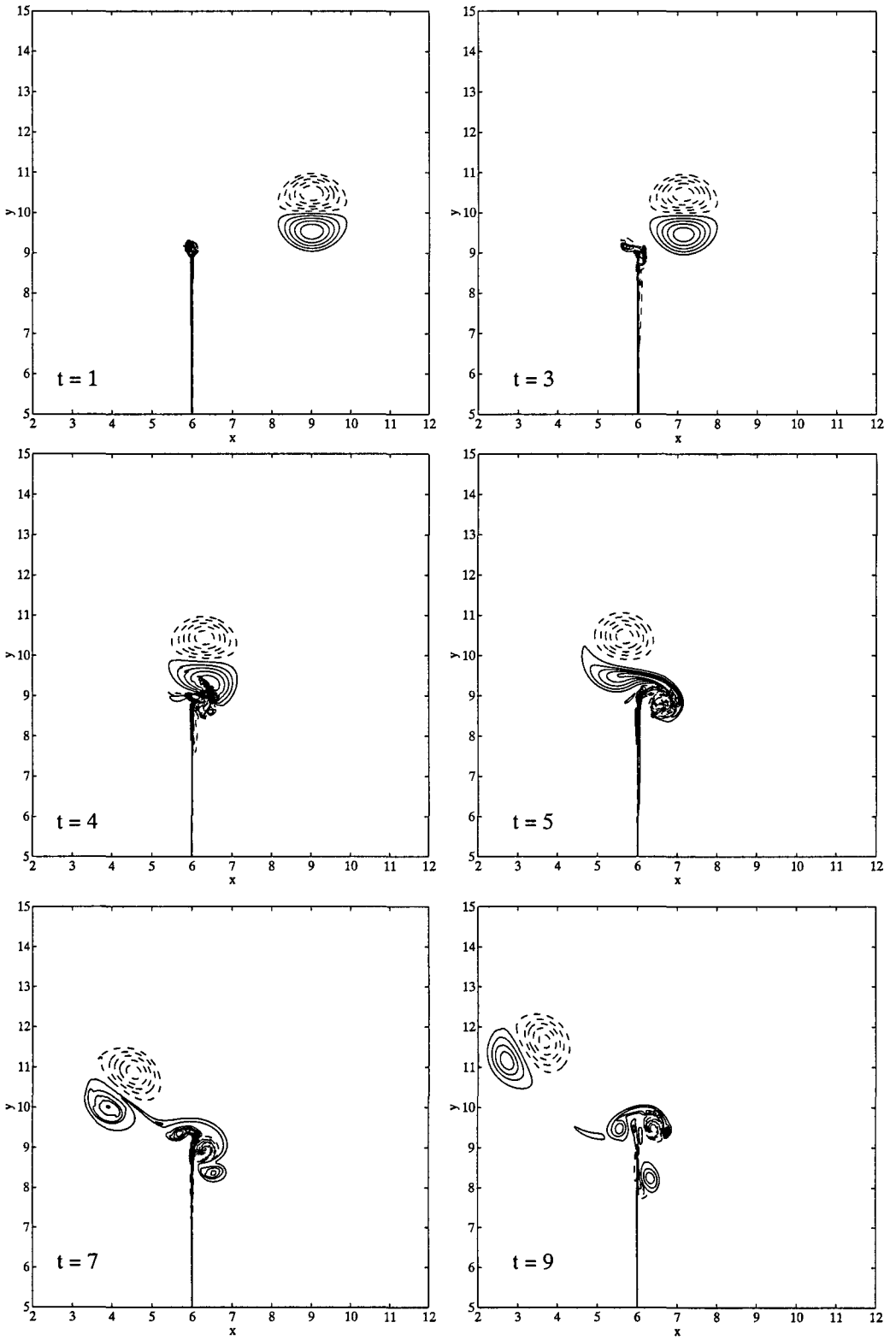

Figure 5.5: *Vorticity contour plots of a dipolar vortex approaching the wall. At* $t = 0$ *the offset is* $\delta = 1.0$. *Dashed lines indicate negative vorticity while solid lines represent positive vorticity.*

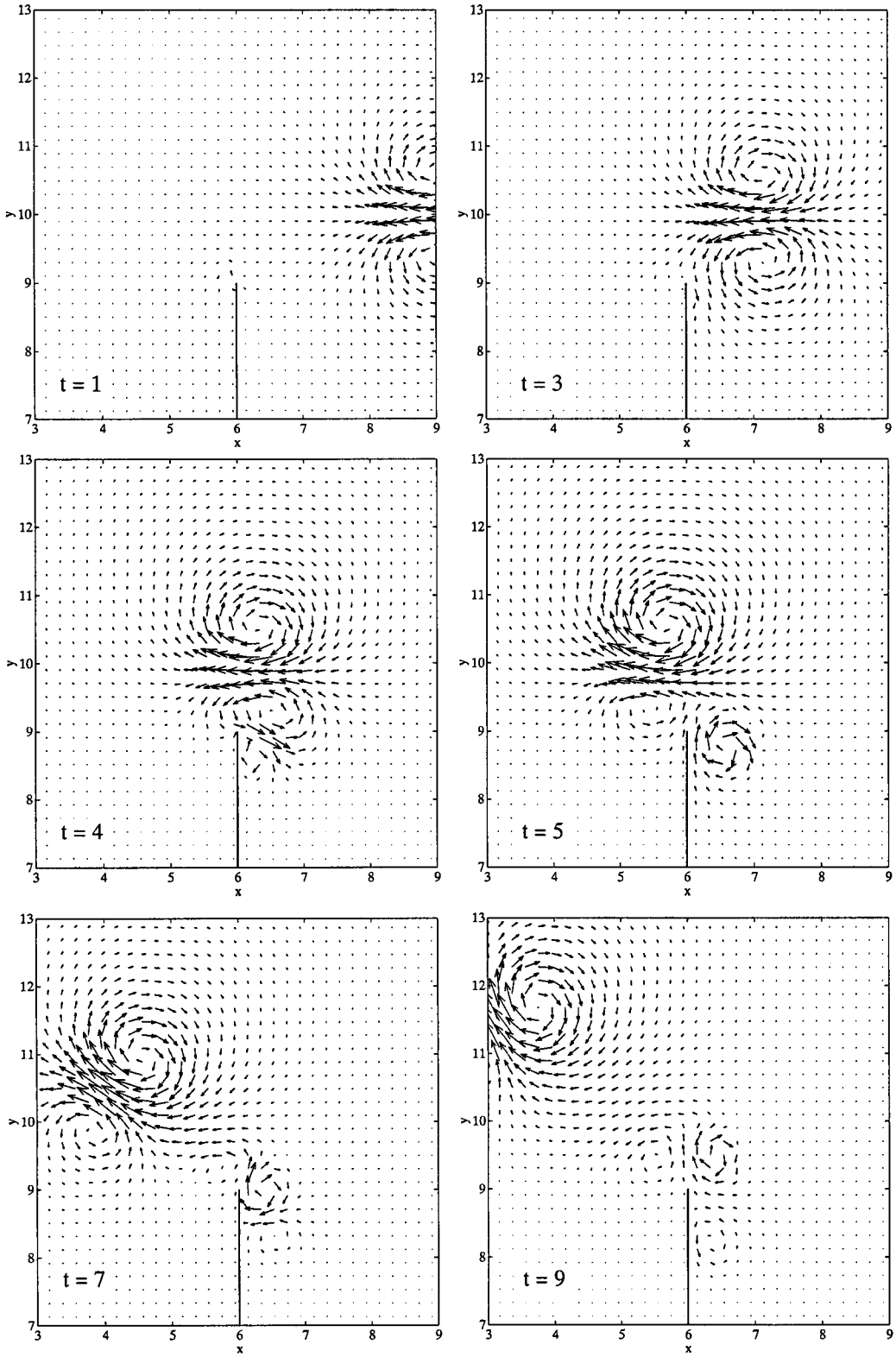

Figure 5.6: *Velocity plots of the same numerical simulation as used in figure 5.5. Only the area around the wall is shown.*

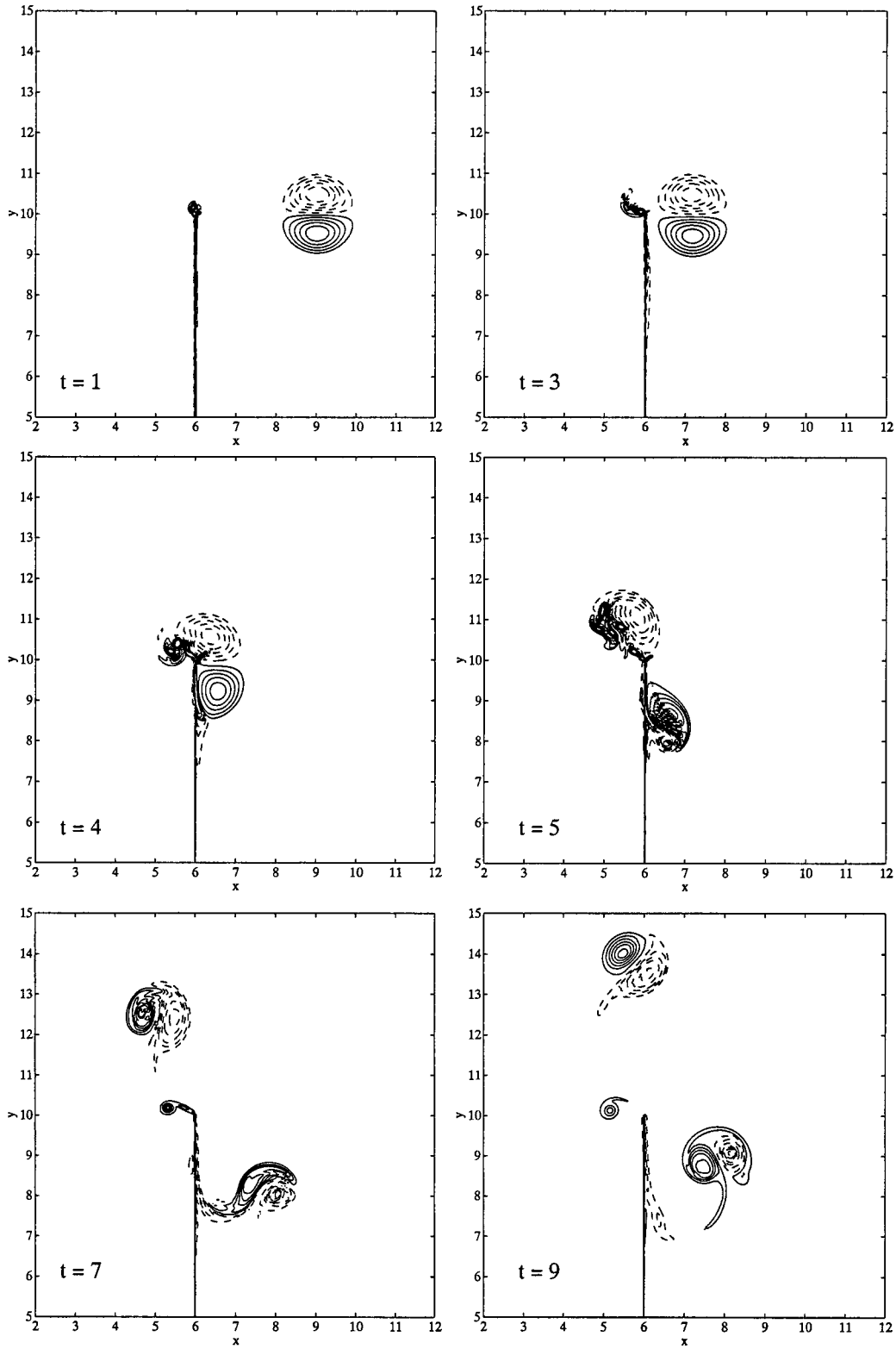

Figure 5.7: *Vorticity contour plots of a dipolar vortex approaching the wall. At* $t = 0$ *the offset is* $\delta = 0.0$. *Dashed lines indicate negative vorticity while solid lines represent positive vorticity.*

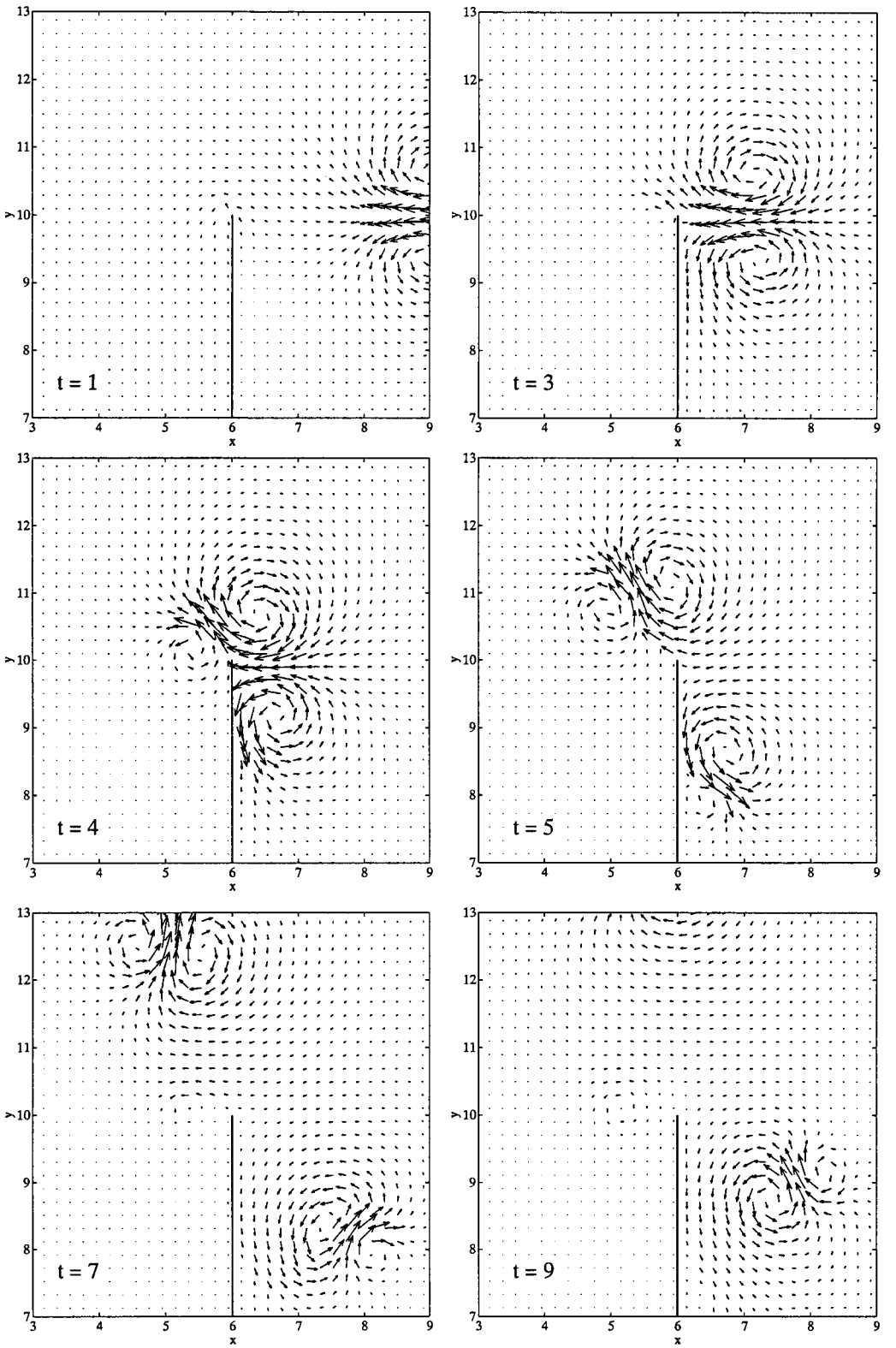

Figure 5.8: *Velocity plots of the same numerical simulation as used in figure 5.7. Only the area around the wall is shown.*

moving away from the wall. The frames at $t = 7$ and $t = 9$ show that again the original vortices are more intense than the secondary vorticity patches since the two dipoles move in a curved path. Still secondary vorticity is generated at the wall. The last frame shows clearly the symmetrical paths of both dipolar vortices. If the offset becomes even more negative, i.e. $\delta < 4$, the behaviour will remain the same.

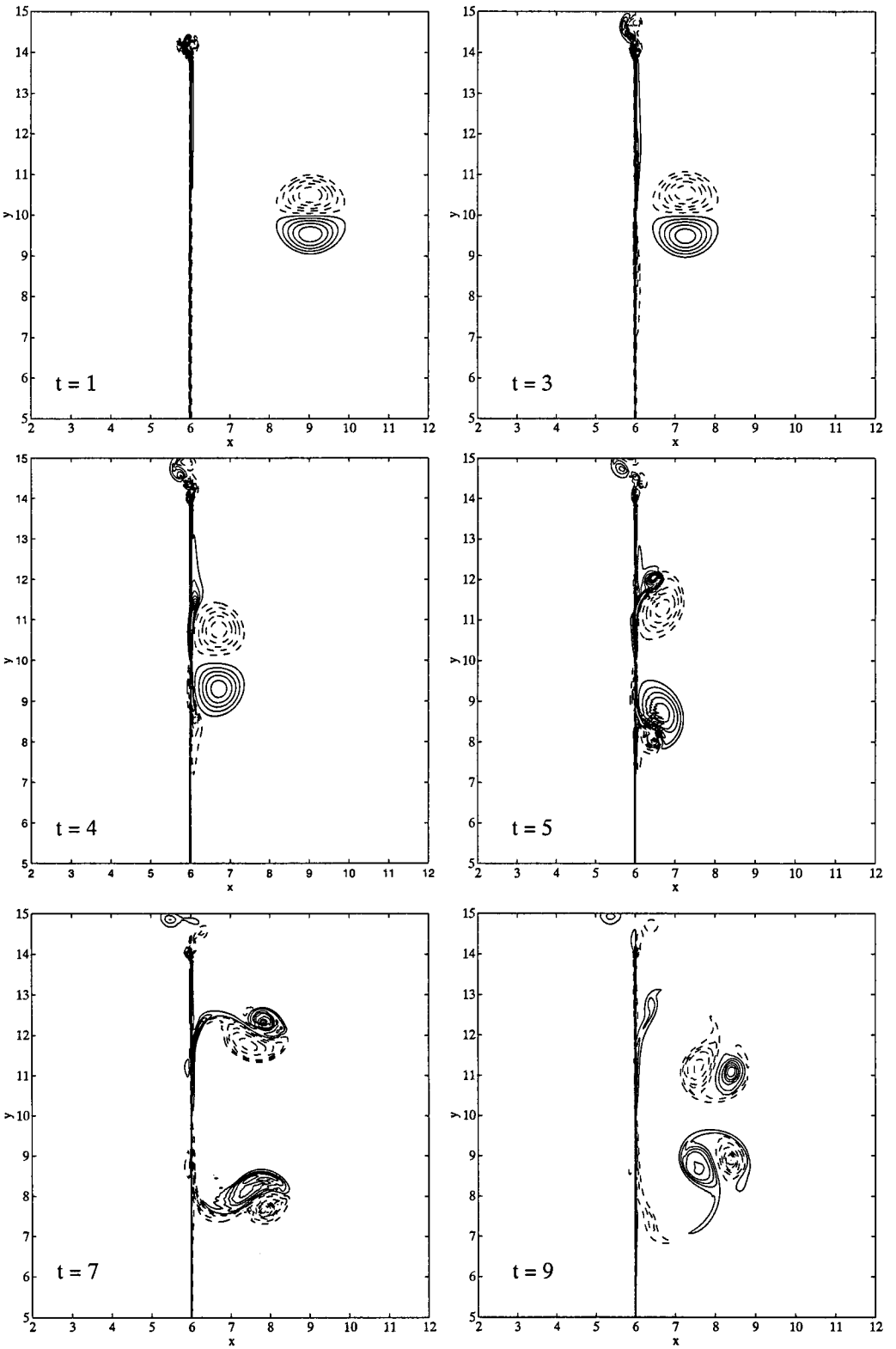

Figure 5.9: *Vorticity contour plots of a dipolar vortex approaching the wall. At* $t = 0$ *the offset is* $\delta = -4.0$. *Dashed lines indicate negative vorticity while solid lines represent positive vorticity.*

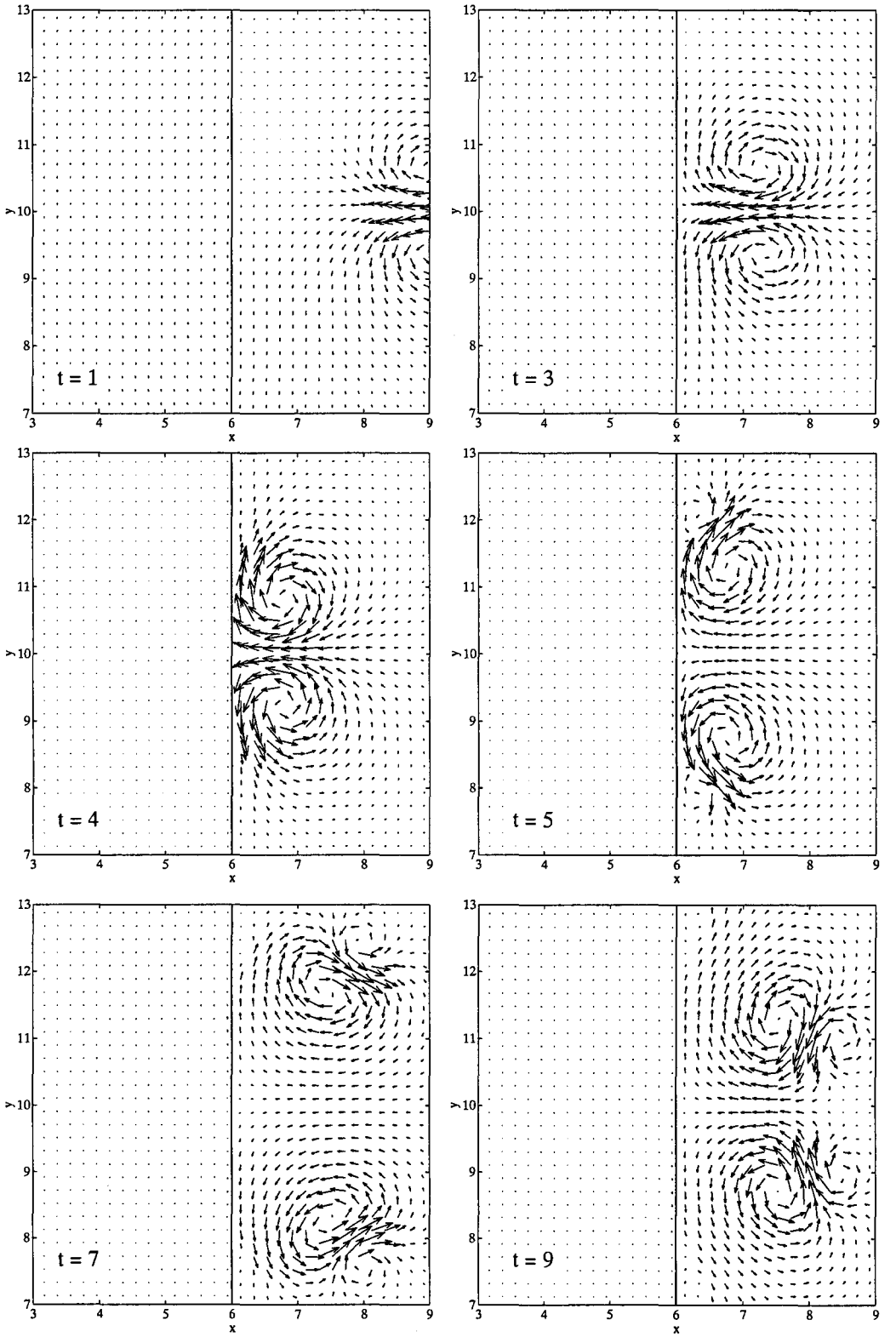

Figure 5.10: *Velocity plots of the same numerical simulation as used in figure 5.9. Only the area around the wall is shown. The top of the wall is at* $y = 14$.

5.3 Results and analysis

5.3.1 Paths of the original and secondary vortices

As shown in the previous section there are four general possibilities for the dipole to behave, depending on the offset δ. In figures 5.11 en 5.12 the paths of the two poles of the dipolar vortex are shown together with some newly formed secondary vorticity poles. These plots are contours of the vorticity at different times plotted in one graph and therefore indicate the evolution of the vortices. The contour was chosen such that it indicates a vorticity equal to $0.70\hat{\omega}$, with $\hat{\omega}$ being the maximum vorticity at $t = 0$.

At offset values $\delta = 3.0$ and $\delta = 2.0$ the dipolar vortex moves in a straight path; for $\delta = 3.0$ it is not influenced by the wall at all. For $\delta = 2.0$ it moves in downward direction, since the middle of the two poles is not at $y = 10$ anymore at $t = 9$. This difference is so small, however, that the dipolar vortex at this offset is considered to be unaffected by the presence of the wall. Secondary vorticity is generated at the top of the wall, it is remarkable that this vorticity is more intense at an offset $\delta = 3$ than it is at $\delta = 2$. It may be expected that the smaller the offset the higher the velocity near the wall and thus more secondary vorticity is generated. Further investigation is needed to explain this difference. At smaller offsets, i.e. $\delta = 1.0$ and $\delta = 0.5$, the positive pole, which is closest to the wall, loses some vorticity to the negative secondary vorticity generated at the right side of the wall. This results in a curved path since the two poles are no longer of equal strength. It was expected that the radius of the dipolar vortex moving away from the wall in case of $\delta = 1.0$ is larger than if $\delta = 0.5$. This conjecture is based on the assumption that for larger offsets less vorticity is removed from the positive pole, therefore the intensities of the two poles are less different resulting in a more straight path. However, this is not what is seen in figure 5.11, the radius of the path of the dipolar vortex is *smaller* for $\delta = 1.0$ than it is for $\delta = 0.5$. This can be explained using figure 5.13. If $\delta = 1.0$ the velocity just above the wall is in positive x-direction. Therefore negative vorticity is generated, this will strip off some of the positive vorticity (as seen in figure 5.5, at $t = 5$) thereby making the positive pole less intense. If $\delta = 0.5$ the velocity at the right side of the wall is still in negative y-direction, thus here too negative vorticity is generated. This will also strip off some of the vorticity of the positive pole. However, the velocity at the top of the wall is in negative x-direction and generates positive secondary vorticity, which will merge with the remains of the original positive pole, thus making it more intense. This increase in vorticity compensates for the larger loss of vorticity due to smaller offset.
Then at offsets $\delta \leq 0$ the two poles split and each merges with secondary vorticity patches to form a new dipolar structure. Figure 5.11 and 5.12 show the paths of these dipolar vortices. The radius of the path of the dipolar structure containing the original negative vortex becomes smaller as the offset becomes more negative.
At $\delta = -3.0$ the paths of the two newly formed dipolar vortices are symmetrical.

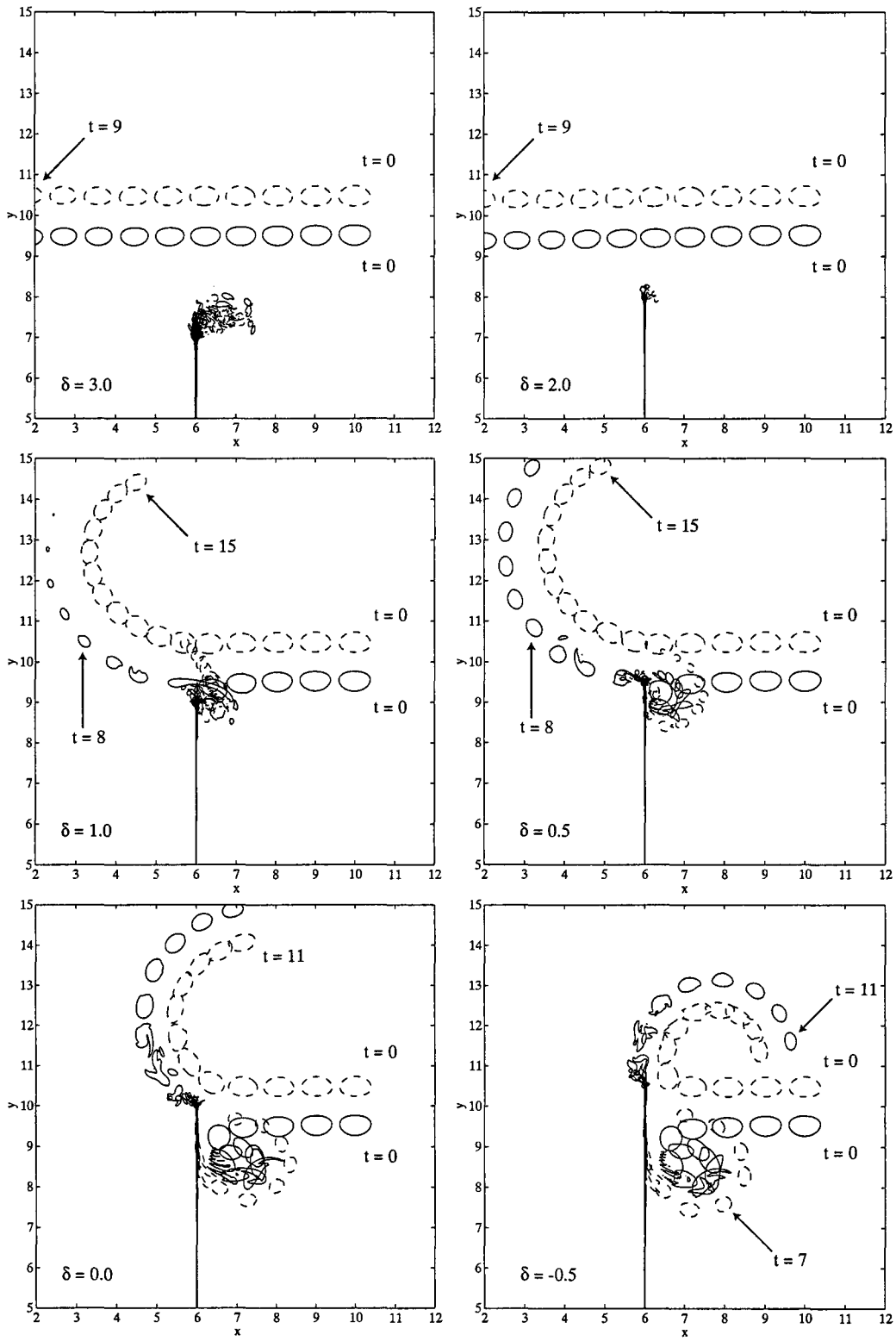

Figure 5.11: *Vorticity contour plots, the contour is drawn at* $0.70\hat{\omega}$. *The offset is varied between* $\delta = 3$ *and* $\delta = -0.5$. *Dashed lines indicate negative vorticity while solid lines represent positive vorticity.*

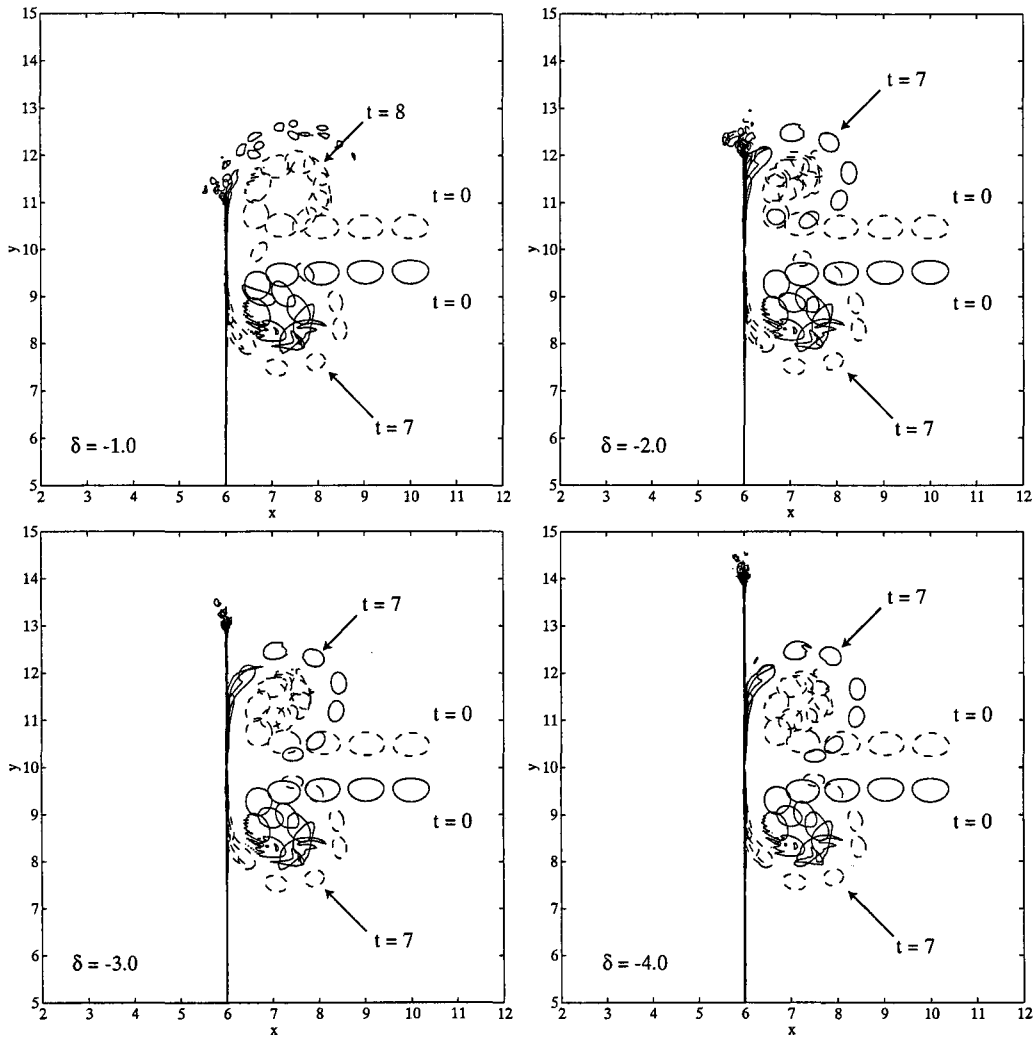

Figure 5.12: *Same as figure 5.12 except that the offset is varied between* $\delta = -1.0$ *and* $\delta = -4.0$.

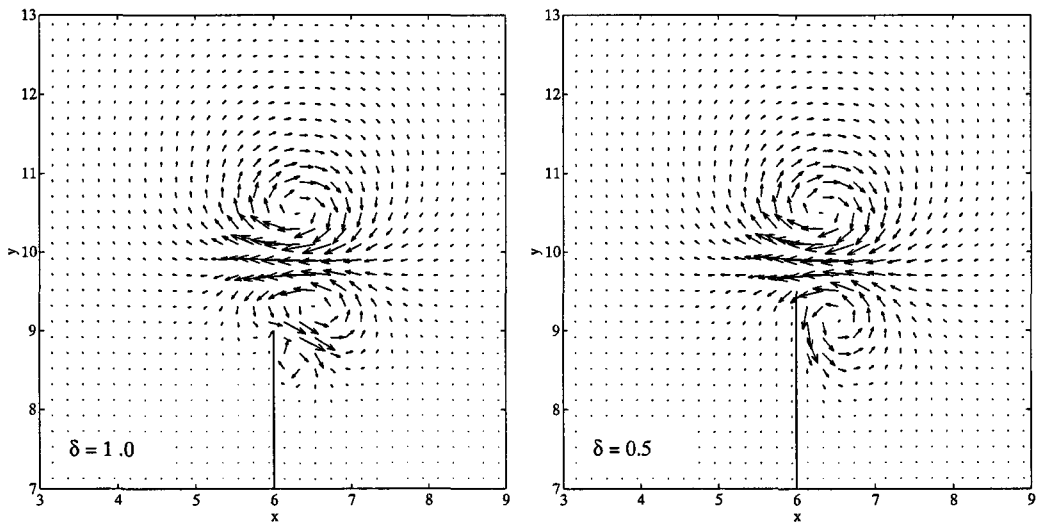

Figure 5.13: *Velocity plots showing the velocity at the top of the wall for offsets* $\delta = 1.0$ *and* $\delta = 0.5$ *at* $t = 4$. *The velocityplot at the top of the wall in the latter figure shows a clear main stream in negative x-direction. The flow with* $\delta = 1.0$ *does not have such a main stream directly above the wall.*

5.3.2 Path of the original negative vortex: a comparison with potential theory

In this section a comparison is performed between the potential model describing the circular paths of two poles of unequal strength (as explained in subsection 4.2.3) and the trajectories of the vortices of the numerical simulations. Only the dipolar structure containing the negative original pole is investigated since the other dipole (for $\delta \leq 0.0$) behaves the same as the dipole described here in case of $\delta = -4.0$.

The ratio of the strengths (circulation) of the two poles of a dipolar vortex, Γ_r, is defined as

$$\Gamma_r = \frac{\Gamma_o}{\Gamma_s} \tag{5.6}$$

with Γ_o the circulation of the original negative pole and Γ_s the circulation of the positive pole. Since the original pole is always more intense than the pole containing secondary vorticity $\Gamma_r \leq -1$. This (Γ_r) is a characteristic property of any dipole and using equation (4.21) the radii of the two poles of a dipolar *potential* vortex can be written in terms of Γ_r:

$$r_o = \frac{-d}{\Gamma_r + 1} \quad \text{and} \quad r_s = \frac{d\Gamma_r}{\Gamma_r + 1} \tag{5.7}$$

Table 5.1: *Calculated circulation depending on the threshold value used to separate the vortex from its surroundings. All determined for* $\delta = 0.0$ *at* $t = 9$.

threshold ($\times MSV_{t=0}$)	Γ_o	Γ_s	Γ_r
0.5	-5.41	3.97	-1.36
1.0	-5.23	3.90	-1.34
2.0	-4.91	3.69	-1.33
3.0	-4.54	3.46	-1.31
5.0	-3.77	2.94	-1.28

with d the distance between the two centroids of the poles and r_o and r_s the radii of the paths of the original negative pole and the positive pole, respectively.

The circulation of a pole can be calculated as an integral of the vorticity, see equation (2.37). To do this a program was used which determines patches where the absolute value of the vorticity is larger than a certain threshold value scaled with the mean squared value of the vorticity at $t = 0$ ($MSV_{t=0}$). The threshold was chosen such that it is as small as possible without including long filaments or protrusions which do not contribute to the dynamics of the system. One example is shown in figure 5.14: it is obvious that the threshold value chosen in figure B is too low because the long tail of vorticity of the negative pole should not be used when calculating the circulation and position of the vortex. The threshold shown in figure C is much better since there the tail is excluded from the calculations. This program also calculates the position of each pole, this is the vorticity weighted average of all points inside the threshold contour, these are the same points as used to calculate the circulation.

To determine the influence of the threshold value on the circulation different values were applied to the same vorticity distribution ($\delta = 0.0$, $t = 9$). The results are shown in table 5.1. It is clear that although the absolute values for the two poles decrease (as is expected) the ratio Γ_r remains approximately the same. Since the threshold at $5.0 \times MSV_{t=0}$ is never used the difference is smaller than 4 %. Also the time evolution of Γ_r is determined. From $t = 7$ to $t = 10$ it varies between 1.37 and 1.35, this is a difference of less than 2 %. Therefore Γ_r is considered to remain constant after the collision. All calculated Γ_r have, unless noted otherwise, an uncertainty of $\pm$ 5 %.

In each simulation first the circular path was drawn based on the values as calculated in the procedure described above. If these paths did not match the results from the simulations adjustments to the calculated values of the positive pole were applied. The radius of the paths can be changed by varying the ratio of the strengths, Γ_r, or the distance d between the poles, see equation (5.7). Here the distance d was kept constant and Γ_r was varied. This is done first, then, with the radii corrected, the position of the positive pole

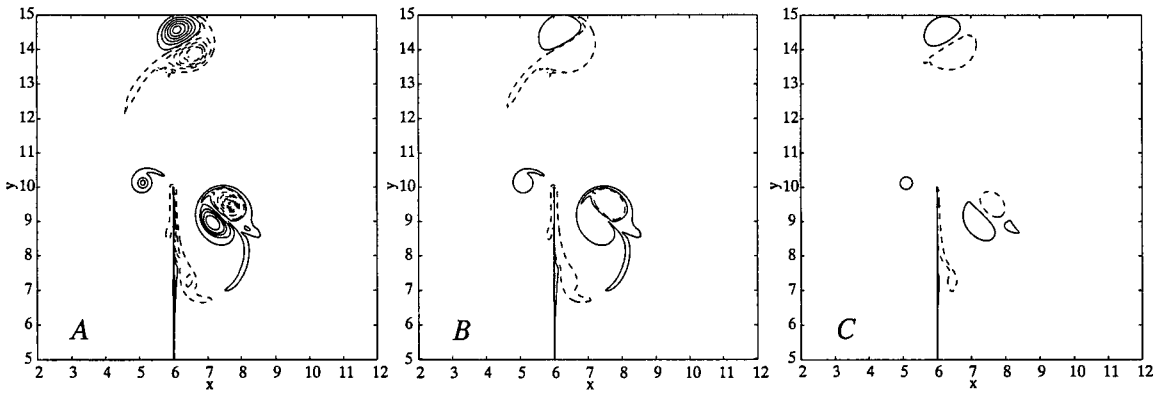

Figure 5.14: *Contour plots of the vorticity for* $\delta = 0$ *at* $t = 10$ *(figure A). Figure B and C only show the contour at one single value of vorticity, at* $0.5 \times MSV_{t=0}$ *respectively* $2.0 \times MSV_{t=0}$. *It is clear that a threshold at* $2.0 \times MSV_{t=0}$ *for the top dipole is much better than one at* $0.5 \times MSV_{t=0}$ *since the long tail in the latter case (figure B) does not contribute to the dynamics of the dipole but it does influence the calculated position and strength of the negative pole.*

is adjusted to compensate for possible tilts in the circular paths. During this repositioning the distance d is kept constant. This is done until an optimal position for the positive pole is found.

Figure 5.15 shows an example of a comparison between the potential model and the results from a numerical simulation ($\delta = 0.5$). The paths of the two poles were determined based on the calculated original values for the positions and strengths of the two vortices as well as on slightly adjusted values to get a better match with the results from the numerical simulations (figure B). The strength and positions of the poles were calculated at $t = 10$ and a threshold of $0.5 \times MSV_{t=0}$ was used, this is shown in figure 5.15 A.

The results of all calculations are given in table 5.2. It is seen that if $\delta > -1.0$ the results of the calculated paths match the results from the numerical simulations with a maximum adjustment of Γ_s of 7.7%. However, if $\delta < -1.0$ the calculated radii no longer correspond to the paths described by the numerical dipolar vortices. Figure A.2 in appendix A shows that for $\delta \leq -2.0$ the trajectories of both the positive and the negative pole can not be matched using the procedure described above. Since the radius of the trajectory of the negative pole is much smaller than the radius of the trajectory of the positive pole the latter was used to determine the optimal values for the adjusted circular path. It is clear that the match between the negative pole's trajectory and the circular path is very poor. The trajectory of the positive pole can be matched by the adjusted circular path, however for $t > 10$ the two outer poles of both dipolar vortices start influencing each other and the trajectory no longer follows the circular path.

A better result for $\delta \leq -2.0$ is obtained if not the strength of the positive pole is adjusted but if the distance d between the two poles is varied. To do this both poles are translated

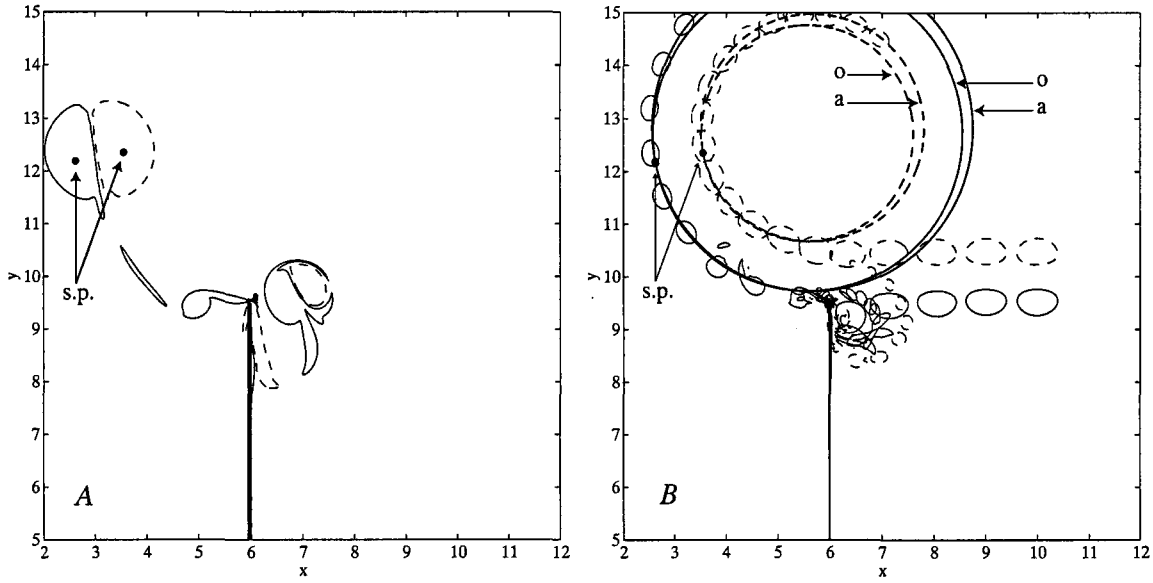

Figure 5.15: *Contour plot of the vorticity for* $\delta = 0.5$ *at* $t = 10$ *at* $0.5 \times MSV_{t=0}$ *(figure A). The centres of vorticity are indicated with dots (*s.p.*). Figure B shows the path of the vortices (same as in figure 5.11) and the calculated circular paths of a similar* potential *dipolar vortex. In both cases positive vorticity contours are indicated with solid lines and dashed contours represent negative vorticity. Four circular paths are shown, the two indicated with an* o *are calculated from the original values for the circulation and position of the poles. The two other paths (marked with an* a*) are based on the adjusted values of the position and strength of the positive pole. Again the dashed line indicates the path of the negative vortex while the solid line represents the path of the positive vortex. Also the starting positions (*s.p.*) are indicated, these are the positions of the potential vortices used to calculate the circular paths. There are two starting positions for the positive pole, one original and one adjusted, however, the two are so close together that het dots almost completely overlap.*

Table 5.2: *Calculated ratio of the strengths* (Γ_r) *and distance d for different offsets. Also shown is the adjusted value for* Γ_r *and the difference between the original and adjusted value in %. The last column gives the distance over which the position of the positive pole was moved to adjust for tilts. Appendix A shows the figures for offsets other than* $\delta = 0.5$.

offset δ	calculated Γ_r	calculated d	adjusted Γ_r	$\Delta\ \Gamma_r$ (%)	Δ position
3.0	-1.00	0.86	-1.00	0.3	0.067
2.0	-1.01	0.90	-1.00	1.3	0.081
1.0	-1.52	0.97	-1.52	0.2	0.058
0.5	-1.46	0.95	-1.44	1.6	0.038
0.0	-1.27	0.78	-1.27	0.0	0.016
-0.5	-1.50	0.69	-1.57	-4.6	0.000
-1.0	-1.83	0.69	-1.97	-7.7	0.000
-2.0	-2.04	0.73	-4.40	-115.4	0.290
-4.0	-1.86	0.73	-3.54	-90.7	0.145

Table 5.3: *Calculated ratio of the strengths* (Γ_r) *and distance d for different offsets. Also shown is the adjusted value for d and the difference between them in %. The last column gives the distance over which the position of the positive pole was moved to adjust for tilts, including the change in* d.

offset δ	calculated Γ_r	calculated d	adjusted d	$\Delta\ d$ (%)	Δ position
-2.0	-2.04	0.73	0.41	-43.9	0.19
-4.0	-1.86	0.73	0.42	-41.2	0.17

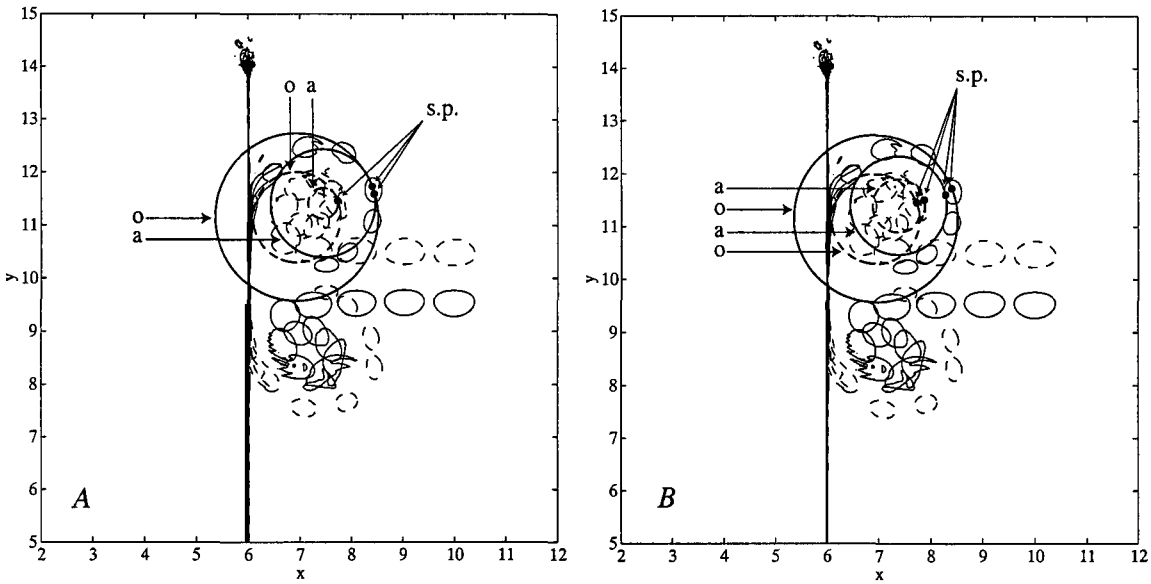

Figure 5.16: *Paths of the vortices for* $\delta = -4.0$ *visualised using contours of the vorticity drawn at* $0.70\hat{\omega}$. *The circular paths are calculated based on the situation at* $t = 8$. *The centres of vorticity are indicated with dots* (s.p.). *The circular path of the negative vortex is indicated by a dashed line while the path of the positive vortex is represented by the solid line. The original circular paths are marked with an* o *while the adjusted paths are indicated with an* a. *Figure* A *shows the calculated circular paths if the circulation of the positive vortex is varied to get a better match while figure* B *shows the circular paths if the distance* d *between the two poles is varied.*

over an equal distance towards each other to adjust the radii of the paths. Then the positive pole is moved a bit more to adjust for tilts, again without changing the distance d between the poles. The inner circle is now in much better agreement with the path of the negative pole and the relative adjustment required is much smaller. Figure 5.16 shows the circular paths for $\delta = -4.0$ if the distance d is varied (figure B) and if the strength of the positive pole is varied (figure A). Results are given in table 5.3.

For $\delta < 1.0$ only the path of the dipolar structure containing the original negative pole is investigated. The dynamics of the other dipolar structure, which contains the original positive pole, is comparable the situation for $\delta = -4.0$ where the two dipolar structures are symmetrical. Therefore also the characteristic properties, Γ_r and distance d, are the same.

It seems that, at least for $\delta \geq -1.0$, the simple potential model predicts the path of the dipolar vortex very well.

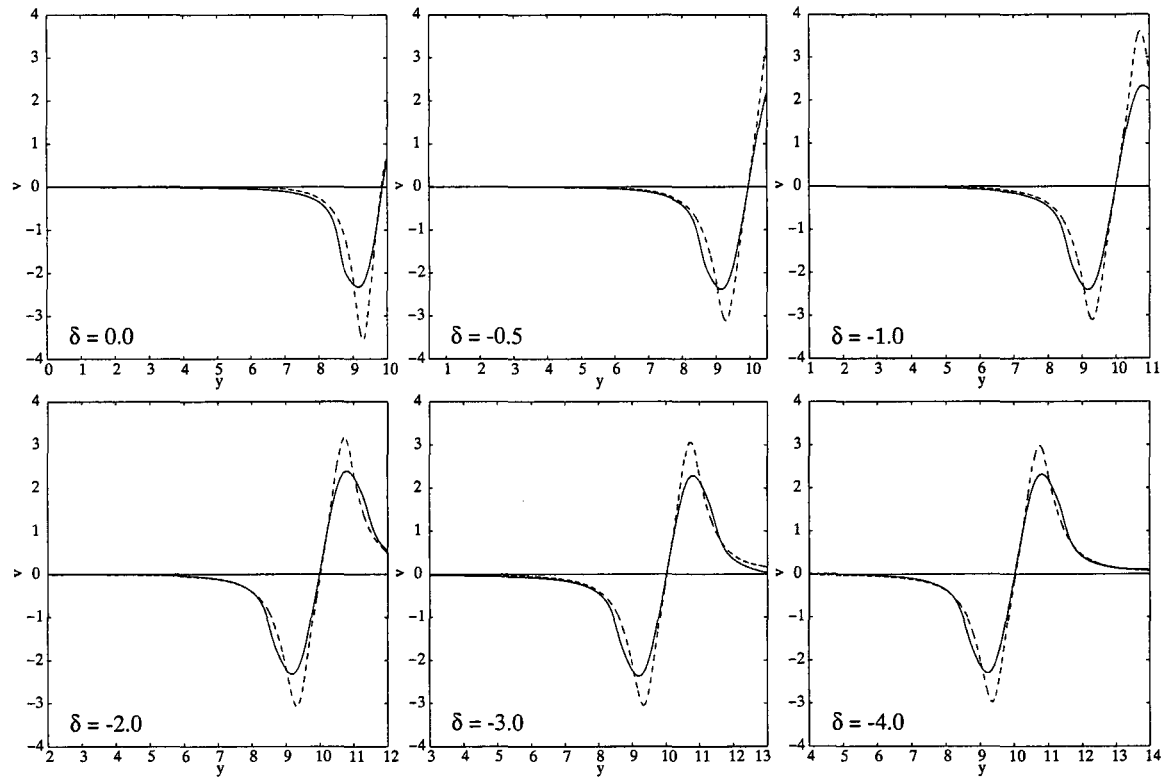

Figure 5.17: *Near-wall velocity $v(x = 6.2a)$ for different offsets δ. The dashed line represents the velocity calculated using the potential model while the solid line indicates results from the numerical simulations.*

5.3.3 Near-wall velocity, a comparison to potential theory

The velocity close to the wall can be used to calculate the secondary vorticity, see equation (2.38). A comparison was conducted with potential theory to see if the velocity around the wall is indeed comparable. The velocity profile at the wall for the numerical simulations was determined at $x = 6.2$, which is a distance $0.2a$ (a is the radius of the dipole at $t = 0$) from the wall. That was the closest distance to the wall while staying away from the boundary layer. The calculations for the profile from the potential model were based on equation (4.1). The distance to the wall is also $0.2a$ and the positions and strengths of the poles were calculated using the procedure as explained in section 5.3.2 with the threshold at $0.5 \times MSV_{t=0}$. These were then mirrored in $y = x$ and translated so that the position relative to the top of the wall is the same as it was in the numerical simulations. The comparison was performed at $t = 4$, the moment at which the original dipolar vortex splits up and the two poles begin to merge with the secondary vorticity patches to form new dipolar structures. The results are shown in figure 5.17.

Table 5.4: *Results from the comparison between numerical simulations and the potential model for different offsets δ. Shown are the amounts of secondary positive circulation based on the numerical simulations ($\Gamma_{num,p}$) as well as based on potential theory ($\Gamma_{pot,p}$) and the difference Δ_p between them in percents (%). Same is done for the negative secondary vorticity indicated with subscripts n.*

offset δ	$\Gamma_{num,p}$	$\Gamma_{pot,p}$	Δ_p (%)	$\Gamma_{num,n}$	$\Gamma_{pot,n}$	Δ_n (%)
0.0	0.05	0.07	34.5	-3.00	-2.89	-3.4
-0.5	0.66	0.90	36.4	-3.24	-3.22	-0.7
-1.0	1.67	2.31	38.5	-3.48	-3.38	-2.7
-2.0	3.01	3.16	5.0	-3.13	-3.45	10.2
-3.0	2.90	3.32	14.6	-3.48	-3.43	-1.2
-4.0	3.18	3.35	5.3	-3.05	-3.37	10.8

The figures clearly show a higher but thinner peak for the potential model profile. Therefore the amount of circulation, equal to the surface integral of the graph, can still be comparable despite the higher peaks of the potential model. The comparison is shown in table 5.4. For small offsets, i.e. $\delta \geq -1.0$, the broader positive peak of the numerical simulations falls outside the integration area. Therefore it cannot compensate for the higher velocity of the potential model which results in a significant ($\approx 35\%$) difference between the calculated circulation using potential theory and the results from the numerical simulations. For other offsets and for the negative peak the results from the numerical simulations and the values found using potential theory match quite well, to within 15%.

The amount of secondary vorticity can also be calculated using the technique described in section 5.3.2, i.e. as an integral of the vorticity. This is done here for the negative secondary vorticity patch. It is not useful to use this technique for the positive patch since it is not confined to the right boundary layer of the wall but also has vorticity above the wall which would influence the calculated circulation but which can not be calculated from the velocity at the wall. A threshold of $0.5 \times MSV_{t=0}$ was used to calculate the circulation of the secondary vorticity patch. The values obtained are compared to $\Gamma_{num,n}$ from table 5.4. The results are shown in table 5.5. They indicate that, except for the situation at $\delta = 0.0$, the results of both methods yield approximately (within 8%) the same results with the integrated vorticity method resulting in a stronger circulation. This difference may be caused by the boundary layer not having the same thickness at every position. The thickness will be larger at places where the velocity is higher, i.e. directly next to the vortex, while it is thinner further away from the vortex. The positions at which the velocity is determined to calculate the circulation are all at the same distance ($0.2 \times a$) from the wall. This will cause an error in the determined circulation.

To see how much of the negative secondary vorticity is actually picked up by the orig-

Table 5.5: *Results from the comparison between the secondary vorticity calculated as a surface integral of the vorticity* ($\Gamma_{iv,n}$ *using a threshold of* $0.5 \times MSV_{t=0}$) *and as determined from the velocity profile at the wall* ($\Gamma_{num,n}$). *Both based on the same numerical simulations.*

offset δ	$\Gamma_{num,n}$	$\Gamma_{iv,n}$	Δ_n (%)
0.0	-3.00	-3.77	20.4
-0.5	-3.24	-3.44	5.8
-1.0	-3.48	-3.73	6.7
-2.0	-3.13	-3.23	3.1
-3.0	-3.48	-3.78	7.9
-4.0	-3.05	-3.18	4.1

Table 5.6: *Comparison between the negative secondary vorticity at the wall* ($\Gamma_{n,t=4}$) *and the positive pole* ($\Gamma_{p,t=4}$) *at* $t = 4$ *and the resulting dipolar structure at* $t = 8$ ($\Gamma_{n,t=8}$ *and* $\Gamma_{p,t=8}$ *the strengths of the two poles*) *based on the numerical simulations. Calculations for* $t = 4$ *were performed using a threshold of* $0.5 \times MSV_{t=0}$ *while at* $t = 8$ *a threshold of* $3.0 \times MSV_{t=0}$ *was used. The last column shows the difference in % between the two ratios.*

offset δ	$\Gamma_{n,t=4}$	$\Gamma_{p,t=4}$	$\Gamma_{r,t=4}$	$\Gamma_{n,t=8}$	$\Gamma_{p,t=8}$	$\Gamma_{r,t=8}$	$\Delta\Gamma_r$ (%)
0.0	-3.77	6.04	-1.60	-2.16	4.00	-1.85	13.5
-0.5	-3.44	6.54	-1.90	-2.42	4.78	-1.98	4.0
-1.0	-3.73	6.60	-1.77	-2.45	4.80	-1.96	9.7
-2.0	-3.23	6.58	-2.04	-2.44	4.82	-1.97	-3.6
-3.0	-3.78	6.59	-1.74	-2.43	4.82	-1.99	12.6
-4.0	-3.18	6.59	-2.07	-2.43	4.83	-1.99	-4.0

inal positive vortex to form a new dipolar structure a comparison is made between the ratio of the strengths of the dipolar structure at $t = 4$ and $t = 8$. All calculations of the circulation are based on integration of the vorticity. The results are given in table 5.6. The difference between the two values for Γ_r at $t = 4$ and $t = 8$ varies with the offset. It is therefore not possible to exactly determine how much of the vorticity of the boundary layer is used in the resulting dipolar structure. It is clear though that most of the secondary vorticity is used to form the dipolar vortex. The ratio of $\Gamma_r \approx 2.0$ at $t = 8$ is the same as was found by Orlandi [2].

Chapter 6

Experiments with background rotation

Apart from numerical simulations experiments were also performed, both in a flow with background rotation and in a stratified fluid. In this chapter the results from the experiments with background rotation are described. As explained in paragraph 3.2 the rotation of the system causes the flow to behave quasi-two-dimensionally. The dipolar vortices are generated by dragging a cylinder through the water and lifting it at the same time. Unfortunately using this technique it is very difficult to create a symmetrical dipolar vortex. The cylinder can be dragged at different velocities and over different distances, both these parameters were varied and the most promising combination, 9.0±0.5 cm in 1.5±0.3 s, was used for the experiments. Still most dipolar vortices were asymmetric and did not move in a straight path. Therefore it was not possible to perform experiments for a full range of offsets, although the starting conditions were set for this range. This makes it impossible to do an analysis as in the previous chapter, i.e. indicate for which offsets the dipole will not be influenced, for which it will split, etc. However, in some experiments the dipolar vortex did move in a straight path. These experiments are described in this chapter and will be compared to numerical simulations. First the results of a dye experiment are shown, then a comparison is performed between the dipole itself and the Lamb model for a dipolar vortex. Finally the paths of the poles of the dipolar vortex are investigated and compared to the results from numerical simulations. The time t is chosen such that in each experiment the centre of the dipolar vortex is $\approx$ 230 mm away from the wall at $t = 0$ s.

6.1 Dye experiment at an offset $\delta \approx 0$

An example of a dye experiment is shown in figure 6.1. The dipolar vortex and the wall are seen in figure A, in figures B and C the vortex moves towards the wall. Then, in figures D, E and F, the dipolar vortex collides against the wall and secondary vorticity is generated. This is most apparent at the top of the wall where a clear dipolar vortex has formed in figure G. The other pole of the original dipolar vortex begins to merge with the secondary

vorticity in figure G resulting in a dipolar structure a seen in figure H. The last figure, I, shows the two new dipolar vortices moving away from the wall. The total duration of the collision as shown in figure 6.1 is 35 s.

6.2 The dipolar vortex

As described in section 2.2 the Lamb dipolar vortex is characterised by a linear ω,ψ relationship within a circle of radius a while the vorticity in the exterior is equal to zero, see equation (2.17). This is in a frame moving with the dipolar vortex. In figure 6.2 A the dipolar vortex is shown 25 s after the cylinder was lifted out of the water. It shows contour plots of both the vorticity and stream function. The scatter plot of the vorticity versus the stream function (figure B) is based on the same data as used for figure A. It indicates a linear relationship between the stream function and the vorticity. However, it also shows that the positive pole is far more intense, the maximum value of the vorticity of the positive pole is ≈ 1.8 times the maximum of the absolute vorticity of the negative pole. Still the ratio of the strengths is not as different as the maximum vorticity suggests, $\Gamma_r = 1.03$. This can be explained using figure 6.2 C, which shows a lower but broader vorticity profile for the negative peak.
It is very difficult to determine the radius of the dipolar vortex directly from the experimental data since there is a gradual transition between interior and exterior. Therefore the distance d between the two centroids of vorticity of the two poles is measured. For a Lamb dipole this distance d is related to the the radius a via $d = 0.92a$. The non-dimensional offset δ is then defined as

$$\delta \equiv \frac{D}{a} = \frac{D}{1.09d}. \tag{6.1}$$

Despite the fact that the dipolar vortex is not exactly a Lamb dipolar vortex equation (6.1) will be used to calculate the dimensionless offset δ.

6.3 Results

Because of the problems encountered while generating the dipolar vortices only four correct experiments were performed of which three will be discussed here. The offsets δ of these three are: 1.4, 0.5 and -1.0. The fourth also had an offset of ≈ 1.4 and is therefore not shown. The three different experiments do show completely different behaviour. Since the cylinder was lifted by hand the velocity of the cylinder was not the same in all experiments resulting in different Reynolds numbers for the different experiments. The Reynolds number for a dipolar vortex is defined as

$$Re = \frac{Ud}{\nu} \tag{6.2}$$

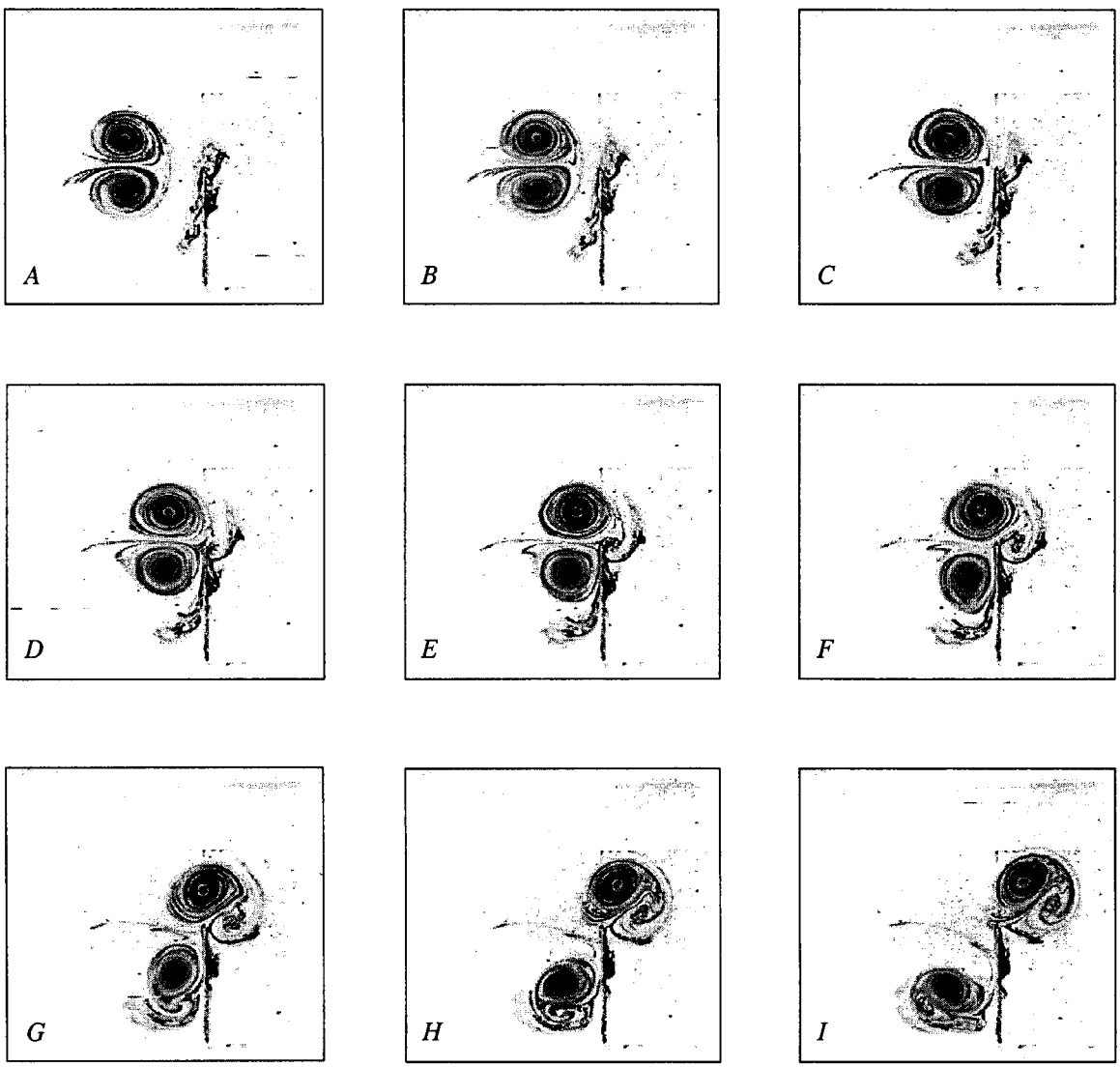

Figure 6.1: *Collision of a dipolar vortex with the wall at an offset* $\delta \approx 0$*, visualised using dye. The total duration of the collision is* 35 *s.*

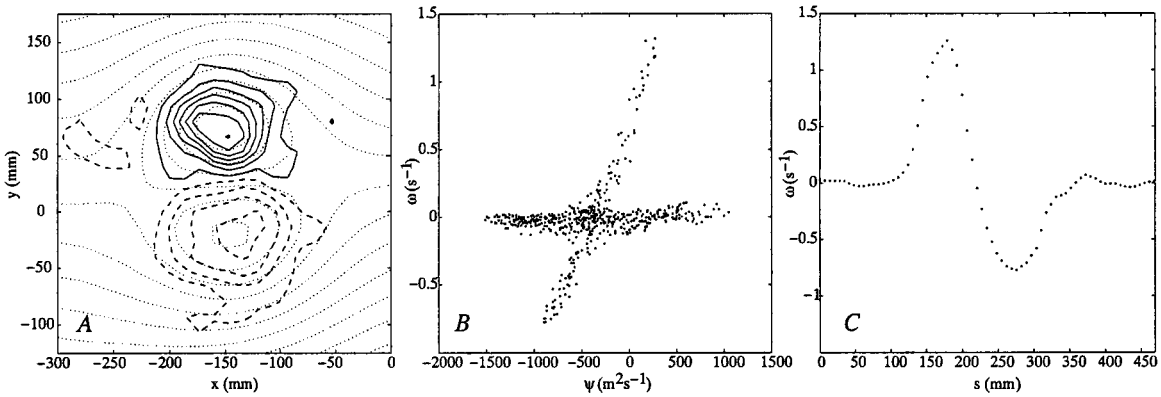

Figure 6.2: *Contour plot of the vorticity and stream function (figure* A*) for a frame moving with the dipolar vortex. The solid lines represent positive vorticity, the dashed lines negative and the dotted lines show isolines of the stream function. Figure* B *is a scatter plot of the vorticity ω against the stream function ψ for the area shown in figure* A*. Figure* C *shows the vorticity distribution along a section* s *through the two tops of the dipolar vortex. This is the situation for $\delta = -1.0$ at $t = 5.1$ s.*

with U the translation velocity of the vortex, d the distance between the centroids of vorticity and ν the kinematic viscosity of the fluid. For the experiments at offsets $\delta = 1.4$, 0.5 and -1.0 the Reynolds numbers at $t = 0$ are, respectively, $Re_{t=0} = 770$, 610 and 800. The results of the different experiments will be discussed in the following sections.

6.3.1 Offset $\delta = 1.4$

Figure 6.3 shows contour plots of the vorticity of the evolution of the dipolar vortex. Figure 6.6 *A* gives a better representation of the path of the dipolar vortex as it shows contours of the vorticity at different moments in one graph. The time interval between these contours is 5.1 s. The offset δ was determined at $t = 15.2$ s since for $t < 15.2$ s the dipolar vortex did not move perpendicular to the wall.
The situation at $t = 0$ s clearly shows a more intense positive pole. However, the ratio of the strengths of the two poles is approximately equal to one, $\Gamma_r = 1.03$. At $t = 20.3$ s and $t = 40.5$ s figure 6.3 shows the generation of positive secondary vorticity at the top of the wall caused by a flow above the wall in negative x-direction. This secondary vorticity patch has a slight influence on the intensity of the original negative pole. This can be seen at $t \geq 40.5$ as from then on the dipolar vortex describes a curved path. This is more clear in figure 6.6 *A*. The curvature of the path is very small, however, and the dipole starting at this offset is therefore probably at the verge of being influenced by the wall and not being influenced by the wall.

6.3.2 Offset $\delta = 0.5$

The evolution of the dipolar vortex starting at an offset $\delta = 0.5$ is shown in figure 6.4. The path of the two vortices is also shown in figure 6.7 *A*. Again the offset was not determined at $t = 0$ s but at $t = 15.2$ s for the same reason as described in section 6.3.1.
The vorticity distribution at $t = 0$ s again shows that the vorticity of the positive vortex is more intense. However, the negative pole is more extensive and the circulation of the latter is 8% higher, $\Gamma_r = 0.92$. At $t = 20.3$ s the vortex has reached the wall and secondary vorticity is generated, negative at the top and positive at the left-hand side of the wall. In the next figure, $t = 40.5$ s, the original dipolar vortex has split into two separate vortices which both form new dipoles with the secondary vorticity from the wall. These dipolar vortices move in curved paths away from the wall ($t = 60.8$ s and further). The dipolar vortex containing the original negative pole has a higher ratio of strengths (Γ_r) when compared to the other dipole and therefore the radius of the trajectory is much smaller.

6.3.3 Offset $\delta = -1.0$

The evolution of the dipolar vortex starting at an offset $\delta = -1.0$ is shown in figures 6.5 and 6.8 *A*. Again the positive pole at $t = 0$ s is far more intense than the negative pole but here too $\Gamma_r = 1.03$. At $t = 0$ s some vorticity has already been generated at the top and side of the wall. In the next frame, $t = 20.3$ s, the dipole has moved towards the wall and the two patches of secondary vorticity have formed. These patches separate from the wall as seen at $t = 40.5$ s and form new dipolar structures with the two original poles. The new dipolar structures move away from the wall in a curved path. The negative secondary vorticity patch is an elongated structure at $t = 40.5$ to 60.8 s. This patch splits but the two patches of negative vorticity remain close to the positive pole, see the situation at $t = 101.3$ s. The other dipolar vortex collides with the wall for a second time and more positive vorticity is generated.

6.4 Comparison between experimental results and numerical simulations

A comparison between the results of the experiments and numerical simulations is performed in this section. Two things are considered, the ratio of the strengths and the radii of the paths of the two poles of the top dipolar vortex.

In the experiments and numerical simulations the original dipolar vortices move towards the wall from different sides. This implies that the top poles of the dipolar vortices are of

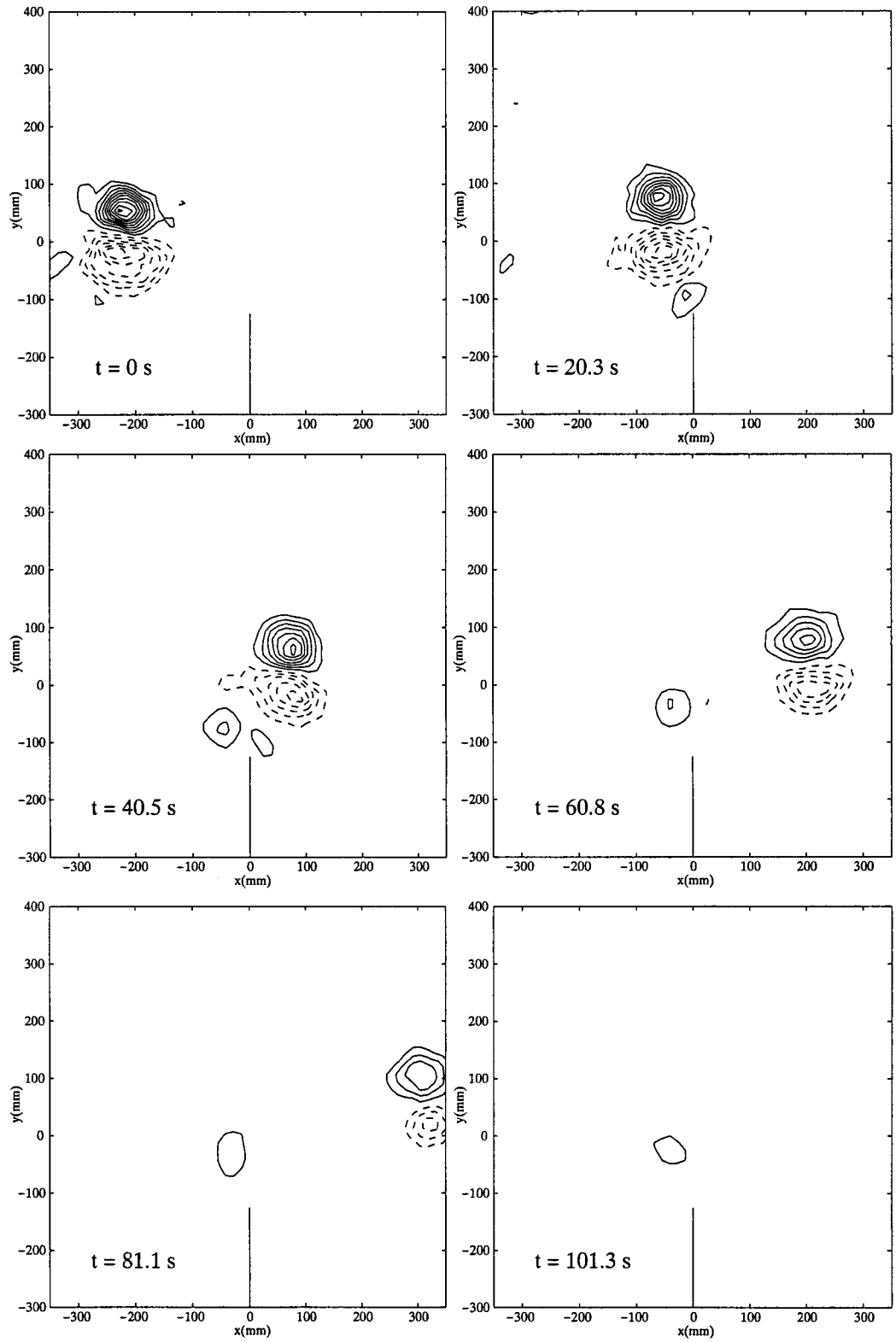

Figure 6.3: *Contour plots of the vorticity of a dipolar vortex approaching the wall. The offset at $t = 15.2$ s is $\delta = 1.4$. The contours are drawn at ± 0.1 s^{-1} and are then raised (positive vorticity) or lowered (negative vorticity) by 0.15 s^{-1}. Solid lines indicate positive vorticity and dashed lines negative vorticity.*

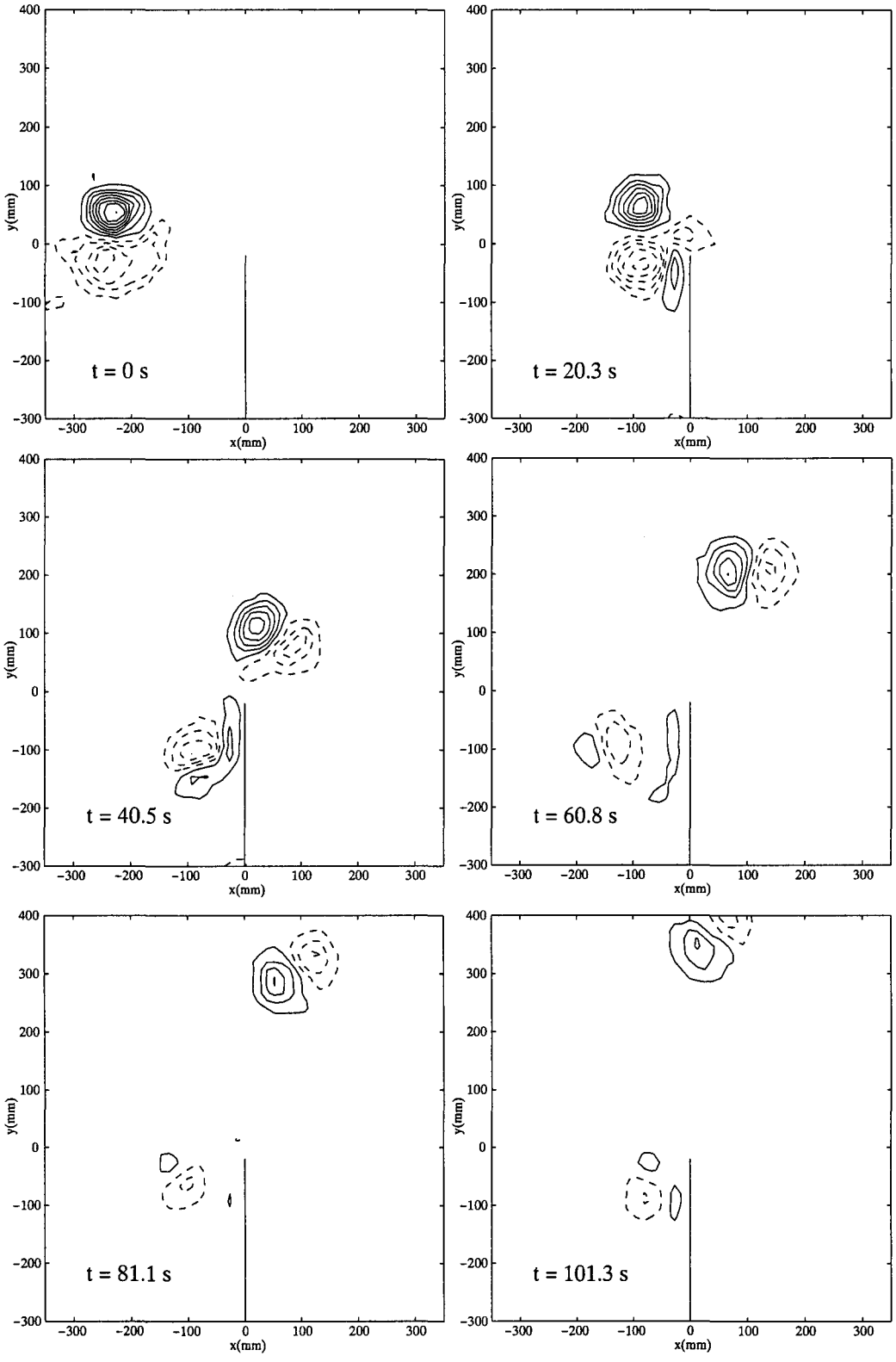

Figure 6.4: *Same as figure 6.3 but with an offset* $\delta = 0.5$.

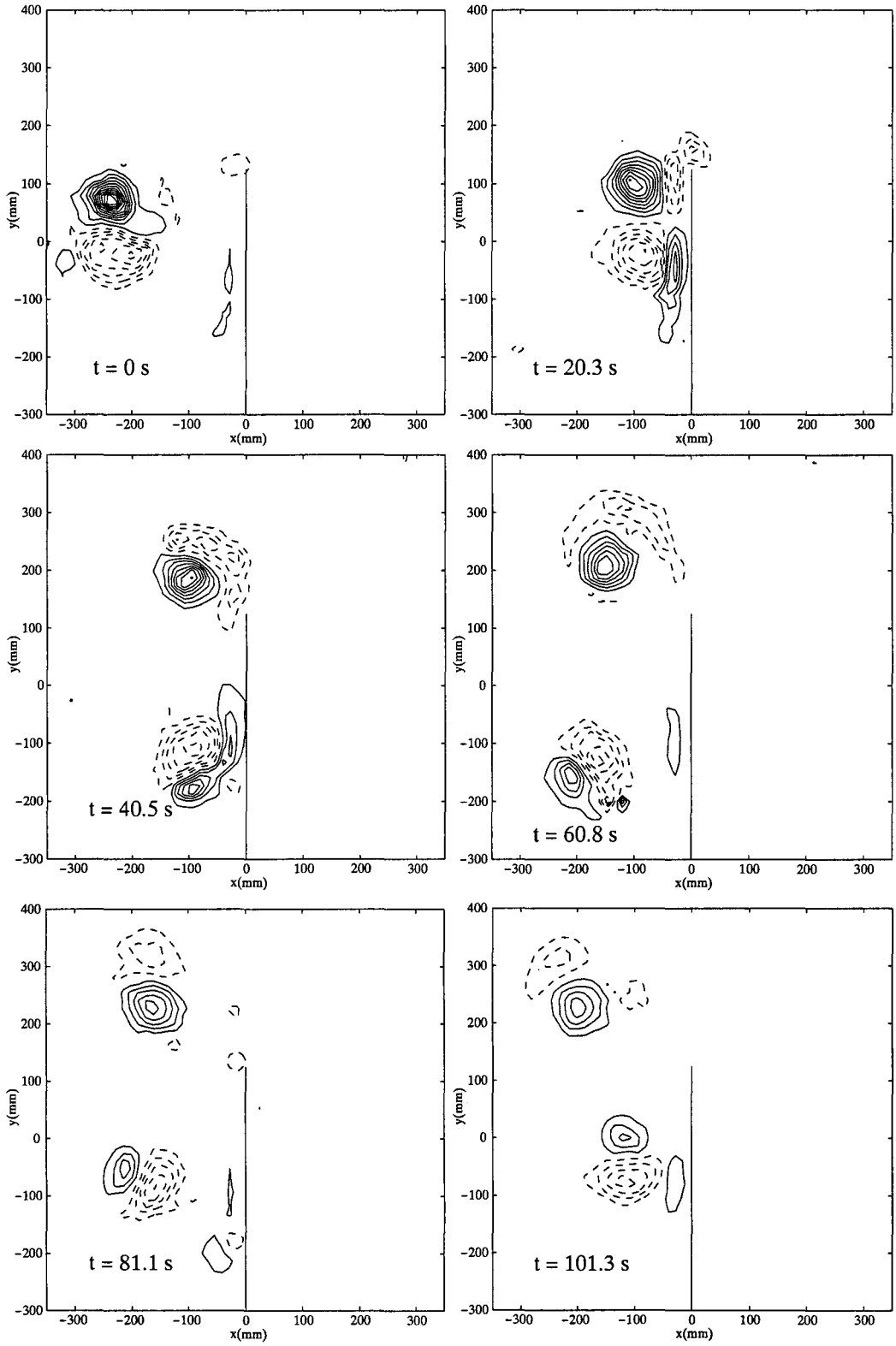

Figure 6.5: *Same as figure 6.5 but with an offset* $\delta = -1.0$.

opposite strength when the two methods are compared. In the experiments the positive pole is above the negative while for the numerical simulations this is just the opposite. The strength and position of the poles and the radii of the paths of the poles are calculated using the method described in section 5.3.2. Again the ratio Γ_r is adjusted until the calculated circular path matches the trajectories of the vortices. The results are shown in figures 6.6 and 6.7 and in tables 6.1 and 6.2. The path of a potential vortex was not calculated for $\delta = -1.0$ since the path of the dipolar structure is not circular. This can be explained using figure 6.5. The patch of negative secondary vorticity is very elongated and splits up after $t = 60.8$ s. The two patches of negative secondary vorticity organise around the positive pole. Since the distribution of negative vorticity around the positive pole is not static the trajectory of the entire structure does not correspond to circular path and can not be described using the potential model. As the negative vorticity is more evenly distributed around the positive vortex the radius of the path of the pole and the velocity of the entire structure becomes smaller. This is seen in figure 6.8 where the curvature of the path increases after $t = 70.9$ s.

Numerical simulations were performed at the same offsets as the experiments and these were compared to the experiments. The results from these simulations are shown in figures 6.6 *B*, 6.7 *B* and 6.8 *B*. Table 6.1 shows the calculated ratio of strengths (Γ_r) for both the experiments and the numerical simulations. The difference in the ratio of the strengths (Γ_r) between the numerical simulations and the experiments is -14 and 8 %. This difference in Γ_r also shows in the comparison of the radii of the poles. This is seen in table 6.2 which indicates an even larger difference between the results from numerical simulations and experiments. However, this was expected since a small change in Γ_r results in a larger difference in the radii of the poles, especially if $-1.5 < \Gamma_r < -1$, see equation (5.7). The difference in the radii are significant and the results from the numerical simulations do not match the results from the experiments. However, only two experiments were performed and to make a good comparison more experiments and simulations are needed. It is clear though that the behaviour of the dipolar vortex is the same for the numerical simulations and the experiments. The path of the vortex is slightly curved after passing the wall at $\delta = 1.4$ while the dipolar vortex splits up in the other two experiments and simulations. Also at an offset $\delta = 0.5$ the upper pole moves past the wall while the lower pole does not, both in simulations and in the experiment. Finally at $\delta = -1.0$ there is a difference in the behaviour of the collision. The negative secondary vorticity in the experiment is generated both at the top and on the left-hand side of the wall while the numerical simulations indicate that secondary vorticity in mainly generated at the top of the wall. Also in the numerical simulations this patch of negative vorticity does not split and the radius of the path of the positive pole remains more constant.

Since these experiments were not very successful another method to generate a dipolar vortex was also used. These experiments were performed in a stratified fluid in which a jet of water is injected. The injected fluid will form a dipolar structure. The results of these experiments are described in the next chapter.

Table 6.1: *A comparison between the ratio of the strengths of the dipolar vortex containing the original positive vortex for experimental results* ($\Gamma_{r,e}$) *and the dipole containing the original negative vortex for the numerical simulations* ($\Gamma_{r,n}$). *Also the difference* Δ *in % is indicated.*

offset δ	$\Gamma_{r,e}$	$\Gamma_{r,n}$	Δ (%)
	$\pm$5%	$\pm$5%	
1.4	-1.00	-1.14	-14
0.5	-1.58	-1.46	8
-1.0	variable	-1.83	variable

Table 6.2: *Comparison between the radii of the poles of the dipolar vortex containing the original positive vortex for experimental results* (r_e) *and the dipole containing the original negative vortex for the numerical simulations* (r_n). *The radius of both the inner (indicated with subscript* in*) and the outer circle, indicated with subscript* ou, *are compared. The difference* Δ *in % is also indicated.*

offset δ	$r_{e,in}$	$r_{n,in}$	Δ (%)	$r_{e,ou}$	$r_{n,ou}$	Δ (%)
	$\pm$ 5 %	$\pm$ 5 %		$\pm$ 5 %	$\pm$ 5 %	
1.4	16.4	7.4	-55	17.3	8.4	-51
0.5	1.72	2.15	25	2.52	3.10	23
-1.0	-	-	-	-	-	-

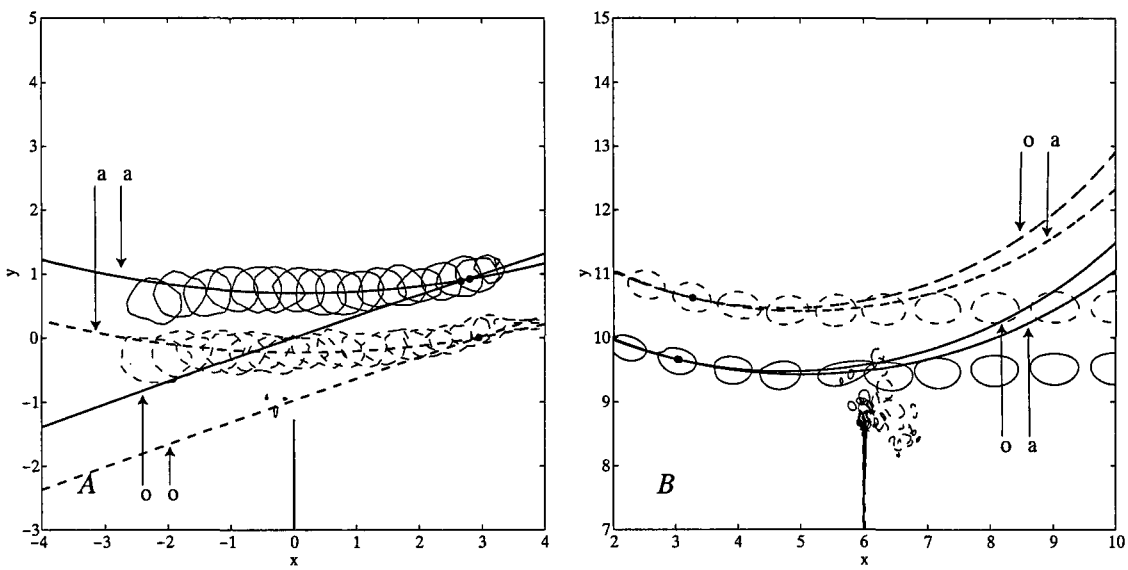

Figure 6.6: *Contour plots of the vorticity of a dipolar vortex approaching the wall at an offset* $\delta = 1.4$. *Figure* A *shows the trajectories of the poles based on the experiment, the contours are drawn at* $\pm 4 \times MSV_{t=0}$. *Figure* B *shows the results from the numerical simulations. The lengths of the experiments are scaled with the radius* (a) *of the dipolar vortex, therefore length scales are comparable between figure* A *and* B. *The circular lines show the paths calculated using potential theory, both based on the original values of the circulation and the position (indicated with an* o*) and on adjusted values to get a better match (indicated with an* a). *Solid lines indicate positive vorticity and dashed lines negative vorticity.*

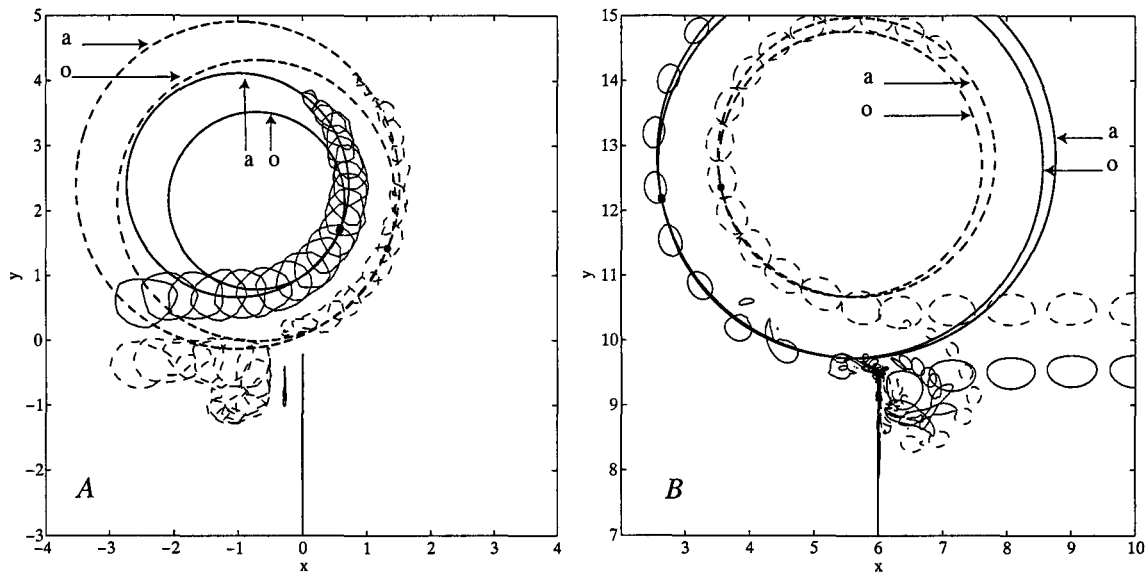

Figure 6.7: *Same as figure 6.6 with an offset* $\delta = 0.5$.

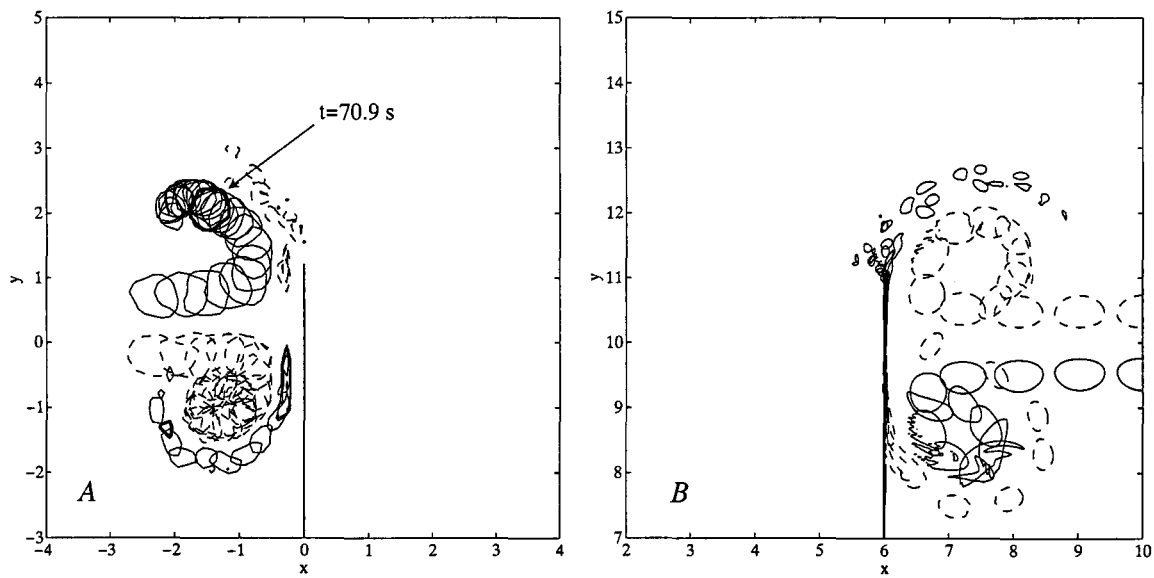

Figure 6.8: *Same as figure 6.6 with an offset* $\delta = -1.0$.

Chapter 7

Experiments in a stratified fluid

The experiments described in this chapter were performed in a stratified fluid. The tank was filled with a two layer stratification with a sharp interface. The lower layer was a 7 cm deep layer of salt water (13.4 % brix) and the top layer consists of another 7 cm of fresh tap water. A vertical wall was placed in the tank. The dipolar vortex is generated using a small diameter nozzle (2 mm) through which fluid is injected. This fluid had the same density as the fluid layer at the level of the nozzle. The injected fluid (3.3 ml in 0.6 s) will form a dipolar structure. The procedure is explained in more detail in section 3.1 and by Flór and Van Heijst (1994) [9]. The Reynolds number based on the diameter of the nozzle d and the injection velocity U is defined as $Re = Ud/\nu = 3500$ which ensures a turbulent jet flow. Again there were problems creating a symmetrical dipolar vortex which moves in a straight path. To overcome these problems the flow rate had to be limited. The setting described above was the maximum flow rate at which the resulting dipolar vortex moves in a straight path.

7.1 Dye experiment at an offset $\delta \approx 0$

Dye experiments were performed in the stratified fluid using dye-coloured fluid for injection. These experiments were used to optimise both the parameters for the injection (amount of fluid injected and flow rate) and the distance from the nozzle to the wall. An example of such an experiment is shown in figure 7.1. Figure A shows the turbulent motion directly after injection. The formation of the dipolar vortex from this turbulent motion is shown in figures B and C. Then, figure D, the dipolar structure collides with the wall. The dipole splits and the two poles form new dipolar vortices as they merge with the secondary vorticity generated at the wall. These new dipolar vortices move away from the wall. This is shown in figures E to I. It is clear that the dipolar vortex, and the upper pole in particular, has not fully developed as it collides with the wall (see figure C and D). Therefore the distance between the wall and the nozzle was increased for the other experiments.

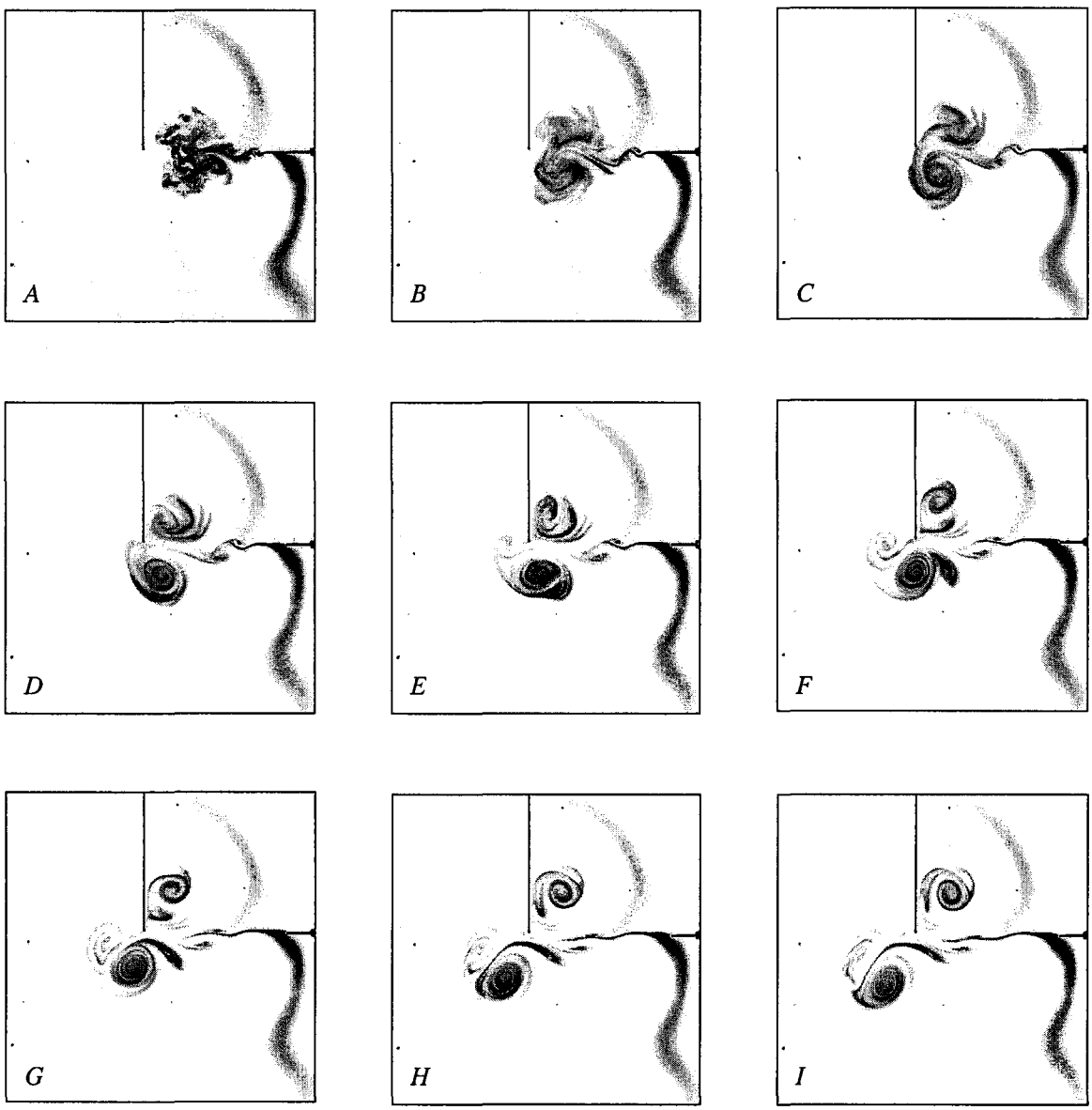

Figure 7.1: *Formation of a dipolar vortex in a stratified fluid (figures* A *to* C*). This dipolar vortex then collides with a solid wall as shown in figures* D *to* I*. The total duration of the experiment shown here is 95 s.*

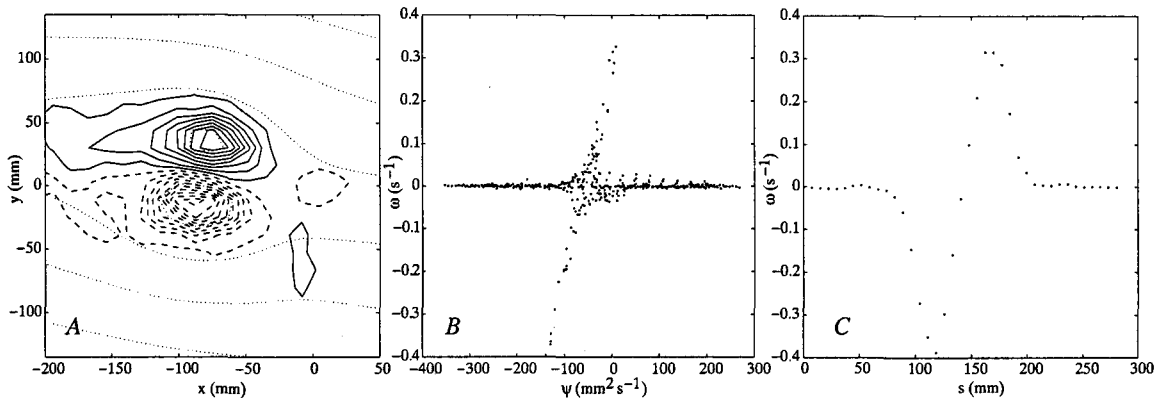

Figure 7.2: *Contour plot of the vorticity and stream function for a frame moving with the dipolar vortex (figure* A*). Solid lines represent positive vorticity, dashed line negative vorticity. The dotted line indicates isolines of the stream function ψ. A scatter plot of the vorticity versus the stream function is shown in figure* B*. The vorticity along a section through the two tops of the dipolar vortex is shown in figure* C*.*

7.2 The dipolar vortex

In this section the same analysis is performed as described in section 6.2. The contour plots of the dipolar vortex are shown in figure 7.2 *A*. Some low intensity vorticity remains in the wake of the vortex but the higher intensity poles do form a circular area and have a linear ω,ψ relationship (figure *B*). The maximum vorticity of the positive pole is slightly less than the maximum absolute vorticity of the negative pole but the ratio of the strengths of the two poles, Γ_r is equal to 1.02. The circulation of the two poles is thus about equal. Again it is difficult to precisely determine the radius of the dipolar structures and therefore equation (6.1) is used to calculate the offset.

7.3 General remarks

7.3.1 Internal waves

The three-dimensional volume of turbulent motion that is formed directly after injection of the fluid collapses under gravity into a two-dimensional layer (as described in section 3.1). This collapse induces internal waves. These can be visualised using the divergence of the velocity. Conservation of mass (equation 2.1)

$$\nabla \cdot v = \frac{\partial u}{\partial x} + \frac{\partial v}{\partial y} + \frac{\partial w}{\partial z} = 0 \tag{7.1}$$

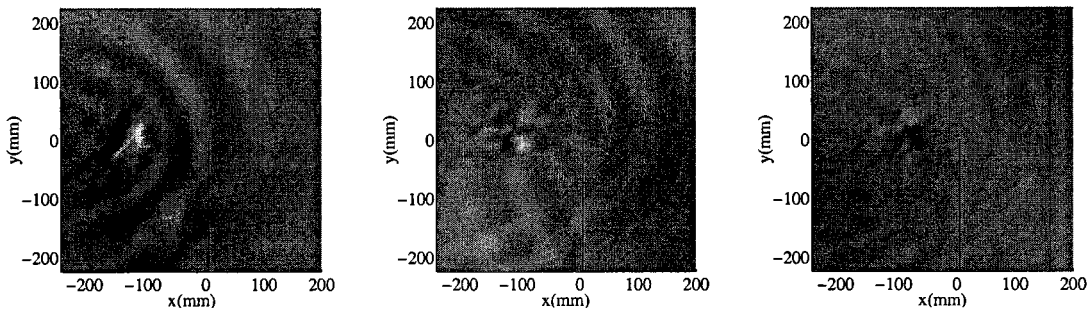

Figure 7.3: *Divergence of the flow at different times after injection showing the quick damping of the internal waves.*

implies that if the divergence of the two-dimensional flow (u,v) is $\neq 0$ the velocity component in z-direction, w, is also $\neq 0$. The divergence after injection of the fluid is shown in figure 7.3 and the waves are clearly visible. It is also apparent that these waves are quickly damped. These waves do not influence the behaviour of the dipolar structure (see also Flór and Van Heijst [9]) and are therefore neglected.

7.3.2 Viscous decay of the dipolar vortex

The dipolar structure decays due to viscous dissipation. Although the flow is quasi-two-dimensional three-dimensional effects do influence the vortices. The decay of the two poles is mainly due to vertical diffusion of vorticity which can be described using

$$\omega = \omega_0(x,y)\,\frac{1}{\sqrt{t}}\,exp(\frac{-t}{\tau_{diff}}), \tag{7.2}$$

with τ_{diff} a time scale and $\omega_0(x,y)$ the vorticity distribution at $t = 0$ (see Flór *et. al.* [17]). Since the circulation is a surface integral of the vorticity the decay of the circulation of the two poles behaves the same as the decay of the vorticity:

$$\Gamma = \Gamma_0\,\frac{1}{\sqrt{t}}\,exp(\frac{-t}{\tau_{diff}}) \tag{7.3}$$

where Γ_0 is the circulation of the pole at $t = 0$. Figure 7.4 *A* shows the decay of the circulation of both poles of the dipolar vortex as function of the time t. A comparison with the model described with equation (7.3) is shown in figure *B*. Here the calculated value for Γ (using $\Gamma_0 = 1$) at a certain time t is set out against the measured circulation at the same time t. The value for τ_{diff} was optimised and is $\tau_{diff} = 1200 \pm 200$ s for both the positive and the negative pole. Least-square linear fits were calculated and are also shown if figure 7.4 *B*. The linear fits were forced through the origin because if $t \rightarrow \infty$ the circulation

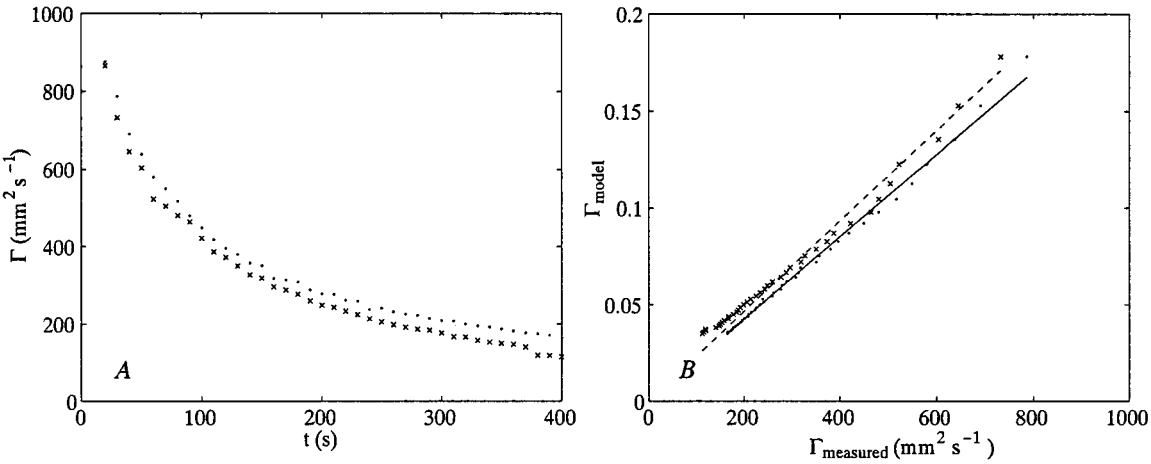

Figure 7.4: *Decay of the circulation of the two poles for* $\delta = 2.28$ *(figure* A*). Figure* B *shows the comparison of the model* $\Gamma_{model} = \frac{1}{\sqrt{t}}\, exp(\frac{-t}{\tau_{diff}})$ *with the measured values of the circulation* ($\Gamma_{measured}$)*. Each point is calculated using equation* (7.3) *at a time* t *which is the same as the time at which the circulation* $\Gamma_{measured}$ *is determined. The dots* ($\cdot$) *indicate values belonging to the positive pole while the crosses* ($\times$) *represent the negative pole. The fit indicated with a solid line in figure* B *represents to the data from the positive pole and the dashed line is for the data of the negative pole. Both fits were forced through the origin. In both figures the absolute value of the circulation of the negative pole was used.*

of the poles in both the model and the experiments should go to zero. The value for Γ_0 was determined, $\Gamma_0 = (4.6 \pm 0.1)10^3$ s^{-1} and $(4.3 \pm 0.2)10^3$ s^{-1} for the positive and the negative pole, respectively. It is clear from figure B that the model describes the decay of the positive pole better then the decay of the negative pole. The decay of the negative pole may be influenced by the presence of the wall. However, the model describes the decay of both poles very well.

7.4 Results

The dimensionless offsets δ are calculated using equation (6.1), and are given in table 7.1. In figure 7.5 the paths of the dipolar vortices are shown for different offsets δ. These figures are contour plots of the vorticity and are drawn at 10 s intervals ranging from $t = 10$ s to $t = 600$ s. The height of the contours (ω_c) varies and is equal to

$$\omega_c = \frac{1}{2n} \sum_{i=1}^{n} |\, \omega| \tag{7.4}$$

with n the total number of grid points (here $40 \times 40 = 1600$), this is calculated for each point of time. Therefore the contour is lowered at approximately the same rate as the

Table 7.1: *Dimensionless offsets δ for the experiments performed in a stratified fluid. Also the distance between the two poles at $t = 20s$ is shown,* d.

Experiment number	distance d (mm)	dimensionless offset δ
1	46.7	2.28
2	45.8	1.69
3	48.4	1.24
4	47.6	0.46
5	48.8	-0.32
6	52.3	-0.90

dipolar vortex decays.
As described in section 7.3.2, viscous dissipation causes the dipolar structure to decay rapidly. This decay will cause the dipole to move slower, see equation (4.19), and finally the translation will stop. This occurs in all experiments, as is clear from figure 7.5; the time interval between the contours is fixed at 10 s and the distance between the contours decreases rapidly. The decay makes it impossible to calculate the radius of the paths after the collision with the wall.

7.4.1 Evolution at different offsets δ

At an offset $\delta = 2.28$ the dipolar vortex is practically uninfluenced by the presence of the wall. Figure 7.5 shows a small patch of positive vorticity which is generated at the left-hand side of the wall. Despite this patch of vorticity the negative pole moves in a straight path. The positive pole does move in a slightly curved path but it is not clear if that is caused by the presence of the wall.
If the offset is reduced to $\delta = 1.69$ a larger patch of positive vorticity is formed at the wall. This patch does remove some of the vorticity from the negative pole of the original dipolar vortex. The dipolar structure is now asymmetrical and moves in a slightly curved path.
At $\delta = 1.24$ a patch of positive vorticity is generated at left-hand side of the wall and the negative pole again loses some vorticity. Since the offset δ is smaller, more negative vorticity is removed and the curvature of the path of the dipole is stronger.
The path of the vortex is not perpendicular to the wall for the experiment with $\delta = 0.46$. The negative pole is more intense than the positive pole and the path shows a clear deflection in downward direction before the vortex reaches the wall. Here the vortex does split up and two new dipolar vortices appear and move away in opposite directions.
For a small negative offset, here $\delta = -0.32$, an almost symmetrical collision is seen in figure 7.5. The original dipole splits up again and two dipolar structures are formed. These move away from the wall in opposite directions. The ratio of strengths (Γ_r) for these dipolar

vortices is -2.4 ± 0.1 and -2.1 ± 0.1 for the upper and lower structure respectively.
At $\delta = -0.90$ the behaviour of the collision with the wall is the same as for the previous offset ($\delta = -0.32$), however, now the collision is symmetrical. The upper dipolar structure has $\Gamma_r = -2.1 \pm 0.1$ while the lower has $\Gamma_r = -2.0 \pm 0.1$.

7.4.2 Comparison to numerical simulations

The evolution of the vortex at offsets $\delta = 2.28$ and 1.69 is comparable to the numerical simulations at $\delta = 2.0$ and 1.4, respectively (see figures 5.11 and 6.6). The trajectory of the dipolar vortex at the larger offset is uninfluenced while the smaller offset results in a slight curvature of the path of the vortex pair. At $\delta = 1.24$ the influence of the wall becomes more distinct. The curvature of the path of the dipolar vortex after the collision is clearly visible and the general behaviour may be compared to the situation of $\delta = 1.0$ in the numerical simulations. The evolution of the dipolar vortex starting at $\delta = 0.46$ is not comparable to the simulation performed at $\delta = 0.5$. The positive pole in the experiment does not move past the wall while in the numerical simulations it does. This is caused by the non-perpendicular approach of the dipolar vortex which effectively gives the dipole a smaller offset. For $\delta = -0.32$ the dipolar structure consisting of the original positive pole and the patch of negative secondary vorticity behaves differently from the comparable vortex in the numerical simulations at $\delta = -0.5$. The negative secondary vorticity in the simulations is generated at the top of the wall while in the experiment it is generated at the left-hand side of the wall. Also at $\delta = -0.90$ the difference between the numerical simulations (at $\delta = -1.0$) and the experiment is that in the numerical simulations the secondary vorticity is generated at the top of the wall rather than at the left-hand side as in the experiments. Besides in the simulations the two dipolar vortices are not symmetrical for $\delta = -1.0$, the situation at $\delta = -2.0$ and -3.0 is more comparable to the experiment at $\delta = -1.0$.

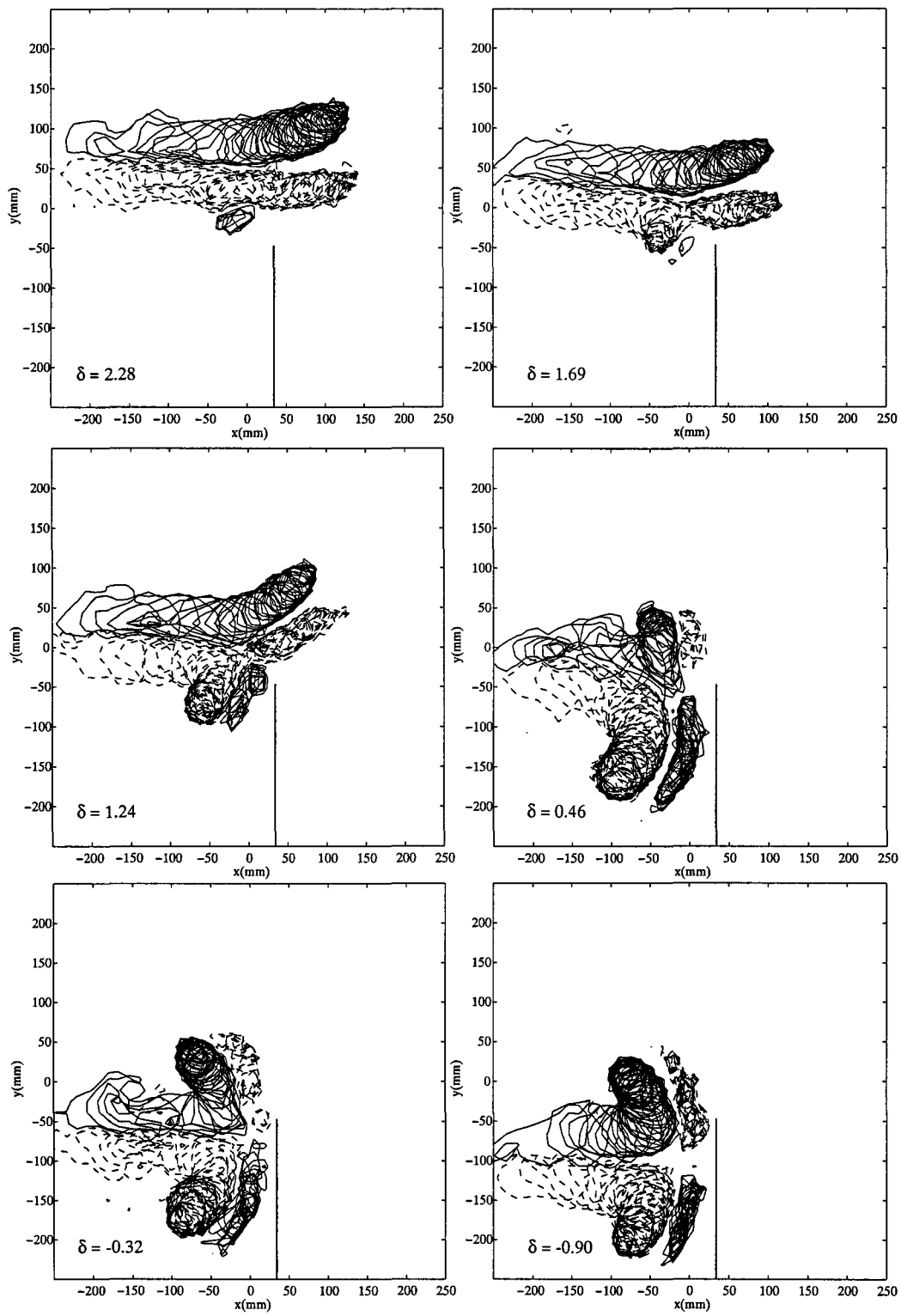

Figure 7.5: *Paths of the dipolar vortex and patches of secondary vorticity for different offsets δ in a stratified fluid. Solid lines indicate positive vorticity while dashed lines represent negative vorticity.*

Chapter 8

Conclusions and recommendations

8.1 Potential model

The analytical-numerical model as derived for a potential dipolar vortex in section 4.1 is unable to predict the trajectory of the vortex. The main deficiency of the model is that it does not take the secondary vorticity into account. This vorticity, originating from the no-slip wall, strongly influences the evolution of the vortex pair. For example, after the dipolar vortex has split up both poles form new dipolar structures with the secondary vorticity, these move away from the wall. In the potential model, however, the two poles split and then move along a path parallel to the wall. The potential model does give a good indication of the velocity induced by the two vortices, as shown in figure 5.17. The amount of secondary vorticity that is generated at the side of the wall corresponds to the secondary vorticity calculated using this model.
The analytical model for two poles in absence of a wall predicts that a dipolar vortex with poles of unequal strength will move in a circular path. Also the radii of the paths of the two poles can be calculated. For offsets $\delta > -2.0$ this model describes the path of the vortices very well.
It may be possible to use potential theory and the Kutta condition to calculate the amount of vorticity generated at the top of the wall. This way the potential model can be extended and maybe the path of the vortices can be predicted with the inclusion of the secondary vorticity vortices. This will give a better prediction of the path of the vortices since then the poles will not move parallel to the wall after the collision but two new dipolar vortices can form which will travel away from the wall.

8.2 Numerical simulations

From the numerical simulations it is clear that there are four general possibilities. The dipolar vortex can remain uninfluenced by the wall. This is the case for $\delta >\sim 1.5$. Another possibility is that the pole closest to wall loses some vorticity to the patch of secondary vorticity that is formed at the top of the wall. This results in a curved path of the dipolar

vortex after it has passed the wall. In the simulations this was visible for offsets $\sim 0.5 < \delta <\sim 1.5$. At offsets $\sim -1.0 < \delta <\sim 0.5$ the dipolar vortex splits up and two new dipolar structures are formed. These vortices move away from the wall in curved asymmetric paths. If $\delta <\sim -2.0$ the two resulting dipolar vortices are symmetrical. Comparisons with potential model are described in section 8.1.

8.3 Experiments with background rotation

The dipolar vortex was created using a cylinder which was lifted out of the water. This was done by hand using a guiding rail to make the cylinder move in a straight line. Since the tank was rotating the procedure of walking with the tank and lifting the cylinder at the same time is not easy. Therefore the generated dipolar structure was often asymmetric and its trajectory a curved path. This may be improved by using a device that lifts the cylinder automatically. For the experiments in which the dipolar vortex did move in a straight path the vortex has a linear relationship between the stream function and the vorticity, indicating that the vortex can be described with the Lamb model for a dipolar vortex. However, the maximum vorticity of the positive pole is much higher than that of the negative pole. Still the ratio of strengths $\Gamma_r \approx 1$. Due to the problems described above only three successful experiments were performed. The evolution of two of these is comparable to the results from numerical simulations. The other experiment shows a different behaviour. More experiments are necessary to perform a better comparison between the results of the numerical simulations and the experiments. However, to do these the lifting of the cylinder should be automated.

8.4 Experiments in a stratified fluid

For these experiments a stratified fluid was used in which fluid was injected horizontally, resulting in the formation of a dipolar structure. The problem with these experiments is that the viscous dissipation of the vorticity is very strong. Therefore the vortices do not really detach from the wall after the collision.
The vortices resemble a Lamb dipolar vortex very well. They are also more symmetrical than the vortices in the rotating fluid. The decay of the poles of the dipolar vortex is compared to a model from Flór *et. al.* [17] and the similarity is very good. The general behaviour of the evolution of the dipolar vortex is comparable to the results from the numerical simulations. Due to the strong dissipation it was not possible to perform a more quantitative comparison.

Bibliography

[1] S.J. Barker and S.C. Crow (1977) The motion of two-dimensional vortex pairs *J. Fluid Mech.* **82**, 659-671.

[2] P. Orlandi (1990) Vortex dipole rebound from a wall *Phys. Fluids A* **2** 1429-1436.

[3] P.K. Kundu (1990) *Fluid Mechanics* Academic Press.

[4] H. Lamb (1932) *Hydrodynamics* Cambridge University Press.

[5] A.R. Paterson (1983) *A first Course in Fluid Mechanics* Cambridge University Press.

[6] M.R. Spiegel (1974) *Complex Variables* McGraw-Hill.

[7] H. Schlichting and K. Gersten (2000) *Boundary Layer Theory* Springer.

[8] G.J.F. van Heijst and J.B. Flór (1989) Dipole formation and collisions in a stratified fluid *Nature* **340**, 212-215.

[9] J.B. Flór and G.J.F. van Heijst (1994) Dipolar vortex structures in a stratified fluid *J. Fluid Mech.* **279**, 101-133.

[10] O.U. Velasco Fuentes and G.J.F. van Heijst (1994) Experimental study of dipolar vortices on a topographic β-plane *J. Fluid Mech.* **259**, 79-106.

[11] J. Pedlosky (1987) *Geophysical Fluid Dynamics*, Springer.

[12] R.J.M. Bastiaans, G.A.J. van der Plas and R.N. Kieft (2002) The performance of a new PTV algorithm applied in super-resolution PIV *Exp. Fluids.* **32**, 346-356.

[13] P.K. Newton (2001) *The N-vortex Problem: Analytical Techniques* Springer.

[14] P.G. Saffman (1992) *Vortex Dynamics* Cambridge University Press.

[15] M. Karweit (1975) Motion of a vortex pair approaching an opening in a boundary *Phys. Fluids.* **18**, 1604-1606.

[16] R. Verzicco, P. Orlandi, A.H.M. Eisinga, G.J.F. van Heijst and G.F. Carnevale (1996) Dynamics of a vortex ring in a rotating fluid *J. Fluid Mech.*. **317**, 215-239.

[17] J.B. Flór, G.J.F. van Heijst and R. Delfos (1995) Decay of dipolar vortex structures in a stratified fluid *Phys. Fluids.* **7**, 374-383.

Appendix A

The circular path of the dipolar vortex after collision

This appendix contains a collection of paths of the dipolar structures for different offsets δ with the calculated and adjusted circular paths of a *potential* dipolar vortex.

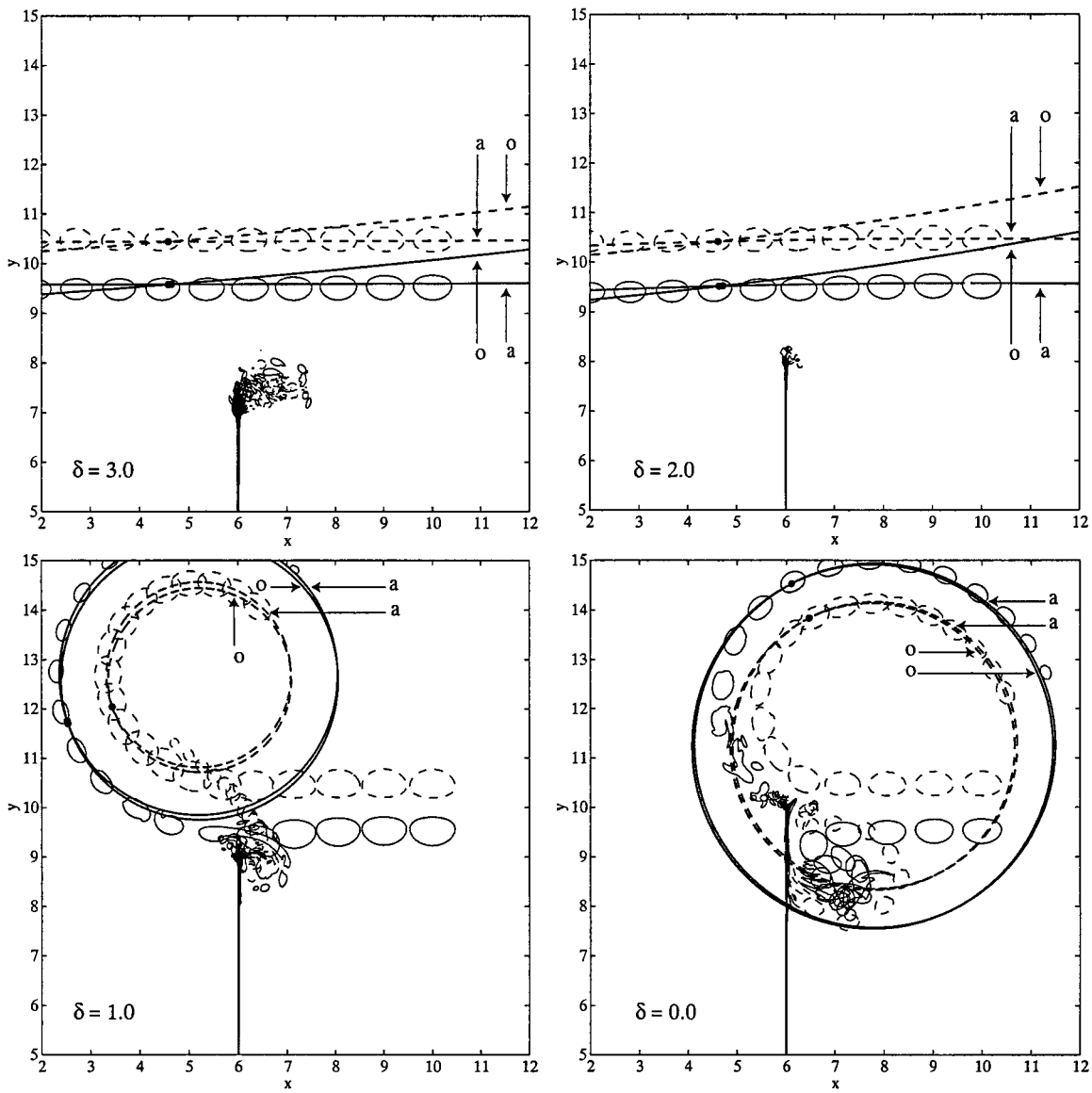

Figure A.1: *Comparison between results from numerical simulations and potential theory. The dashed lines represent (the paths of) negative poles while solid line indicate positive vorticity. Lines denoted with an* o *are the original unadjusted paths based on the calculated positions and strengths of the poles. Lines marked with an* a *are based on adjusted values. The dots indicate the calculated and adjusted starting positions on which the radii of the potential paths are based. The offset is varied between* $\delta = 3.0$ *and* $\delta = 0.0$.

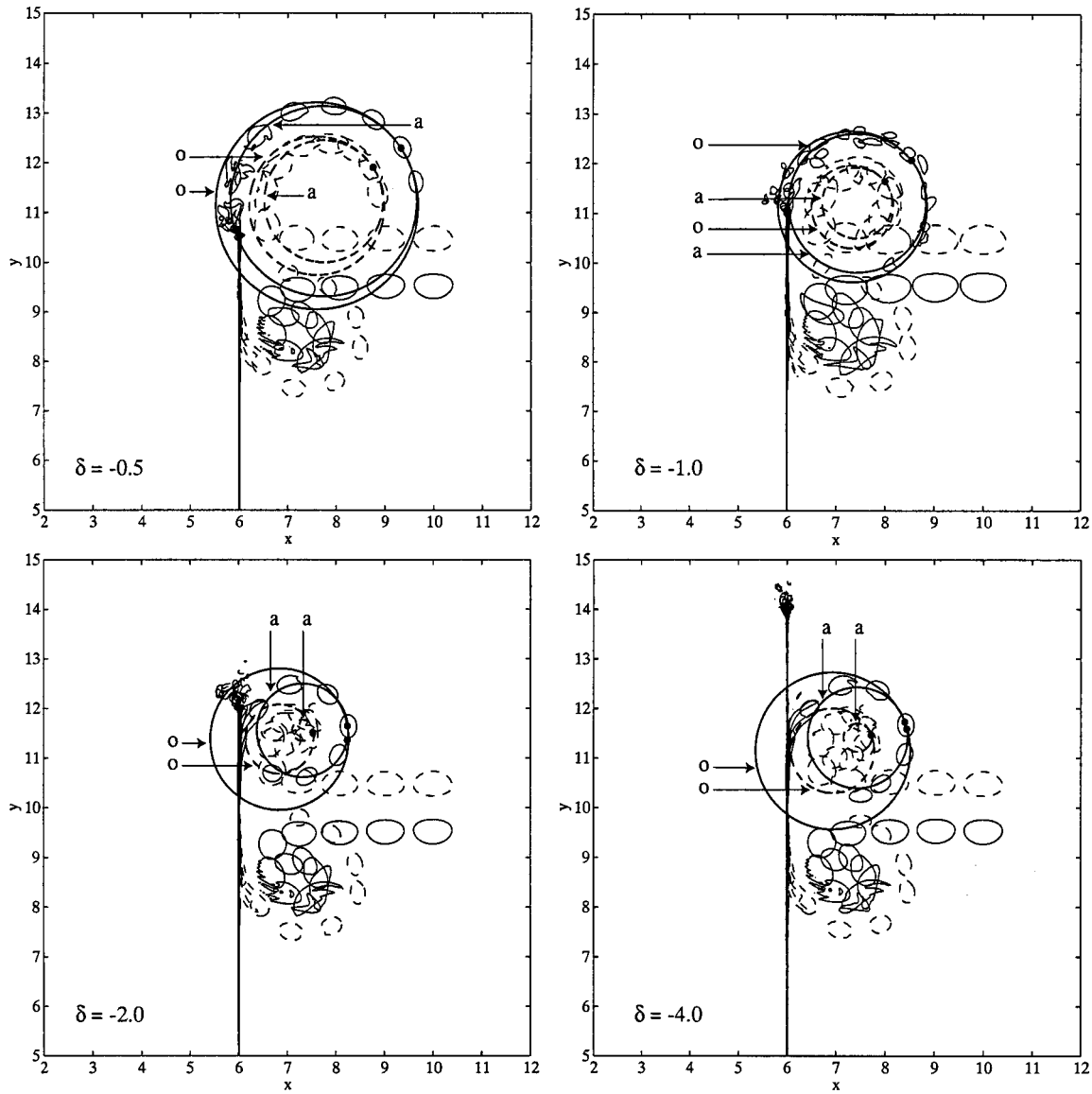

Figure A.2: *Same as figure A.1 except that the offset is varied between* $\delta = -0.5$ *and* $\delta = -4.0$.

Appendix B

Technology assessment

The study of the atmosphere of the earth is important for the prediction of the weather, both on short and long term (climate). It is also important to understand the large-scale flows in the oceans as they too are of great influence on the global climate. These large-scale oceanic flows are responsible for the transport of, e.g. heat and pollution. The North Atlantic Drift is an example of such a flow which transports heat from the Gulf of Mexico to northern Europe, which makes the climate more temperate.

As described in the introduction (chapter 1) the flow in the atmosphere and oceans is in good approximation two-dimensional. A lot of research has been performed to better understand the processes that take place in these flows. The present study, as described in this report, is only a small part of this research. It is of special relevance to better comprehend the flow around obstacles. An example is the interaction of large-scale geophysical vortices with a mountain ridge (here approximated with the wall). Also in the flow around the sharp edge of airfoils and aircraft- and helicopter rotors the interaction between vortices and a sharp edge can be of great influence.